A SIMULATION OF THE SINGLE SCAN ACCURACY OF A TWO-DIMENSIONAL PULSED SURVEILLANCE RADAR

Johan J Bras

A Dissertation Submitted to the Faculty of Electrical and Electronic Engineering University of Cape Town in partial fulfillment for the degree of Master of Science in Engineering

Cape Town 1991

ABSTRACT

The following dissertation considers the single-scan two-dimensional positional accuracy of a pulsed surveillance radar. The theoretical aspects to the positional accuracy are considered and a generalized analytical approach is presented.

Practical position estimators are often complex, and theoretical predictions of their performance generally yield unfriendly mathematical equations. In order to evaluate the performance of these estimators, a simulation method is described based on replicating the received video signal. The accuracy of such a simulation is determined largely by the accuracy of the models applied, and these are considered in detail. Different azimuth estimation techniques are described, and their performances are evaluated with the aid of the signal simulation.

The best azimuth accuracy performance is obtained with the class of analogue processing estimators, but they are found to be more susceptible to interference than their binary processing counterparts. The class of binary processing estimators offer easily implemented techniques which are relatively insensitive to radar cross-section scintillation characteristics. A hybrid estimator, using both analogue and binary processing, is also evaluated and found to give an improved accuracy performance over the binary processing method while still maintaining the relative insensitivity to radar cross-section fluctuation.

Declaration

I, Johan J Bras, declare that this dissertation is my own work. It is being submitted in partial fulfillment of the requirements for the degree of Master of Science in Engineering at the University of Cape Town. It has not been submitted before for any degree or examination at any other University.

signature removed

30 th day of September, 1991

CONTENTS

PREFACE

Current radar systems utilize advanced processing techniques to optimize detection, accuracy and resolution performance. Although the detection range of these systems is still calculated with the basic range equation, prediction of the accuracy and resolution performance of such systems generally require detailed simulations. A number of papers and reports have been published detailing the particular performance characteristics of specific processing techniques. Quite often, however, these evaluations are applicable to very specific situations, and comparative evaluations usually require certain further assumptions or interpolations between results to be made. The following dissertation examines the positional accuracy of a pulsed surveillance radar utilizing various position estimators. These evaluations are such that comparisons are possible. Particular emphasis has been placed on the azimuthal positional accuracy of the system.

I am indebted to Professor M.R. Inggs for his guidance, patience and time in helping me to complete this dissertation.

I would also like to thank my employer, ESD-South, as well as the Armaments Corporation of South Africa (ARMSCOR) for granting me the opportunity to undertake this study. Further, I would like to mention mr S. Rich whose radar enthusiasm inspired me to start this dissertation, and Dr. R.M. Braun who assisted me with this dissertation during its infancy stage.

Finally, I would like to thank my wife in particular for all her encouragement, and especially patience, as well as her assistance in preparing the final document. Without her continued support this study would surely not have been possible.

LIST OF ILLUSTRATIONS

LIST OF TABLES

1.0 INTRODUCTION

1.1 STATEMENT OF THE PROBLEM

The primary functions of a radar are the detection, positional estimation and resolution of objects. Radars may generally be categorized according to their functions, such as two-dimensional- and three-dimensional surveillance radars, height finding radars, tracking radars and multi-function phased array radars. Further distinctions such as pulsed or continuous wave radar are possible within each category, depending on the technical features of the system. An abundance of information on radar has been published during the post-World War II period detailing the capabilities of- and the limitations imposed on the performance of the different radar systems. Technological advances have enabled radars to approach the theoretical performances predicted in the literature.

A multitude of processing techniques have been developed in the quest for optimum performance. The complexity of these processing techniques is often of such a nature that it precludes the prediction of performance via analytical techniques. In many instances, the advantages of a given processing technique have been investigated with the aid of simulations, and many articles have been published detailing the achieved results. In the majority of cases the conditions assumed in the simulations have differed, and comparative evaluations are quite often difficult to make without further assumptions.

1.2 SCOPE AND OBJECTIVES OF THE STUDY

The following dissertation considers the positional accuracy of a pulsed surveillance radar utilizing different processing techniques such that comparative evaluation is possible. The primary objectives of the report may be itemized as:

1. Determination of the theoretical positional accuracy of a two-dimensional surveillance radar.

2. Establishment of the influence of different estimation techniques on the azimuth accuracy of a system.
3. Establishment of the influence of target characteristics, system parameters and land clutter on the azimuth accuracy.

1.3 METHOD OF ANALYSIS

The evaluation of the radar performance has been achieved with the aid of simulations. Basically two approaches may be followed in radar simulation:

1. The simulation may be of a functional nature in which the radar outputs are represented by samples of a statistical distribution.
2. The simulation may model the received video signal.

With the functional simulation, details of the actual pulse waveform and processing are not treated explicitly, but rather appear as system losses. The video signal simulation attempts to create a replica of the received radar signal as realistically as possible. The latter technique has been applied in the evaluation of the radar performance in the following investigations.

The accuracy of a video simulation is determined largely by the targets and environmental models applied. An additional limitation to the accuracy of the video simulation is imposed by the finite number of trials performed. These limitations have been minimized by the application of detailed target and clutter models, and the utilization of a large (typically 500) number of trials for each value estimated.

1.4 SUMMARY

Chapter 2 examines the theoretical positional accuracy of an optimal system for both range and azimuth in a thermal noise environment. A generalized approach is described based on the analysis of variance technique which enables the theoretical performance of certain processing methods to be predicted.

Chapter 3 details the practical limitations imposed on the azimuth accuracy of a system. The simulation approach and models applied to evaluate the performance of different processing configurations are described in chapter 4, while chapter 5 outlines the method used to evaluate the different estimators and discusses the simulation results achieved. The azimuth accuracy results are presented in the form of the standard deviation of angle estimates, and for each estimator. Finally, conclusions are drawn in chapter 6.

2.0 THEORETICAL RADAR ACCURACY

2.1 RANGE ACCURACY

The ability of a radar system to measure the time delay between a transmitted signal and reception of the signal in the presence of noise is influenced by

- the signal bandwidth and the spectral density of the received signal
- the receiver response to the receive signal
- the received signal energy relative to the noise spectral density
- the processing technique applied.

The ideal range estimator consists of a matched filter which maximizes the signal- to- noise ratio at the filter output, and a differentiator and zero-crossing detector which enables determination of the instant at which the filter output achieves its peak value. Woodward [53] has shown that for the case of the matched filter, the range accuracy is given by:

$$\sigma_t = 1 / \sqrt{(\beta * E/N_0)} \qquad (2.1\text{-}1)$$

where:

β = rms bandwidth of signal

$$\beta = \left[\frac{\int (2\pi f)^2 \, \| A(f) \|^2 \, df}{\int \| A(f) \|^2 \, df} \right]^{0.5} \qquad (2.1\text{-}2)$$

The expression for range accuracy may also be expressed in terms of a "relative difference slope" K, which in the case of the matched filter is equal to the rms signal bandwidth:

$$\sigma_t = \frac{1}{K_o\sqrt{(2*E/N_o*n)}} \qquad (2.1\text{-}3)$$

Equation (2.1-3) is applicable to single pulse range estimation as well as coherent pulse trains. In practice the receive filter may not be optimally matched to the signal spectrum, resulting in a reduced output signal-to-noise ratio and a reduced error sensitivity K. The reduced signal-to-noise ratio is expressed in a filter mismatch loss factor L_m, yielding:

$$\sigma_t = \frac{1}{K\sqrt{(2*E/N_o*n*L_m)}} \qquad (2.1\text{-}4)$$

Barton [2] states that the error slope may be determined from the rms bandwidths of the filter output signal and the filter characteristic according to:

$$K = \frac{\beta_x^2}{\beta_h^2 * \sqrt{L_m}} \qquad (2.1\text{-}5)$$

where :

β_x is the rms bandwidth of the filter output voltage spectrum

β_h is the rms width of the squared filter transfer function.

For signals containing no intrapulse frequency modulation or coding, simplified error expressions may be obtained, normalized to the pulse width τ_3 :

Matched filter:

$$\frac{\sigma_t}{\tau_3} = \frac{1}{1.63*\sqrt{(2*E/N_o)}} \qquad (2.1\text{-}6)$$

Mismatched filter:

$$\frac{\sigma_t}{\tau_3} = \frac{\beta_h/\beta_x * \sqrt{L_m}}{1.63 * \sqrt{(2*E/N_o)}} \qquad (2.1\text{-}7)$$

The effects of practical signal processing on the range accuracy are generally accounted for by introducing various loss factors. Typically, the use of a detector (envelope or square law) results in a loss due to the discarding of phase information, while the effect of antenna pattern modulation on received signal energy is accounted for with a beamshape loss factor. The normalized range error may then be expressed as [2]:

$$\frac{\sigma_t}{\tau_3} = \frac{\sqrt{(S/N+L_p)}}{K*\tau_3*(S/N)} * \sqrt{\left[\frac{L_p}{2*n*L_m}\right]} \qquad (2.1\text{-}8)$$

where:

L_p is the beamshape loss factor

L_m is the filter mismatch loss.

For pulse compression radars utilizing a uniform spectrum compressed pulse with weighting on the received spectrum to reduce the time sidelobes, an expression for the error normalized to the compressed pulse width is given by:

$$\frac{\sigma_t}{\tau_3} = \frac{1}{K*\tau_{compressed}*\sqrt{(2*E/N_o)}} \qquad (2.1\text{-}9)$$

where:

$\tau_{compressed}$ is the compressed pulse width

K is the error slope (2.1-5).

For a linear chirp pulse the range-doppler coupling effect will cause the output of the matched filter to be displaced in range as a result of a doppler component by an amount:

$$\delta R = \frac{\pm \tau_t * f_d * c}{2 * B_{chirp}} \qquad (2.1\text{-}10)$$

where:

B_{chirp} is the chirp pulse bandwidth

f_d is the doppler content of the received signal

τ_t is the duration of the chirp pulse (the sign depends on the chirp slope).

2.2 AZIMUTH ACCURACY

The measurement of the azimuth position of an object by radar aims to establish the location of the object within the azimuth resolution cell with the smallest error. For a scanning pulsed radar, the estimates of the angle are made by locating the centroid of the received signal envelope. The signal from the receiver is an envelope detected pulse train, modulated by the two-way pattern of the antenna. Theoretically, if the beam pattern were known exactly, and no noise entered the system from any source, the angular position could be determined exactly. In practice, however, the existence of receiver noise, target scintillation and other noise sources limit the achievable accuracy.

Various authors have examined the problem of azimuth estimation in the literature, utilizing both analytical techniques as well as Monte Carlo simulations. In an early work, Bernstein [9] examined the azimuth accuracy of search radars employing a maximum likelihood estimator. Bernstein limited his investigation to rapidly fluctuating targets exhibiting Rayleigh amplitude statistics. In the paper an analytical formulation is made for unquantized and quantized video by deriving the joint probability density function at the receiver output and showing that the problem of ascertaining the target azimuth is equal to estimating the parameter of a stochastic distribution. Bernstein further shows that for search radars an optimum azimuth estimator does not exist. No closed form expression for the azimuth accuracy of the maximum likelihood estimator could be found by Bernstein and quantitive results were obtained by Monte Carlo simulations.

Dinneen and Reed [17] evaluated the azimuth accuracy of a class of beam-splitting estimators employing binary quantized video. Their investigation is limited to the evaluation of a sine wave in additive gaussian noise (as investigated by Rice), and as with the work by Bernstein, no closed form analytical expressions are derived and quantitive results are presented based on Monte Carlo simulations.

In a paper titled 'Maximum Angular Accuracy of a Pulsed Searched Radar' Swerling [45] derives an analytical expression for angular accuracy. In the paper, the lower bound imposed on the accuracy of an azimuth estimate by receiver noise and target fluctuation is analyzed by applying a theorem of statistical estimation cited by H. Cramer [15]. The derivation, which is applicable to unbiased estimators, assumes that the antenna beamwidth is large compared to the angle rotated by the beam between successive pulses, and that the angle step size between pulses is sufficiently small to allow the beam motion between transmission and reception of any given pulse to be neglected. Simplified expressions are presented for the non-fluctuating target applicable to the limiting cases of small-and large midbeam signal-to-noise ratios:

Small signal-to-noise ratios:

$$\sigma_{\min} = \frac{1}{\sqrt{[0.5 * \int f'^2(u)\,du]}} * \frac{\beta}{X_o * \sqrt{N}} \qquad (2.2\text{-}1)$$

Large signal-to-noise ratios:

$$\sigma_{\min} = \frac{2}{\sqrt{\left[\dfrac{\int f'^2(u)}{f(u)}\,du\right]}} * \frac{\beta}{X_o * \sqrt{N}} \qquad (2.2\text{-}2)$$

where:

N is the number of pulses transmitted in a beamwidth of 2β

2β represents the 1/e power beamwidth

X_o represents the midbeam signal-to-noise power ratio f(u) is the two-way power gain pattern of the antenna.

For the fast fluctuating target case, the lower bound on the azimuth estimate is given as:

$$\sigma_{\min} = \frac{1}{\sqrt{0.5 * \dfrac{\int f'^2(u)\,du}{[1 + X_0 f(u)]^2}}} * \frac{\beta}{X_0 * \sqrt{N}} \qquad (2.2\text{-}3)$$

The analysis made by Swerling considers the optimum achievable accuracy for the case where only the amplitude information of the returned pulses after envelope detection is used. In a subsequent paper, Cooper [14] examines the effect on the lower bound of the achievable azimuth accuracy if the pulse amplitudes are quantized into two levels. Cooper concludes that "for many cases of practical interest, the additional limitation in accuracy may be neglected".

Different authors have examined the azimuth accuracy of specific estimators using Monte Carlo simulations:

- Walter, Atkin and Bickel [51] considered the maximum likelihood, end condition and scan density estimators. The end condition estimator detects the presence of a target by scanning binary quantized data for a specific pattern, while the scan density estimator detects a target by establishing whether the density of hits within a specified width exceeds a predetermined level. The paper concludes that the end condition and scan density estimators exhibited shifts in the mean of the estimates as a function of signal-to-noise ratio, and that their performance is inferior to that of the maximum likelihood estimator.

- Hansen [22] considered the performance of the analogue moving window detector for fixed and fast fluctuating targets and a sinx/x antenna pattern.

- Cantrell and Trunk [13] considered a two-pole filter in their simulations. Two techniques for estimating the azimuth position were considered, one which detects the peak signal location and one performs a beam splitting function by comparing the filter output to a fixed threshold. They concluded that the standard deviation of the azimuth estimate is only fifteen percent greater than the lower bound derived by Swerling for the beam-splitting technique, and that the estimator using a maximum value yields a constant mean bias but a 100% worse estimate than the lower bound.

- Galati and Studer [20] considered the binary moving window detector for Swerling target models zero, one and two as well as partially correlated targets assuming a gaussian antenna pattern.
- Accarino and Giaccari [1] considered the application of a dedicated micro processor executing a specific extraction algorithm and showed that the utilization of such a technique could improve the performance of conventional plot extractors.

It has been shown by Barton that the ideal estimator is achieved by sensing the derivative of the response function in the coordinate of interest. Skolnik [42] shows that, under the assumptions of large signal-to-noise ratio, gaussian receiver noise and independence of errors due to different parameters, the rms error of a radar measurement M for the ideal estimator can be expressed as:

$$\delta M = \frac{k*M}{\sqrt{(2*E/N_0)}} \qquad (2.2\text{-}4)$$

where:

E is the received signal energy

N_0 is the power spectral density

k is a measurement factor.

For the case of angular measurement, Skolnik shows that the theoretical accuracy is dependant on an effective antenna aperture width γ and a signal energy to noise spectral density R according to:

$$\sigma_\theta = \frac{1}{\gamma/\lambda * \sqrt{R}} \tag{2.2-5}$$

where:

λ is the wavelength of the radiated signal

γ is the effective antenna aperture width.

Barton [2] applies a normalizing constant L_s in his equation for rms angular error:

$$\sigma_\theta = \frac{1}{L_s/\lambda * \sqrt{R}} \tag{2.2-6}$$

Comparison with the equation given by Skolnik shows that the normalizing constant L_s is in effect the effective antenna aperture width. Barton further considers the impact of losses, mismatching and signal processing on the rms angular accuracy. For coherent pulse integration, and taking into account an antenna pattern scanning loss, the normalized rms angular error is expressed by:

$$\frac{\sigma_\theta}{\theta_3} = \frac{\sqrt{L_p}}{K_p * \sqrt{(2 * n * E/N_o * L_m)}} \tag{2.2-7}$$

Non-coherent integration is considered by introducing a detector loss, yielding:

$$\frac{\sigma_\theta}{\theta_3} = \frac{\sqrt{(E/N_o + L_p)}}{K_p * E/N_o} * \frac{\sqrt{L_p}}{\sqrt{(2 * n)}} \tag{2.2-8}$$

where:

K_p is the antenna slope factor

L_p is the two-way antenna scanning loss

n is the number of pulses integrated

L_m is the matching loss in the receiver

E/N_0 is the signal-to-noise ratio at the beam center.

For the event of a gaussian beam (two-way) and no mismatching loss, Barton shows that the rms accuracy will be approximately

$$\frac{\sigma_\theta}{\theta_3} = \frac{0.565}{S/N\sqrt{n}} \qquad n > 1 \qquad (2.2\text{-}9)$$

for the case of non-coherent integration assuming a small signal-to-noise ratio. For coherent pulse integration, Barton shows an azimuth accuracy:

$$\frac{\sigma_\theta}{\theta_3} = \frac{0.490}{\sqrt{(S/N*n)}} \qquad n > 1 \qquad (2.2\text{-}10)$$

Swerling shows that the optimum angular accuracy for a gaussian antenna pattern is approximately

$$\frac{\sigma_\theta}{\theta_3} = \frac{0.58}{S/N\sqrt{n}} \qquad (2.2\text{-}11)$$

assuming a small signal-to-noise ratio and non-coherent pulse integration. Generally, the accuracy limitation due to thermal noise is approximated by [6]

$$\frac{\sigma_\theta}{\theta_3} = \frac{\theta_3}{10} \qquad (2.2\text{-}12)$$

assuming a reasonable signal-to-noise ratio for target detection.

2.3 GENERALIZED ACCURACY

The analytical evaluation of estimate accuracies often requires certain assumptions to be made regarding the scattering object characteristics in order to achieve some tractable form of expression. More often than not, however, the analytical expressions derived are very complex and not easily computed. In 1958, C. M. Walter [50] published a paper intended to "derive a reasonably simple method of evaluating and optimizing the performance of a wide class of target detection and position estimation type data processing schemes". The approach taken by Walter to estimate the azimuth accuracy is based on the analysis of variance technique. This approach requires knowledge of the first order (mean) and second order (variance) moments of the multi-variate probability distribution describing the target as observed by the radar. In the paper, Walter considers the class of unbiased estimators based on a single threshold examination of integrated pulse amplitudes (figure 2.3-1).

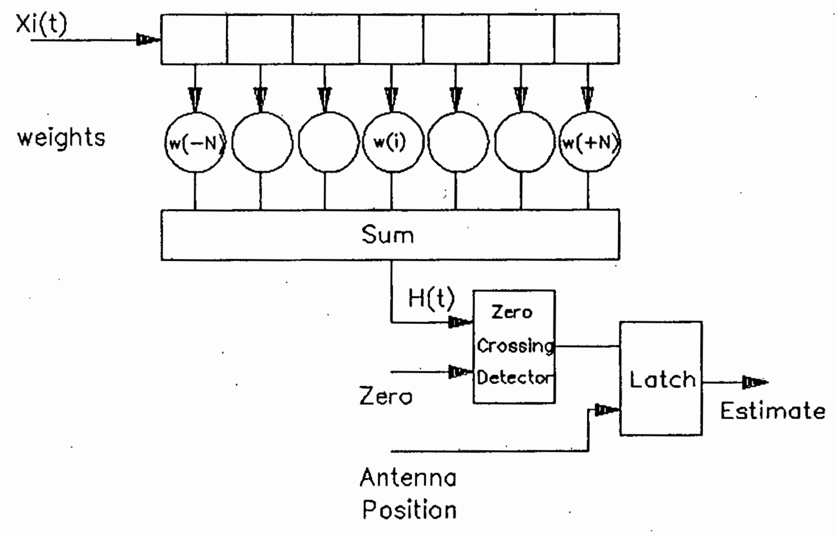

Figure 2.3-1: Unbiased estimator

$$H(\tau) = \sum_{i=-N}^{i=+N} w_i(\tau_0) * x_i(\tau) \qquad (2.3\text{-}1)$$

where:

τ is the generalized azimuthal coordinate

$w_i(\tau_0)$ is the weight applied to the i th pulse

$x_i(\tau)$ is the signal amplitude of the i th received pulse. The sequence of pulse amplitudes $\{x_{-N}(\tau),..,x_0(\tau),..,x_{+N}(\tau)\}$ is representative of the returned signal amplitudes for a beam pointing angle τ.

In the event of a symmetrical antenna pattern and odd-symmetrical weights the true target position is represented by the azimuth coordinate at which the response function (2.3-1) is zero.

Applying a Taylor series expansion to the response function (2.3-1), and neglecting any higher order terms, Walter shows that the minimum estimate variance for an unbiased estimator is given by:

$$\sigma_\tau{}^2 = \frac{\sigma_{H(\tau)}{}^2}{\left[\dfrac{\partial <H(\tau)>}{\partial \tau} \right]^2_{\tau=\tau_0}} \qquad (2.3\text{-}2)$$

where:

$$H(\tau) = \sum_{i=-N}^{i=+N} w_i(\tau_0) * x_i(\tau) \qquad (2.3\text{-}3)$$

$$\sigma_{H(\tau)}{}^2 = \sum_{i=-N}^{i=+N} w_i{}^2(\tau) * \sigma_{x(\tau)}{}^2 \qquad (2.3\text{-}4)$$

$$\sum_{i=-N}^{i=+N} w_i(\tau) * \partial/\partial\tau[\, x_i(\tau)]_{\tau=\tau_0} = \left[\frac{\partial <H(\tau)>}{\partial \tau} \right]_{\tau=\tau_0} \qquad (2.3\text{-}5)$$

The expression for the minimum estimate variance as derived by Walter agrees with the measure of error noted by Skolnik [42] as "the ratio of the rms noise voltage to the slope of the response function evaluated at the threshold crossing".

Application of the expression as derived by Walter allows the minimum estimate variance to be derived if the statistics of the received signal amplitudes are known. Using the statistics derived by Bernstein [9] to describe the amplitudes of the received signal after envelope detection

$$f(x) = \frac{x/\sigma_n^2}{1+K_m^2 * g_i^4} * \exp\left[\frac{(x/\sigma_n)^2}{1+K_m^2 * g_i^4} \right] \qquad (2.3\text{-}6)$$

it can be shown that the first and second order moments of the returned signal amplitudes will be [31]:

$$<x> = \sigma_x * \sqrt{(\pi/2)} * \sqrt{(1+K_m^2 * g_i^4)} \qquad (2.3\text{-}7)$$

$$\sigma_x^2 = \frac{(4-\pi)}{2} * \sigma_x^2 * (1+K_m^2 * g_i^4) \qquad (2.3\text{-}8)$$

where:

K_m is the voltage signal-to-noise ratio on the beam axis

g_i is the normalized one-way voltage gain

$<x>$ is the mean video signal amplitude, σ_x is the standard deviation.

Assuming a one-way antenna voltage pattern g_i of

$$g_i = \frac{\sin(i * \pi/N)}{(i * \pi/N)} \qquad (2.3\text{-}9)$$

the minimum angular estimate standard deviation may be expressed as (assuming unity rms noise):

$$\sigma_T = \frac{\sum_{i=-N}^{i=+N} \left\{ w_i^2 * \frac{(4-\pi)}{2} * \left[k_m^2 \frac{\sin^4(i*\pi/N)}{(i*p/N)^4} + 1\right] \right\}^{0.5}}{\sum_{i=-N}^{i=+N} w_i * \sqrt{(\pi/2)} \; \frac{2*k_m^2}{\sin^4(i*p/N) \sqrt{\left[k_m^2 \frac{\sin^4(i*\pi/N)}{(i*\pi/N)^4} + 1\right]}} * \frac{\sin^4(i*\pi/N)}{(i*\pi/N)^4} \left\{ \frac{\cos(i*\pi/N)}{\sin(i*\pi/N)} \quad \frac{1}{i*\pi/N)} \right\}} \tag{2.3-10}$$

The assumption of an antenna pattern given by equation (2.3-9) implies a null-to-null beamwidth of 360 degrees, and a two-way power gain pattern -3 dB beamwidth of 120 degrees.

The performance of unbiased estimators for the above case can now be determined assuming different weighting functions. Figures 2.3-3 through 2.3-5 illustrate the normalized estimate standard deviation for

a. pseudo-centre of gravity weights

$w_i = i/N \qquad -N <= i <= +N$

b. rectangular weights

$w_i = -1 \qquad -N <= i < 0$

$w_i = +1 \qquad 0 < i <= +N$

$w_i = 0 \qquad i = 0$

c. optimum weights for a maximum likelihood estimator as calculated by Bernstein [9]

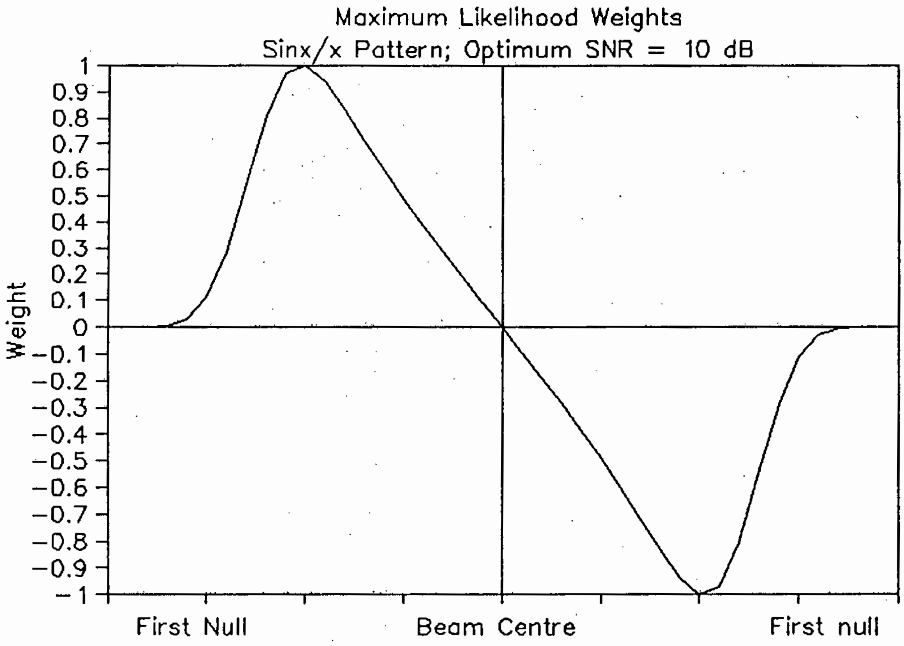

Figure 2.3-2: Maximum likelihood weights

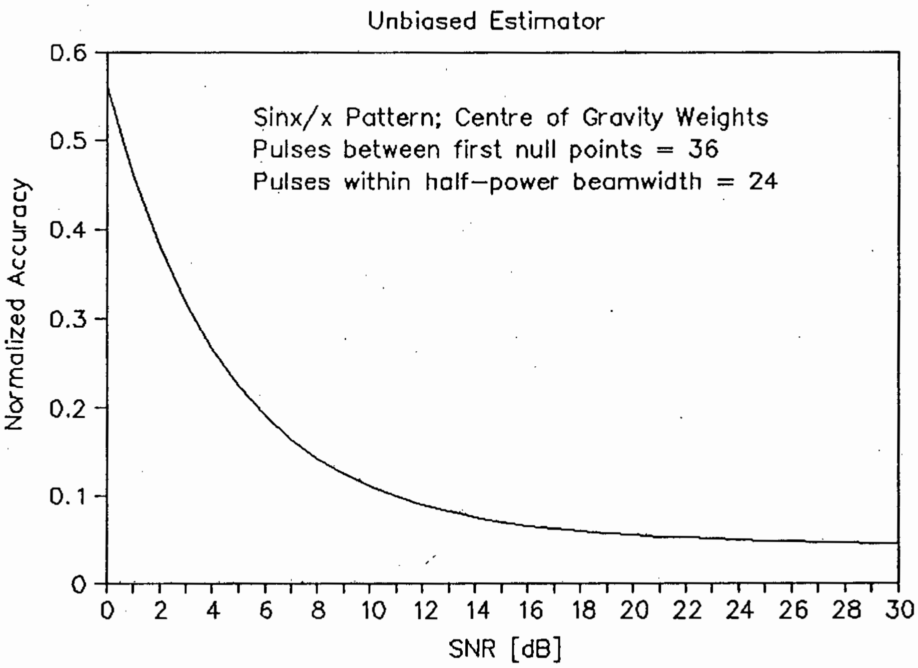

Figure 2.3-3: Azimuth accuracy with centre-of-gravity weights

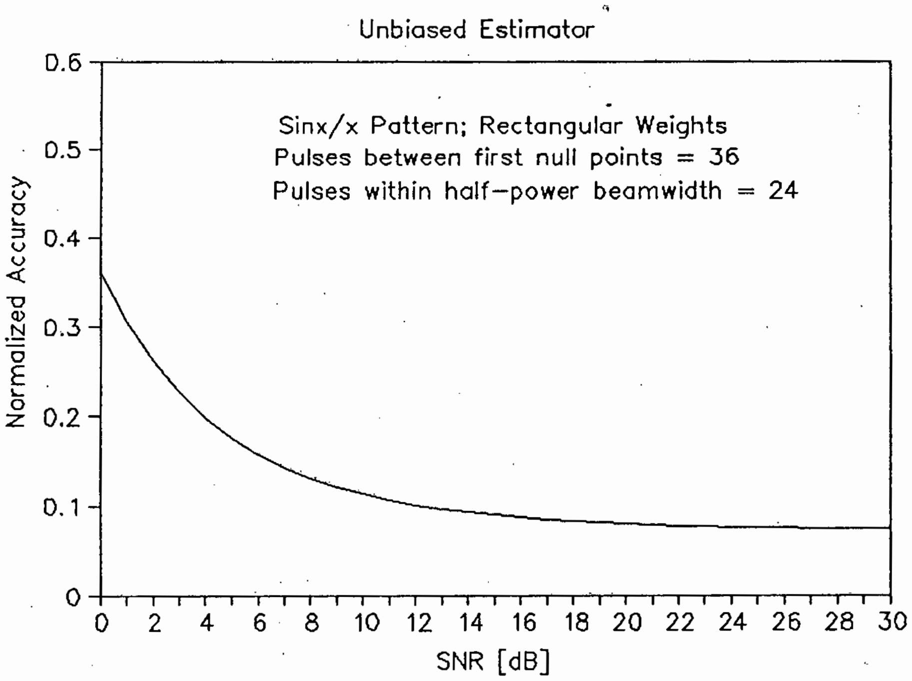

Figure 2.3-4: Azimuth accuracy with rectangular weights

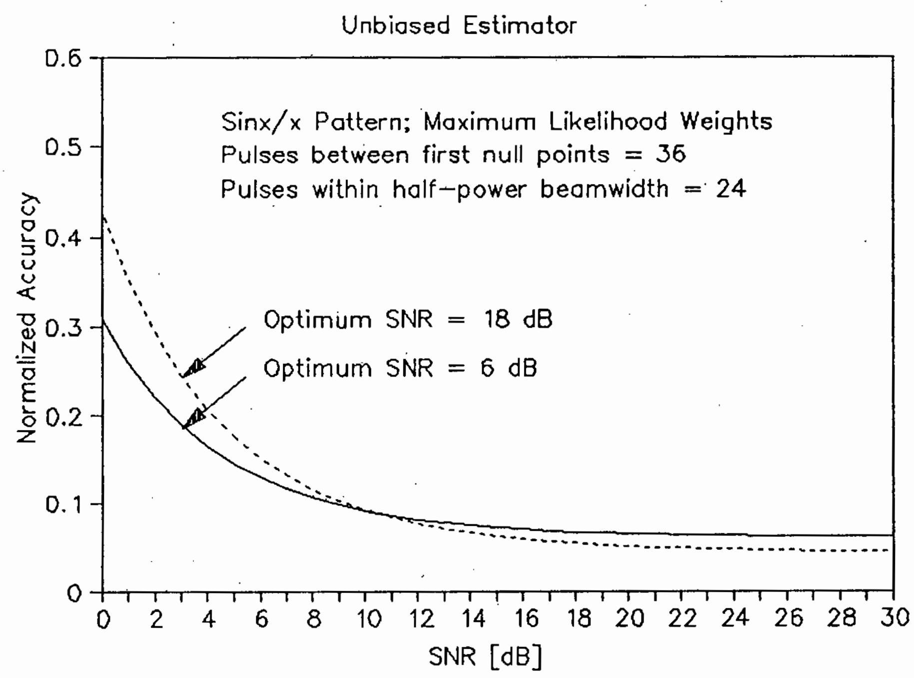

Figure 2.3-5: Azimuth accuracy with maximum likelihood weights

In order to facilitate comparison of the estimate minimum standard deviation for a sin x/x pattern with that achievable with a gaussian pattern, a gaussian one-way voltage gain pattern is defined of the form:

$$g_i = \exp[-c*(i*\pi/N)^2] \qquad (2.3\text{-}11)$$

This pattern must yield the same -3 dB two-way power gain beamwidth as the sin x/x pattern, resulting in:

$$g_i = \exp[-0.158*(i*\pi/N)^2] \qquad (2.3\text{-}12)$$

The minimum estimate standard deviation applying the statistics derived by Bernstein can then be written as:

(2.3-13)

$$\sigma_s = \frac{\sum\limits_{i=-N}^{i=+N} \{ w_i^2 * \frac{(4-\pi)}{2} * [k_m^2 \exp(-0.632*(i*\pi/N)^2 + 1] \}^{0.5}}{\sum\limits_{i=-N}^{i=+N} w_i * \sqrt{(\pi/2)} \frac{2*k_m^2}{\sqrt{[k_m^2 \exp(-0.632*(i*\pi/N)^2 + 1]}} * -0.632 \exp(-0.632*(i*\pi/N)^2 + 1]\}^{0.5}}$$

Figures 2.3-7 through 2.3-9 illustrate the normalized accuracy assuming the centre-of-gravity, rectangular and maximum likelihood weights.

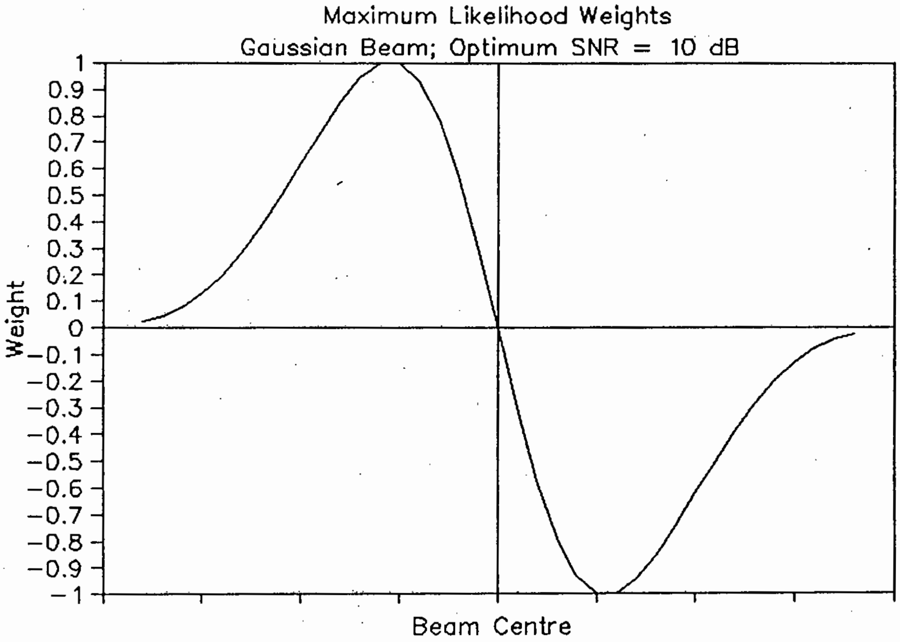

Figure 2.3-6: Maximum likelihood weights

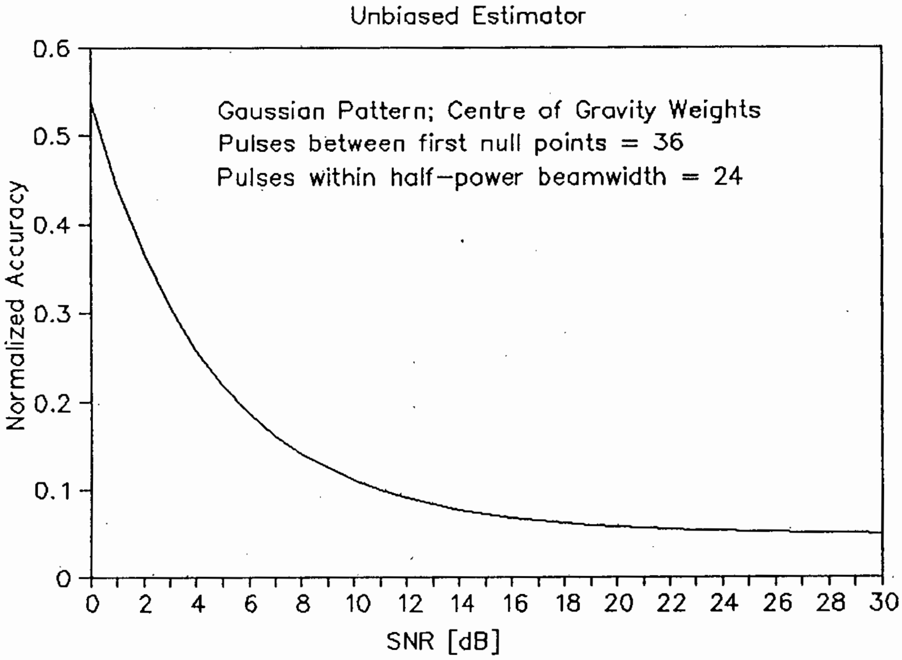

Figure 2.3-7: Azimuth accuracy with centre-of-gravity weights

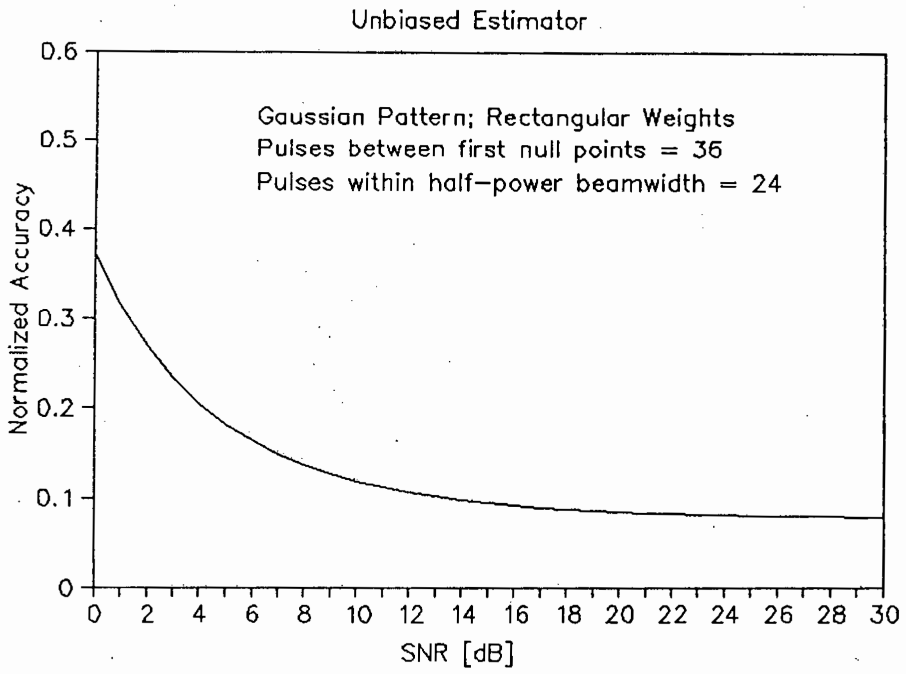

Figure 2.3-8: Azimuth accuracy with rectangular weights

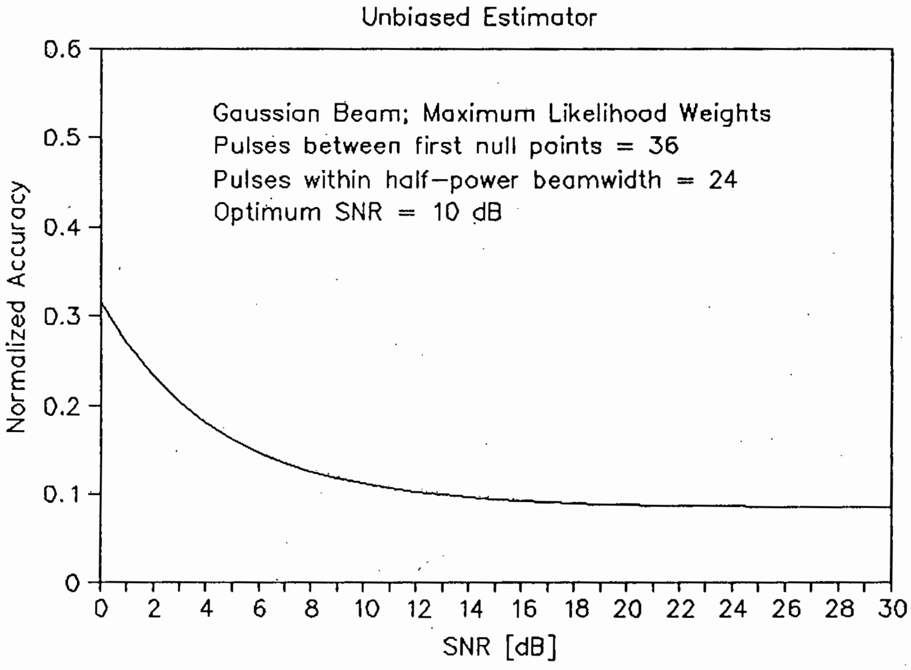

Figure 2.3-9: Azimuth accuracy with maximum likelihood weights

In the event of the gaussian pattern, the maximum likelihood weights are given by:

(2.3-14)

$$w_i = \frac{2*\tau^2*k_m^2*(-0.316)*(i*\pi/N)*\exp\{-0.632*(i*\pi/N)^2\}}{[1+k_m^2*\exp\{-0.632*(i*\pi/N)^2\}] * [1-\exp\{\frac{-\tau^2/2}{1+k_m^2*\exp\{-0.632*(i*\pi/N)^2\}}\}]}$$

In the statistics derivation, Bernstein assumed a fast fluctuating target in gaussian noise. For the non-fluctuating case, the voltage output of an envelope detector is given by [30]:

(2.3-15)

$$f(x) = \exp\left[\frac{-(x^2+A^2)}{2*\sigma_n^2}\right] * I_0\left[\frac{Ax}{\sigma_n^2}\right] * \frac{x}{2\sigma_n^2}$$

where:

σ_n is the rms noise component

A is the peak signal amplitude

$I_0(.)$ is a zero-order Bessel function of the first kind.

Skolnik [42] relates the signal amplitude and rms noise component to the power signal-to-noise ratio according to:

(2.3-16)

$$\frac{A}{\sigma_n} = \frac{\text{signal amplitude}}{\text{rms noise voltage}} = \frac{\sqrt{2}*(\text{rms signal voltage})}{\text{rms noise voltage}}$$

$$= \sqrt{(2*S/N)}$$

The statistics for the envelope detected signal may be derived as [40]:

(2.3-17)

$$<x> = \sigma_n*\sqrt{(\pi/2)}*\exp(-\frac{A^2}{4\sigma_n^2})*[(1+\frac{A^2}{2\sigma_n^2})*Io(\frac{A^2}{4\sigma_n^2})+\frac{A^2}{2\sigma_n^2}*I1(\frac{A^2}{4\sigma_n^2})]$$

$$<x^2> = 2*\sigma_n^2*(1+\frac{A^2}{2\sigma_n^2}) \qquad (2.3\text{-}18)$$

where:

$<x>$ represents the mean signal amplitude

$<x^2>$ represents the mean of the squared amplitude.

In terms of power signal-to-noise ratio, the statistics may be re-written as:

(2.3-19)

$$<x> = \sigma_n*\sqrt{(\pi/2)}*\exp(-\frac{S/N}{2})*[(1+S/N)*I_0(\frac{S/N}{2})+S/N*I_1(\frac{S/N}{2})]$$

$$<x^2> = 2*\sigma_n^2*(1+S/N) \qquad (2.3\text{-}20)$$

$$\sigma_x^2 = <x^2> - <x>^2 \qquad (2.3\text{-}21)$$

Assuming a sin x/x one-way voltage beam pattern (2.3-9), the single pulse signal-to-noise ratio may be written as:

$$S/N_i = k_m^2 \frac{\sin^4(i * \pi/N)}{(i * \pi/N)^4} \qquad (2.3\text{-}22)$$

In order to evaluate the minimum standard deviation of the azimuth estimate for the non-fluctuating case, the quantities $[\sigma_{H(s)}]^2$ (2.3-4) and $\partial H(\tau)/\partial(\tau)$ (2.3-5) need to be calculated. Application of the statistics for the non-fluctuating case yields the following expressions:

$$(2.3\text{-}23)$$

$$\frac{\partial \langle x(\tau) \rangle}{\partial(\tau)} = 4\sqrt{(2\pi)} * S/N * \left[\frac{\cos(i * \pi/N)}{\sin(i * \pi/N)} - \frac{1}{(i * \pi/N)}\right] * \exp\left(\frac{S/N}{2}\right) *$$

$$\left[I_0\left(\frac{S/N}{2}\right) - I_1\left(\frac{S/N}{2}\right) - 2S/N * I_1\left(\frac{S/N}{2}\right) \right]$$

$$(2.3\text{-}24)$$

$$\sigma_x^2 = 2 * [1 + S/N] - (\pi/2) * \exp(-S/N) *$$

$$\left[(1 + S/N) * I_0\left(\frac{S/N}{2}\right) + S/N * I_1\left(\frac{S/N}{2}\right) \right]^2$$

Evaluation of expressions (2.3-23) and (2.3-24) require the zero- and first order Bessel functions to be calculated. This may be achieved by approximating the Bessel function with a power series [28]:

$$I_0(x) = 1 - \frac{x^2}{2^2(1!)^2} + \frac{x^4}{2^4(2!)^2} - \frac{x^6}{2^6(3!)^2} + \ldots \qquad (2.3\text{-}25)$$

$$I_1(x) = \frac{x}{2} - \frac{x^3}{2^3 * 2! * 1!} + \frac{x^5}{2^5 * 3! * 2!} - \frac{x^7}{2^7 * 4! * 3!} + \ldots \qquad (2.3\text{-}26)$$

For large x, the number of terms required in the power series for a reasonable accuracy becomes prohibitive, and the Bessel functions may then be approximated by:

$$I_0(x) = 1/\sqrt{(\pi x)} * [\cos(x) + \sin(x)] \qquad (2.3\text{-}27)$$

$$I_1(x) = -1/\sqrt{(\pi x)} * [\cos(x) - \sin(x)] \qquad (2.3\text{-}28)$$

The correlation behaviour of a scattering object is of particular importance in the evaluation of the accuracy performance of an estimator. Standard radar texts calculate the limiting cases of no correlation i.e. pulse-to-pulse independent fluctuation, and complete correlation between pulses. The effects of a partially correlated scattering object are obtained by interpolation between the limiting cases. Application of the analysis of variance technique permits the effect of partial correlation to be calculated. Assuming an exponential correlation of the form:

$$\rho(\tau) = \exp(-\gamma * \|\tau\|) \qquad (2.3\text{-}29)$$

where:

$$\gamma = 2 * \pi * B_0 * T_{prf} \qquad (2.3\text{-}30)$$

B_0 is the scintillation bandwidth

T_{prf} is the transmit pulse period.

Walter shows that the normalized correlation coefficient for a partially correlated scattering object in gaussian noise is given by:

$$\rho_{\alpha\beta} = \frac{k_m^2 * g_\alpha^2 * g_\beta^2 * \rho(\|\alpha - \beta\|)}{(k_m^2 g_\alpha^2 + 1) * (k_m^2 g_\beta^2 + 1)} \qquad (a \neq b) \qquad (2.3\text{-}31)$$

$$\rho_{\alpha\beta} = 1 \qquad (a = b)$$

where:

k_m is the axial signal-to-noise voltage ratio

g_α, g_β are normalized one-way antenna power gain patterns; $g_0 = 1$

$\rho_{\alpha\beta}$ is the normalized correlation coefficient between consecutive pulses amplitudes x_α and x_β

$\rho(\|\alpha - \beta\|)$ is the correlation function for a target, with α and β defining the video pulse indices.

The output probability density function is still assumed to be Rayleigh distributed, but with the samples being correlated. It has been shown [49] that the variance of the response function is given by:

$$H(\tau) = \sum_{i=-N}^{i=+N} w_i * x_i \qquad (2.3\text{-}32)$$

$$\sigma_{H(\tau)}^2 = \sum_{i=-N}^{i=+N} w_i^2 (k_m^2 g_i^2 + 1) + \left[\sum_{\alpha=-N}^{\alpha=+N} \sum_{\beta=-N}^{\beta=-\alpha-1} w_\beta \, w_{\beta-(N+\alpha-1)} \, \sigma_\beta \, r_{\beta-(N+\alpha-1)} \, \rho_{\beta,(N+\alpha-1)}\right] * 2 \qquad (2.3\text{-}33)$$

where:

$$\sigma_k = (k_m^2 g_k^4 + 1)^{0.5} \qquad (2.3\text{-}34)$$

N represents the number of pulses within the null-to-null beamwidth

ρ is the normalized correlation coefficient representing the degree of correlation between consecutive pulses.

Assuming a sin x/x pattern, Walter calculated the azimuth standard deviation for different values of γ. Barton [2] establishes the normalized azimuth estimate standard deviation for a gaussian antenna pattern and a weighting function which is the derivative of the two-way signal envelope. Barton further defines a parameter $n_e - 1$ defined as the number of independent samples. A correspondence between the parameter γ used by Walter, and $(n_e - 1)$ used by Barton is given by [20]:

$$(n_e - 1) = t_o/t_c = (n/2)^{*}\gamma \qquad (2.3\text{-}35)$$

where:

t_o is the observation time of the radar i.e. the time during which the detected object is within the radar beam

t_c represents the correlation time of the scattering object

$t_c = 1/(\pi B_o)$

B_o is the scintillation half-power beamwidth

n represents the number of pulses within the half-power beamwidth.

Figure 2.3-10 illustrates the normalized azimuth estimate as a function of the scintillation bandwidth for a sin x/x antenna pattern and maximum likelihood weights.

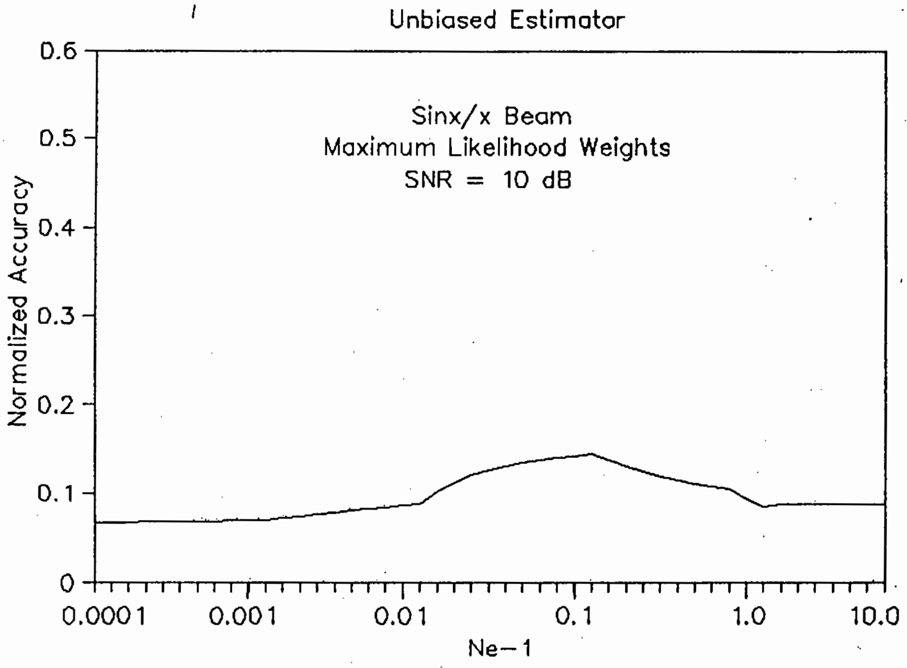

Figure 2.3-10: Azimuth accuracy for a partially correlated scatterer

3.0 AZIMUTH ACCURACY LIMITATIONS

3.1 CLUTTER AND INTERFERENCE

The general expression for noise induced error in an arbitrary coordinate z is given by Barton [2] as:

$$\sigma_z = \frac{\sqrt{\eta}}{k_z\sqrt{(2*S/N*n)}} \qquad (3.1\text{-}1)$$

where:

k_z is the relative difference slope in the z-coordinate

η is the relative efficiency factor relating the actual S/N ratio received in the measurement channel to the ideal S/N ratio.

Analogous to the noise induced error, a signal-to-interference ratio S/I can be utilized to express the error caused by interference as:

$$\sigma_z = \frac{\sqrt{\eta}}{k_z\sqrt{(2*S/I*n_e)}} \qquad (3.1\text{-}2)$$

where:

n_e is the number of independent samples integrated

S/I represents the ratio of signal power to interference power.

For a search radar, the equation may be expressed as:

$$\sigma_z = \frac{z_3}{(k_p/\sqrt{L_p})*\sqrt{(2*S/I*n_e)}} \qquad (3.1\text{-}3)$$

where:

k_p is the antenna pattern slope factor

L_p is the antenna pattern loss factor to account for the non-ideal antenna pattern.

A point source of interference with a small displacement from the actual scattering object may introduce an error given by [6]:

$$\sigma_z = \frac{\|z_i\|}{\sqrt{(2 * S/I * n_e)}} \qquad (3.1\text{-}4)$$

Clutter return in general will exhibit the characteristics of a distributed target return, and will practically always follow a Rayleigh amplitude distribution within a resolution cell. Such distributed clutter will introduce an azimuth error according to:

$$\sigma_a = \frac{\theta_3}{(k_p/\sqrt{L_p}) * \sqrt{(2 * S/I * n_e)}} \qquad (3.1\text{-}5)$$

where:

θ_3 is the half-power beamwidth.

In order to calculate the magnitude of the error for land clutter, the signal-to-interference ratio must be evaluated. The equivalent land clutter radar cross-section may be expressed as:

$$\sigma_c = \sigma^o A_c \qquad (3.1\text{-}6)$$

where:

$$\sigma^o = 0.00032/\lambda \qquad (3.1\text{-}7)$$

A_c represents the clutter reflecting area.

Blake [11] has shown that the area of intersection for surface clutter is determined by the radar resolution cell and the grazing angle ψ:

$$\psi = \sin^{-1}\left(\frac{2a_e h_1 + h_1^2 - R_1^2}{2a_e R_1}\right) \qquad (3.1\text{-}8)$$

where:

h_1 is the height of the antenna above the ground

a_e represents the earth radius

R_1 is the slant range from the radar to the point of intersection with the land clutter.

For high grazing angles, the illuminated area is approximated by

$$A_c = \pi/4 * R_c^2 * h_a * h_e * \csc(\psi) \qquad (3.1\text{-}9)$$

while for low grazing angles, the approximate expression is given by:

$$A_c = R_c * h_a * c * \tau/2 * \csc(\psi) \qquad (3.1\text{-}10)$$

where:

R_c is the slant range to the clutter cell

h_a is the half-power beamwidth in azimuth

h_e is the half-power beamwidth in elevation

τ is the pulse length.

The signal-to-interference ratio may thus be derived using the range equation:

$$\frac{P_r}{P_c} = \frac{G_t G_r \sigma}{G_{tc} G_{rc} \sigma_c} \qquad (3.1\text{-}11)$$

where:

G_t represents the transmit gain of the antenna in the direction of the detected object

G_{tc} represents the transmit gain of the antenna in the direction of the clutter source

G_r represents the receive gain of the antenna in the direction of the detected object

G_{rc} represents the receive gain of the antenna in the direction of the clutter source.

The above equation expresses the antenna transmit- and receive gains as separate entities for the returned signal and clutter power to account for the fact that the scattering object and the clutter are not necessarily at the same altitude. The resultant azimuth error due to clutter interference may thus be derived using equations (3.1-5) and (3.1-11):

$$\sigma_a = \frac{\theta_3}{(k_p/\sqrt{L_p}) * \left[2 * \dfrac{G_t G_r \sigma}{G_{tc} G_{rc} \sigma_c} * n_e\right]^{0.5}} \qquad (3.1\text{-}12)$$

Practical systems will employ clutter reduction techniques in order to improve detection in clutter areas. The improvement in angular accuracy as a result of this may be derived by multiplying the signal-to-interference ratio with an improvement factor in equation (3.1-12)

3.2 MULTIPATH ERROR

A multipath error may be introduced into a radar measurement if a reflected signal from a scattering object traverses to the radar via multiple paths of different length. The majority of reflections in radar are due to surface reflections, and these reflections affect measurement in all four radar coordinates. In the elevation coordinate, surface reflections result in lobing of the antenna pattern in the vertical plane. The lobing results from an inter-action between the direct- and reflected path signals. Detection calculations utilize the two-way propagation factor to predict the signal strength at the radar. The returned signal at the radar is a composite result of four effects:

a. a direct path for transmission and reception

b. a direct transmit path and reflected receive path

c. a reflected transmit path and direct receive path

d. a reflected transmit and reflected receive path

In the analysis of angular multipath errors, Barton [5] states that only the return path to the radar is significant as the transmit path affects only the amplitude and phase of the signal reflected from the object.

Reflections from a surface are characterized by a reflection coefficient which defines the fraction of an incident wave which is reflected. Smooth surfaces exhibit a specular reflection characteristic. The reflection coefficient is given by:

$$\rho = \rho_o \, \rho_s \qquad (3.2\text{-}1)$$

where:

ρ_o is the Fresnel reflection coefficient

ρ_s is the scattering factor accounting for surface irregularities.

$$\rho_s = \exp\left[-\left\{\frac{4\pi * \sigma_h \sin(\psi)}{\lambda}\right\}^2\right] \qquad (3.2\text{-}2)$$

where:

σ_h is the rms height variation of the surface.

The specular nature of the reflections changes with grazing angle for a particular surface rms height variation and radar wavelength. Generally, the specular scattering changes to diffuse scattering when the grazing angle exceeds twice a critical angle given by [3]:

$$\psi_c = \sin^{-1}\left(\frac{0.665*\lambda}{\sigma_h}\right) \qquad (3.2\text{-}3)$$

The diffuse scattering will cause the resultant signal to vary rapidly about its free-space value, but will add little to the average signal power.

The effect of specular reflections on the azimuth accuracy may be evaluated by considering the propagation factor, similar to the detection analysis in elevation multipath. The amplitude and phase of the received signals are affected by:

a. the magnitude of the reflection coefficient

b. the magnitude of the antenna pattern factor at the angle of the ray

c. a cross-section difference of the scattering object due to different aspect angles

d. a phase shift introduced by the path length

e. a phase shift introduced as a result of the reflection

f. a possible phase difference of the pattern factors for the direct and reflected rays.

Two scenarios may be identified in the consideration of specular reflection azimuth multipath errors:

a. The path difference between the direct and reflected rays is less than a range resolution cell. This scenario will result in the direct and reflected signals combining at the antenna, identical to the case of elevation multipath (figure 3.2-1).

b. The path difference between the direct and reflected rays exceeds a range resolution cell. The returns from the reflected paths appear in a different range cell to those from the direct path. The direct path propagation will yield a peak signal when the nose of the antenna beam is pointing at the scatterer. However, the reflected signal from the indirect path will yield a peak in the angular region between the scattering surface and the scattering object. Depending on the range separation between these two returns and the rules applied in the plot estimation algorithms in the data processor, the signal returns may be used to form a single plot, with a consequent angular error (figure 3.2-2).

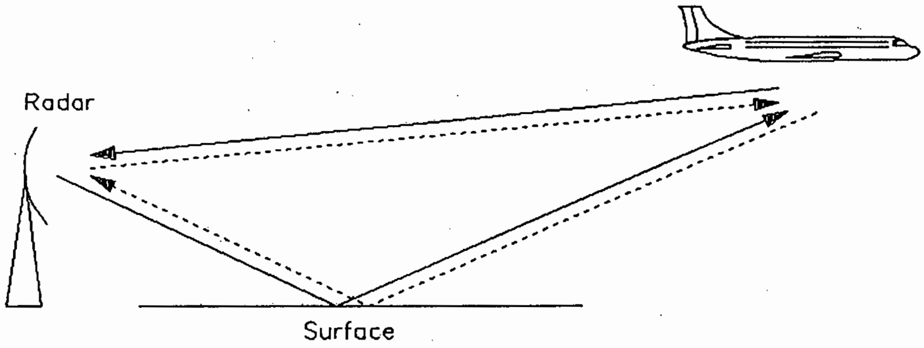

Figure 3.2-1: Path difference less than a resolution cell

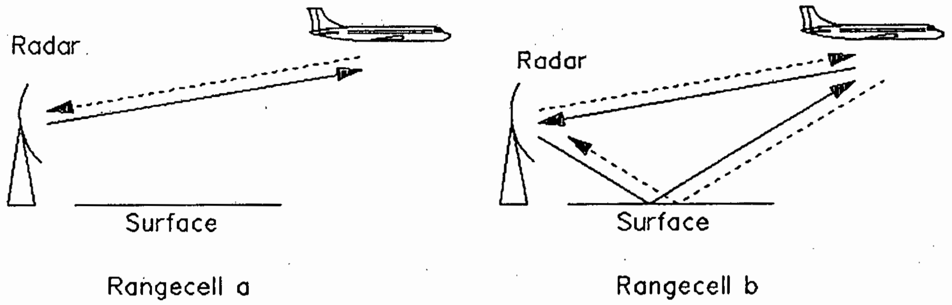

Figure 3.2-2: Path difference larger than a resolution cell

The electric field intensity at the radar due to the direct ray may be expressed as:

$$E_d = f(\theta_d) * E_o \qquad (3.2\text{-}4)$$

where:

E_o is the free-space electric field intensity experienced at the radar as a result of the reflected signal from the scattering object.

$f(\theta_d)$ is the antenna pattern factor at angle θ_d

The electric field intensity at the radar due to a reflected ray is given by:

$$E_r = \rho * E_o * f(\theta_r) * \exp(-j\alpha) \qquad (3.2\text{-}5)$$

where:

ρ is the reflection coefficient

α is the phase shift introduced due to the reflection, additional path length and possible phase difference in antenna pattern factor at angles θ_d and θ_r .

The total electric field intensity at the radar receiver may be expressed as the sum of the direct and reflected intensities:

$$E = E_d + E_r$$

$$= E_o[\ f(\theta_d) + \rho * f(\theta_r) * \exp(-j\alpha)\ ] \qquad (3.2\text{-}6)$$

Following the derivations made by Blake [11], the propagation factor may be expressed as:

$$F = \|[\ f(\theta_d) + \rho * f(\theta_r) * \exp(-j\alpha)\ ]\|$$

$$= \|f(\theta_d)\| * \sqrt{[1 + x^2 + 2*x*\cos(\alpha)]} \qquad (3.2\text{-}7)$$

where:

$$x = \rho * f(\theta_r)/f(\theta_d) \qquad (3.2\text{-}8)$$

$$\alpha = 2\pi * \delta R/\lambda + \phi + (\beta_r - \beta_d) \qquad (3.2\text{-}9)$$

δR is the path length difference

β_r-β_d is the phase difference introduced by the antenna between the direct and reflected rays

ϕ is the phase shift introduced by the reflection.

The path length difference δR may be derived from geometry (Appendix A) as:

$$\delta R = \sqrt{[\ \{\|R\sin(\theta_o)\| + 2R_c\}^2 + \|R\cos(\theta_o)\|^2\ ]} - R \qquad (3.2\text{-}10)$$

where:

R is the slant range between the radar and the detected object

R_c is the offset between the radar and the reflecting surface

θ_o is the angle of the detected object relative to the scattering surface (Appendix A).

Assuming a sin x/x antenna pattern with a nose pointing angle θ_i, the pattern for the direct path will yield an antenna pattern factor

$$f_d(\theta_i) = \frac{\sin(\theta_i - \theta_o)}{(\theta_i - \theta_o)} \qquad (3.2\text{-}11)$$

while the reflected path will yield:

$$f_r(\theta_i) = \frac{\sin(\theta_i - \theta_r)}{(\theta_i - \theta_r)} \qquad (3.2\text{-}12)$$

where:

θ_o is the angle of the detected object relative to the scattering surface (Appendix A).

For the scenario where the path length difference exceeds a range resolution cell, the direct ray will exhibit an antenna modulation of the received pulse train according to (3.2-11), with the peak of the pulse train modulation occurring when the nose of the beam coincides with the scattering object. In a different range ring, the pulse train amplitude will be modulated by the composite propagation factor (3.2-12). Figure 3.2-3 illustrates the expected pulse train modulations in the direct- and composite returns assuming that the reflecting surface is offset at an angle 32 degrees from the scattering object and that the reflection introduces a 180 degrees phase shift.

Assuming a sin x/x antenna pattern with a nose pointing angle θ_i, the pattern for the direct path will yield an antenna pattern factor

$$f_d(\theta_i) = \frac{\sin(\theta_i - \theta_o)}{(\theta_i - \theta_o)} \qquad (3.2\text{-}11)$$

while the reflected path will yield:

$$f_r(\theta_i) = \frac{\sin(\theta_i - \theta_r)}{(\theta_i - \theta_r)} \qquad (3.2\text{-}12)$$

where:

θ_o is the angle of the detected object relative to the scattering surface (Appendix A).

For the scenario where the path length difference exceeds a range resolution cell, the direct ray will exhibit an antenna modulation of the received pulse train according to (3.2-11), with the peak of the pulse train modulation occurring when the nose of the beam coincides with the scattering object. In a different range ring, the pulse train amplitude will be modulated by the composite propagation factor (3.2-12). Figure 3.2-3 illustrates the expected pulse train modulations in the direct- and composite returns assuming that the reflecting surface is offset at an angle 32 degrees from the scattering object and that the reflection introduces a 180 degrees phase shift.

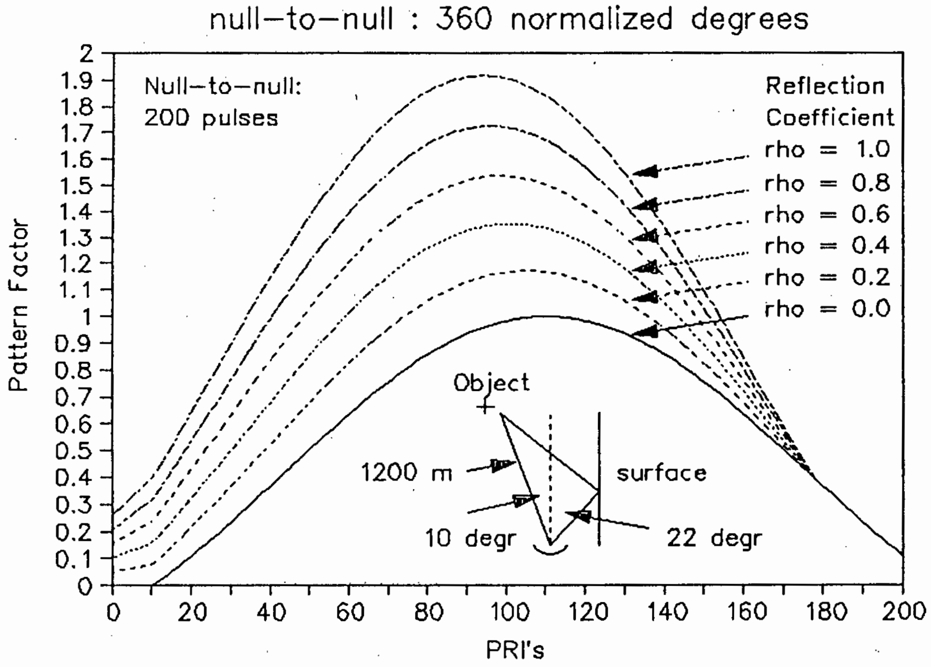

Figure 3.2-3: Pattern propagation factor with multipath

It is apparent from figure 3.2-3 that a bias will be introduced into the scatterer angular position related to the shift in the peak of the received amplitude pulse train. If the path length is sufficiently small to result in the direct and reflected path range bins being adjacent, combination of both range bins to produce a single plot will reduce the angular bias.

3.3 GLINT AND SCINTILLATION

Implicit to the equations for azimuth and range accuracy in thermal noise is the assumption that a scattering object may be considered as a point scatterer. At practical radio frequencies, however, the scattering object is usually large with respect to the transmitted signal wavelength. A shift of range, angle and doppler as a function of aspect angle will be exhibited by such a scattering object. These effects are due to the inter-action of the reflected signals from the multiple scatterers comprising the object. Nathanson [33] categorizes two forms of measurement noise originating from a complex scattering object:

a. Glint which refers to the observed angle fluctuations due to variations of apparent angle of the echo phase front received by the radar antenna.

b. Scintillation which describes the fading or variation in amplitude strength of the received signal at the radar antenna.

Barton [2] states that the effect of glint will be significant if the physical dimensions of the scattering object exceed about one percent of the radar resolution cell in any coordinate. Theoretical derivations for a two-point target enable the angular error due to glint to be determined precisely. For complex scatterers, however, the glint error is difficult to determine theoretically, and the effect on angular accuracy is evaluated by drawing an analogy between the object scatterers distributed over part of the radar resolution cell and bandlimited noise.

The probability density of the apparent object angle resulting from glint is typically gaussian [43]. If the angular error is expressed in terms of linear distance units representing the displacement between the apparent and true target centers, the error is independent of range. Skolnik [43] states that the magnitude of the angular error σ_a is proportional to the radius of gyration R_0 of the object, and is essentially independent of radio frequency:

$$\sigma_a = R_0/\sqrt{2} \qquad (3.3\text{-}1)$$

Scintillation affects the angular accuracy of a radar due to the variations in the echo amplitude distorting the antenna pattern modulated return from the reflector. The magnitude of error introduced is largely influenced by the degree of correlation present between consecutive pulse amplitudes. For an object with uniformly distributed scatterers, the correlation time is given by (3.3-2):

$$t_c = \frac{\lambda}{2 * w_a * L_x} \qquad (3.3\text{-}2)$$

where:

t_c is the correlation time

w_a represents the object rotation rate relative to the radar

L_x is the object span perpendicular to the radar line of sight.

The correlation function is determined by the scintillation spectrum of the object. A Markoffian spectrum will yield an exponential correlation function, while a gaussian spectrum results in a gaussian correlation function [2]. For the situation where the correlation time is less than the inter-pulse period (corresponding to the Swerling 2 model), the scintillation error is given by [2]:

$$\sigma_s = \frac{0.215*\theta_3}{\sqrt{n}} \qquad (3.3\text{-}3)$$

For beam-splitting estimators, the scintillation error is approximated by [2]:

$$\sigma_s = 0.19*\theta_3*\sqrt{[1-\rho(t_o)]} \qquad (3.3\text{-}4)$$

where:

t_o is the target observation time

θ_3 is the half-power beamwidth.

4.0 RADAR SIGNAL SIMULATION

4.1 MODELLING THE RADAR RETURN SIGNAL

4.1.1 Signal Return

In order to model the received radar signal in a simulation process, the signal returned from a scatterer is described as a function of time. This is achieved by expressing the basic radar range equation in terms of the instantaneous received power at some instant t:

$$P_R(t) = \frac{P_T(t-\tau)\, G_T\, G_R\, \lambda^2 \sigma}{(4\pi)^3\, R^4} \qquad (4.1.1\text{-}1)$$

where:

$P_R(t)$ is the received power

$P_T(t)$ is the peak transmitted power

G_T is the antenna transmit gain

G_R is the antenna receive gain

λ is the transmitted wavelength

σ is the radar cross-section

R is the radar slant range to the detected object.

To express this equation in terms of a voltage relationship, the transmitted power is defined as a function of a complex voltage signal $\psi(t)$ such that:

$$P_T(t) = \psi(t) * \psi^*(t) \qquad (4.1.1\text{-}2)$$

The transmitted signal is reflected by a scatterer which is defined in terms of a complex reflection coefficient γ. This reflection coefficient represents that portion of the transmitted signal voltage that is reflected and the phase shift introduced to the reflected signal:

$$\gamma = \sqrt{\sigma} * \exp(j\phi) \qquad (4.1.1\text{-}3)$$

The reflected signal may thus be expressed as:

$$\psi_R(t) = \psi_T(t-\tau) * \left[\frac{G_T\, G_R\, \lambda^2}{(4\pi)^3\, R^4}\right]^{0.5} * \gamma \qquad (4.1.1\text{-}4)$$

This equation is valid if it is assumed that the single point scatterer and the antenna are stationary. For a moving scatterer and scanning antenna, the antenna gain, complex reflection coefficient, round-trip delay time and scatterer range may no longer be considered as constants, but become functions of time:

$$(4.1.1\text{-}5)$$

$$\psi_R(t) = \psi_T[t-\tau(t)] * \left[\frac{\lambda^2}{(4\pi)^3\, R^4(t)}\right]^{0.5} * [\, G_T(t)\, G_R(t)\,]^{0.5}\, \gamma(t)$$

Mitchell [32] has shown that, for a processing interval T, the received signal from a single point scatterer may be expressed as

$$(4.1.1\text{-}6)$$

$$\psi_R(t) = \psi_T[t-\tau(t)] * \left[\frac{\lambda^2}{(4\pi)^3\, R^4}\right]^{0.5} * [\, G_T\, G_R\,]^{0.5}\, \gamma\, *$$

$$\exp(-j*4\pi*R/\lambda) * \exp[j*2\pi*(f_c + f_d)t]$$

where:

f_c is the transmit frequency

f_d is the doppler frequency of the scatterer.

if it is assumed that:

a. The total range displacement of the scatterer during the processing interval T is small compared to the range resolution of the system.

b. The change in doppler frequency for an accelerating scatterer is small compared to the doppler resolution of the system.

c. The angle rotated by the scanning antenna during the processing interval T is small compared to the angular resolution of the system.

The simulation of the received signal from a single scatterer enables the simulation of the received signal from distributed scatterers by superimposing all the individual returns to form a composite signal. Following this approach, the received signal from multiple scatterers is expressed as [32]:

(4.1.1-7)

$$\psi_R(t) = \exp(j*2\pi*f_c*t) * \sum_{k} V_k \, \mu_T(t-\tau_k) * \exp(j*2\pi*f_{dk}t)$$

where:

$$V_k = \frac{\lambda}{(4\pi)^{3/2} R_k^2} [\, G_T \, G_R \,]^{0.5} * \gamma \exp\left(\frac{-j*4\pi*R_k}{\lambda}\right) \quad (4.1.1\text{-}8)$$

V_k represents a phasor of the k^{th} scatterer

R_k represents the range to the k^{th} scatterer.

However, generating the video for each individual scatterer and superimposing all the signals becomes to computationally intensive for large numbers of scatterers. This can be overcome by grouping scatterers which are unresolvable in terms of range, azimuth and doppler into resolution cells and representing the return from such a cell by a single phasor signal:

(4.1.1-9)

$$\psi_R(\theta,t) = \exp(j*2\pi*f_c t) * \sum_{l} \sum_{m} \sum_{n} \frac{\lambda}{(4\pi)^{3/2} R_m^2} \gamma(\theta_l,\tau_m,f_{dn}) *$$
$$[\, G_T(\theta_l-h) * G_R(\theta_l-\theta) \,]^{0.5} * \mu(t-\tau_m) * \exp(j*2\pi*f_{dn}*t)$$

where:

m is an index to the range cells within one pulse repetition interval

n is an index to the doppler samples within the received spectrum

l is an index to the antenna pointing angles per repetition interval

f_c is the transmit frequency

$\gamma(\theta_l,\tau_m,f_{dn})$ is the complex reflection coefficient of the scatterer

$\mu(t-\tau_m)$ is the complex transmitted pulse.

In equation (4.1-9), the factor

$$\sum_l \gamma(\theta_l,\tau_m,f_{dn}) * [\, G_T(\theta_l-\theta) * G_R(\theta_l-\theta) \,]^{0.5} * \exp(j*2\pi*f_{dn}*t)$$

may be considered to be a random phasor [32].

In the event of independent contributing scatterers within the resolution cell as is typically applicable for cells with many individual scatterers, or cells where one scatterer dominates, the ensemble average power of the random phasor may be derived from an average radar cross section for the cell:

$$\| < U(\theta,\tau_m)^2 > \| = \sum_l \sigma(\theta_l,\tau_m)\, G_T(\theta_l-\theta)\, G_R(\theta_l-\theta) \qquad (4.1.1\text{-}10)$$

This ensemble average power is distributed amongst all the spectral components of the signal such that:

$$\sum_n \| < U(\theta,\tau_m,f_{dn})^2 > \| = \| < U(\theta,\tau_m)^2 > \| \qquad (4.1.1\text{-}11)$$

where:

$\| < U(\theta,\tau_m)^2 > \|$ denotes the ensemble average power of the phasor U.

The radar receiver is generally matched to the transmitted signal, and the received signal is mixed down to baseband prior to processing. Simulation of the baseband signal when the radar transmits a pulse train can be achieved by simulating each pulse independently according to:

(4.1.1-12)

$$\psi_R(\theta,t) = \sum_{l}\sum_{m}\sum_{n} \frac{\lambda}{(4\pi)^{3/2} R_m^2} \gamma(\theta_l,\tau_m,f_{dn}) * [\, G_T(\theta_l-\theta) * G_R(\theta_l-\theta)\,]^{0.5} * \mu(t-\tau_m) * \exp(j*2\pi*f_{dn}*t)$$

This expression applies to a fan-beam antenna where the pointing angle θ is measured in a plane normal to the fan-beam, and the increments in angle are uniform. Simulation of the received signal for a 3-D radar will require a further summation in the above expression to account for the elevation pattern.

However, if the pulses may be considered as coherent, and the pulses are transmitted at uniform intervals, the received pulse train can be simulated with a simplified expression:

(4.1.1-13)

$$\psi_R(\theta,t,lT_r) = \sum_{m}\sum_{n} \frac{\lambda}{(4\pi)^{3/2} R_m^4} U(\theta,\tau_m,f_{dn}) *\mu(t-\tau_m) * \exp(j*2\pi*f_{dn}*t)$$

In this expression, the phasor $U(\theta,\tau_m,f_{dn})$ actually has a phase term associated with it ($\exp[-j*4\pi*R_m/\lambda]$). However, in the practical case the range R_m will not be measurable to a fraction of a wavelength, and consequently the phasor is considered to be random. The phasor represents the return from a resolution cell at pointing angle θ, range $c*\tau_m/2$ and with a doppler frequency f_{dn}. The phasor may be derived from:

$$U(\theta,\tau_m,f_{dn}) = \sum_{l} \gamma(\theta_l,\tau_m,f_{dn}) * [\, G_T(\theta_l-\theta) * G_R(\theta_l-\theta) \,]^{0.5} \qquad (4.1.1\text{-}14)$$

For independent scatterers, the ensemble average of the complex reflection coefficients within the resolution cell may be considered as the average radar cross section of the cell, and the power of the phasor representing the return from this resolution cell is given by equation (4.1.1-10). The total phasor power will be distributed amongst its spectral components (4.1.1-11).

In order to assume coherent processing, the signal amplitude and phase of the received signal must be stable, which inherently implies that the antenna gain, scatterer doppler and range need to be constant during the processing interval T in which the received pulses are considered to be coherent. Following this approach, the total time during which the scatterer is illuminated by the antenna can be subdivided into "coherent processing intervals", and the expression derived for coherent pulses may be applied to each interval.

In order to increase the accuracy of the simulation, the power associated with the return from a representative scatterer within a resolution cell is shared with neighbouring cells if the scatterer does not fall in the centre of the cell. The fraction of power shared is derived from the displacement of the scatterer from the cell centre assuming a linear relationship between position and amount of power shared. In a one-dimentional case, a deviation of x from the cell centre if will result in a fraction x/X of the returned power being allocated to the neighbouring cell if the displacement between two resolution cells is X.

Modelling of the received signal according to the aforementioned expressions enables:

a. A representation of the returned signal at each sampling instant after pulse transmission.

b. A frequency spectrum to be associated with a scatterer as is typically required for ground clutter return.

c. The treatment of extended scatterers such as large aircraft and clutter.

d. The implementation of non-linear receiver processing such as sensitivity-time-control, limiting and analogue-to-digital conversion.

In practice, the radar signal simulation is quite often performed with a simplified expression:

$$\mu(\theta,t,lT_r) = \text{radar cross-section} * G(\theta_l-\theta) * \exp(j*2\pi*f_d/f_{prf}*l) \qquad (4.1.1\text{-}15)$$

This expression follows from the modelled signal, if the following assumptions are made:

a. The returned signal consists of a single doppler component

b. The signal is only represented at the instant for which a scatterer is present

c. The scatterer only occupies one resolution cell, and does not contribute to any neighbouring cells

d. The measured range to the scatterer is accurate to a fraction of a wavelength enabling returned signal to only experience a phase shift as a result of scatterer velocity

e. A single transmit and receive antenna gain.

4.1.2 Noise

The performance of a radar is ultimately limited by receiver noise resulting from thermal effects associated with electron conduction in the receiver components. In the absence of external noise factors attributable to transmission lines and the antenna, the noise power contribution of a thermal nature is expressed by:

$$P_n = k * T_e * B_n \qquad (4.1.2\text{-}1)$$

where:

k is the Boltzmann constant

T_e is the effective noise temperature

B_n is the noise bandwidth.

For radar receivers of the superheterodyne type, the receiver bandwidth is approximately equal to that of the intermediate stage. The frequency response characteristics of many practical radar receivers are such that the half-power bandwidth and noise bandwidths do not differ appreciably [42], and the noise bandwidth is often equated to the half-power bandwidth.

The effects of external noise are incorporated in the noise power by the definition of a system noise temperature which is defined as the effective noise temperature including the effects of antenna temperature:

$$P_n = k\,T_s\,B_n \qquad (4.1.2\text{-}2)$$

$$T_s = T_e + T_{antenna} \qquad (4.1.2\text{-}3)$$

Receiver noise may generally be characterized by a white spectrum with a power spectral density

$$S_n(w) = No = kT_s \qquad (4.1.2\text{-}4)$$

and a gaussian statistical property. The noise power out of the receiver intermediate frequency filter can be derived as [16]:

$$P_o = N_o \int \| H(f) \|^2 \,\delta f = N_o\,E_p \qquad (4.1.2\text{-}5)$$

where:

E_p represents the energy contained in the matched pulse.

In the event of noise being sampled, the noise power is influenced by the sampling rate. For this case it can be shown [32] that the ensemble average noise power in each noise sample is:

$$p_n = N_o/\delta T \qquad (4.1.2\text{-}6)$$

In the simulation process, δT represents the time between consecutive noise samples. If δT is equal to the reciprocal of the half-power bandwidth, the equation transforms to:

$$p_n = N_o B_n = \sigma_n^2 \qquad (4.1.2\text{-}7)$$

The intermediate frequency filter limits the bandwidth of the receiver noise, enabling the bandpassed process to be expressed in terms of its quadrature components. Di Franco and Rubin [16] have shown that for this case, the first and second order statistics of the noise and its quadrature components are characterized by zero mean and equal variance distributions:

$$\sigma_n^2 = \sigma_i^2 = \sigma_q^2 \qquad (4.1.2\text{-}8)$$

$$\mu_n = \mu_i = \mu_q = 0 \qquad (4.1.2\text{-}9)$$

Furthermore, sample values of the in-phase and quadrature waveforms at the same time instant are independent. The simulation of noise thus requires the generation of independent gaussian samples with zero mean and variance equal to the noise power per sample:

$$\sigma_n^2 = N/\delta T = kT_s/\delta T \qquad (4.1.2\text{-}10)$$

4.2 MODELLING THE RADAR RECEIVE PATH

4.2.1 Block Diagram

A block diagram of the pulsed radar assumed in the accuracy evaluations is given in figure 4.2.1-1.

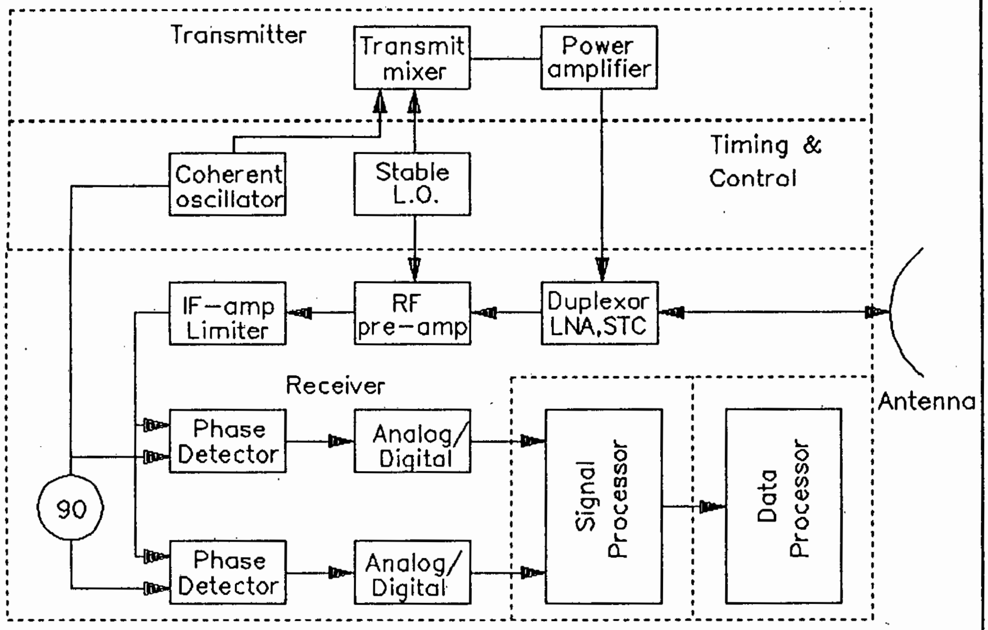

Figure 4.2.1-1: Radar Block Diagram

The radar may be considered to consist of a transmitter-, an antenna-, a receiver-, a timing and control unit-, a signal processor- and a data processor subsystems. For evaluation purposes, the transmitter, timing and control and data processor subsystems have been regarded as "black boxes", and only the antenna, receiver and signal processor subsystems have been considered.

The radar receiver may employ coherent processing or non-coherent processing. Coherent processing utilizes both the amplitude and phase information across the complete pulse train received when the antenna scans past a reflecting object. With the coherent processor the pulse train is integrated prior to envelope- or square law detection.

Non-coherent processing only utilizes the phase and amplitude information of a single pulse. Typically, non-coherent processing employs matched filtering on an individual return, and integration is performed after detection.

The process of coherent integration yields a higher detection performance than its counterpart, but requires more complex hardware with more stringent stability constraints, and complete knowledge of the received signal phase during integration. The output signal-to-noise ratio of the coherent integrator for integration of N pulses will be N times the signal-to-noise ratio for the single pulse. A representative single pulse is then given by:

$$(S/N)_N = \sum_{k=1}^{N} (S/N)_k \qquad (4.2.1\text{-}1)$$

For non-coherent integration, the output signal-to-noise ratio of the integrator will be less primarily due to the fact that the signal is rectified prior to integration which reduces some of the noise cancellation present in coherent integration.

4.2.2 Antenna Subsystem

The antenna subsystem in the radar receive path is represented by an antenna gain factor given by:

$$G(\theta,\phi) = G_M \, \| \, f(\theta,\phi) \, \|^2 \qquad (4.2.2\text{-}1)$$

where:

$f(\theta,\phi)$ is the antenna pattern factor

G_M is the maximum power gain at the nose of the beam.

The antenna pattern factor defines the relative strength of the free-space field radiated by the antenna as a function of the azimuth angle θ and elevation angle ϕ. The most generally applied approximation to the pattern of typical directional antenna's is the gaussian pattern factor [8]:

$$f(\theta) = \exp[-1.385\ (\theta/\theta_3)^2] \qquad (4.2.2\text{-}2)$$

The gaussian pattern factor is representative for beam patterns near the beam axis up to the half-power points of the beam. However, the gaussian pattern has no sidelobes, and can therefore not be generated by a practical antenna as this would require an infinite antenna aperture. A more realistic approximation is achieved by a sin x/x pattern [8]:

$$f(\theta) = \frac{1 + \cos(\theta)}{2} * \frac{\sin[k\sin(\theta)]}{[k\sin(\theta)]} \qquad (4.2.2\text{-}3)$$

where:

$$k = \frac{1.3916}{\sin(\theta/2)} \qquad (4.2.2\text{-}4)$$

The sin x/x pattern is applicable to narrow-beam antenna's ($\theta_3 < 90$ degrees) with a uniformly illuminated rectangular aperture. The first sidelobe level is 13.26 dB below the main lobe. In practice, lower sidelobes are usually achieved by weighting the illumination function. This may be modelled by modifying the antenna pattern factor past the first null [11]:

$$(4.2.2\text{-}5)$$

$$f(\theta) = 10^{-[S-13.26]/20} * \frac{1 + \cos(\theta)}{2} * \frac{\sin[k\sin(\theta)]}{[k\sin(\theta)]}$$

where:

S is the specified sidelobe level in dB.

A simplification of the above is possible is it is assumed that $\cos(\theta) \simeq 1$ and $\sin(\theta) \simeq \theta$. Then:

$$f(\theta) = \frac{\sin[2.783*(\theta/\theta_3)]}{[2.783*(\theta/\theta_3)]} \quad (\theta < \theta_3) \qquad (4.2.2\text{-}6)$$

(4.2.2-7)

$$f(\theta) = 10^{-[S-13.26]/20} \frac{\sin[2.783*(\theta/\theta_3)]}{[2.783*(\theta/\theta_3)]} \qquad (\theta > \theta_3)$$

A uniformly illuminated circular aperture gives rise to a pattern factor of the form [8]:

$$f(\theta) = \frac{2*I_1[3.24*(\theta/\theta_3)]}{[3.24*(\theta/\theta_3)]} \qquad (4.2.2\text{-}8)$$

The corresponding level of the first sidelobe is reduced to 17.6 dB in comparison with the 13.26 dB for the rectangular aperture.

4.2.3 Sensitivity Time Control

The received power at the radar antenna is proportional to the inverse fourth power of the slant range to the scatterer. The implication of this is that a scatterer at a given range will yield the same power return as a second scatterer with 1/16 of the radar cross section at half the slant range. The consequent dynamic range requirements imposed on the receiver are impractical. In order to overcome this, sensitivity time control may be implemented. With this technique, the radar sensitivity is varied with time in such a way that the received echo strength is independent of range. A practical model with which the sensitivity time control may be emulated is achieved by scaling the received pulse amplitude with a factor:

$$a_{STC} = (R_k/R_o)^2 \qquad (4.2.3\text{-}1)$$

where:

R_k is the slant range to the scatterer

R_o represents the sensitivity-time-control cut-in range.

4.2.4 Matched Filter

In almost all practical radar receivers, a matched filter or an approximation of a matched filter is employed in order to maximize the peak-signal to rms noise level at the output of the receive filter. The receiver intermediate frequency amplifier is generally matched to the single-pulse radar transmissions, or to each single pulse in a coherent waveform transmission (non-coherent processor). The matched filter design is such that its amplitude response minimizes the effect of thermal noise at its output, and its phase response maximizes the signal response of the filter. The amplitude response is generally achieved by a bandpass analogue filter which limits the width of the frequency spectrum to the extent possible. The phase response is implemented with either analogue (SAW) or digital (FFT) techniques.

The simplest transmitted pulse waveform is given by a rectangular pulse. Its corresponding matched filter is given by a sin x/x response with a half-power bandwidth of $0.884/\tau$ and an output signal-to-noise ratio:

$$S/N = 10 * \mathrm{Log}_{10}[A^2/(2\sigma_n^2)] \qquad (4.2.4\text{-}1)$$

where:

A is the pulse amplitude

σ_n is the noise standard deviation.

Approximations of the matched filter are often implemented as a result of hardware simplifications or due to characteristics required to reject other interference. The approximation of the matched filter results in a degraded output signal-to-noise ratio. This degradation is reflected in a mismatch loss factor L_m utilized in the various analytical equations. Furthermore, a bandwidth mismatch degradation may also be experienced if the filter bandwidth is not selected for an optimum value.

4.2.5 Limiter

The current trend in radar systems is to preserve a wide dynamic range in the receiver, and to achieve a constant false alarm rate by various CFAR techniques. However, many systems still employ limiting in the intermediate frequency stage to prevent saturation of filters and analogue-to-digital convertors. A possible model for this limiting is given by:

$$\rho^2 = (v_r^2 + v_c^2) / C \qquad (4.2.5\text{-}1)$$

$$V_r = v_r/\rho \text{ and } V_i = v_i/\rho \qquad (4.2.5\text{-}2)$$

where:

C is the clip level

$v = v_r + j^*v_i$ represents the received phasor.

4.2.6 Analogue-to-Digital Conversion

Digital signal processing requires the received radar echo to be translated from an analogue representation to a digital representation. Application of a n-bit convertor introduces a quantization into the signal representation. The resolution of such a n-bit convertor is given by

$$q = \frac{E_{max}}{(2^n - 1)} \qquad (4.2.6\text{-}1)$$

where:

E_{max} is the maximum voltage swing at the input to the convertor.

The dynamic range in decibels for an n-bit convertor is given by [43]:

$$6n - 9 - 20^*\text{Log}_{10}(\sigma_n/q) \qquad (4.2.6\text{-}2)$$

Several errors may accompany the analogue to digital conversion process which adversely affect the radar performance:

a. Phase and gain errors in the phase detectors preceding the convertors which results in the generation of spurious components of the input signal at the image frequency. The relative level of the spurious component is determined by [24]:

(4.2.6-3)

$$S[dB] = 10 * \text{Log}_{10} [(\gamma/2)^2 + \{\sin(\delta/2)^2\}]$$

where:

γ is the amplitude quadrature error and δ is the phase quadrature error

b. DC offset which is equivalent to introducing a spectral component at zero doppler frequency

c. Quantization noise given by $1/\sqrt{12}$ levels. If k levels of thermal noise are present, the increase in total noise due to quantization is given by:

(4.2.6-4)

$$(k^2 + 1/12) / k^2$$

d. A straddling loss due to the sampling rate of the convertor. This loss may be reduced significantly if more than one sample is taken per half-power pulse width.

In the model applied, the quantization step q of the convertor is related to a limiting power level C and the number of bits n in the convertor according to:

$$\sqrt{C} = (2^n - 1)*q \qquad (4.2.6\text{-}5)$$

where:

C is the power limiting level

q is the quantization step size.

The digital representation for the in-phase and quadrature signal amplitudes is then simply V_r/q and V_i/q

4.2.7 Detector

Prior to integration, the in-phase and quadrature signals are combined in an envelope or square law detector. The detection criteria most appropriate to the radar detection problem is the Neyman-Pearson criterion which maximizes the probability of detection for a given false alarm probability by comparing the likelihood ratio to a given threshold. Skolnik [43] states that for small signals, the Neyman-Pearson detector reduces to a square law detector, while for large signals it reduces to linear detector.

4.2.8 Constant False Alarm Rate Processing

In order to maintain a constant false alarm rate in a clutter environment, a CFAR circuit is usually applied. The CFAR circuit adapts the decision threshold in the radar processor to suit the clutter environment which is generally assumed to be uniformly distributed. Two common techniques utilized to achieve constant false alarm rate processing are the cell-averaging CFAR (CA-CFAR) and the cell averaging CFAR with greater-of selection (CAGO-CFAR). Figure 4.2.7-1 illustrates the two CFAR techniques.

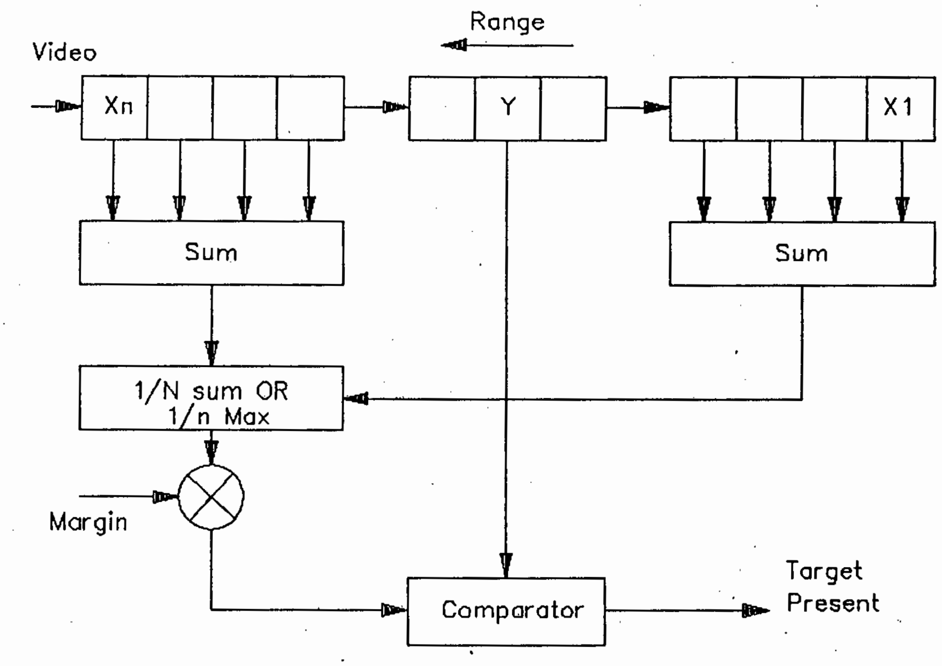

Figure 4.2.8-1: CA-CFAR and CAGO-CFAR

An estimate of the mean clutter power surrounding the test cell Y is made by the two reference windows. The cell averaging CFAR determines the average amplitude over the two reference windows, while the greater-of selection determines the average amplitude of each reference cell individually, and subsequently selects the larger estimate. The determined average is scaled with a margin to establish the detection threshold. Generally, the test cell is separated from the reference cells by guard cells in order to prevent 'spill-over' from a target in the test cell from influencing the mean estimates. H. Rohling [37] introduced the ordered-statistic CFAR (OS-CFAR) to overcome the deficiencies of the previously mentioned CFAR mechanisms, which are primarily:

- Masking of targets
- Interdependence between the clutter extent and the length of the reference window for optimum detection probability.

The ordered statistic CFAR is very similar to the cell averaging CFAR in architecture, and differs only in the mechanism applied to establish an estimate of the clutter level. In contrast to the averaging process applied, the contents of the reference cells are ranked according to increasing amplitude, and the contents of one certain rank position in the sequence is used as an estimate. Typically the rank position will be in the range between the median and maximum value (figure 4.2.7-2).

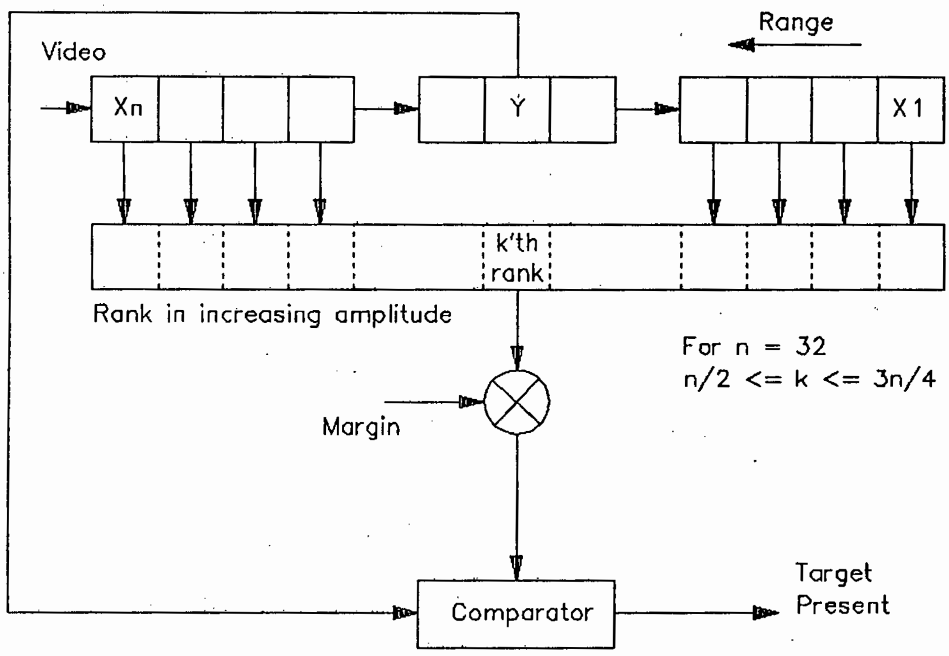

Figure 4.2.8-2: OS-CFAR

4.3 TARGET MODELS

The detection and estimation performance of a radar is largely dependant on the signal-to-noise ratio available at the receiver. This ratio is defined by the radar equation, and is amongst other parameters dependant on the scatterer radar cross section (RCS). Nathanson [33] defines the radar cross section of an object as proportional to the far-field ratio of reflected to incident power density. The RCS for a scatterer exhibits three distinct regions of behaviour, the regions being distinguished by the ratio of radar wavelength relative to the scattering object size. For scattering objects smaller than the radar wavelength, a Rayleigh cross section behaviour may be assumed. This region is categorized by the RCS being sensitive to polarization of the signal, and near isotropic scattering characteristics. Although targets are not normally in the Rayleigh region, precipitation particles such as raindrops and some forms of chaff are.

Scattering objects which are large compared to the radar wavelength exhibits an optical region behaviour which is characterized by strong aspect dependance. The RCS of complex reflectors in this region may be approximated by considering the reflector to consist of individual scatterers which do not interact, and regarding the total RCS as the vector some of the individual reflectors.

The resonance region is identified by the radar wavelength being comparable to the scattering object size. For this region, no simple generalizations are possible [33]. Generally, targets of interest exhibit an optical region behaviour, and as such are modelled by some theoretical statistical distribution. The majority of real targets are only approximations to the ideal scattering mechanisms which yield the applied statistical models. It is, however, of interest for simulation purposes to evaluate the physical mechanisms underlying the statistical models. Swerling originally proposed four fluctuation models to represent the behaviour of practical targets. However, in a later work [46] it is indicated that the Swerling models do not necessarily describe or even encompass the RCS fluctuation behaviour of all targets of interest, and that three broader families of target RCS models of which the Swerling models are a subset, are more representative of a wide variety of practical targets. The three families of models are categorized as:

a. The Chi-square family which encompasses the Swerling, Marcum and Weinstock target models.

The model is given by the following general distribution:

(4.3-1)

$$w(x,<x>) = \frac{k}{(k-1)!} \frac{k}{<x>} \left[\frac{kx}{<x>} \right]^{k-1} \exp \left[\frac{-kx}{<x>} \right] \qquad x > 0$$

For the event that the Chi-square distribution has two degrees of freedom, the distribution represents the Swerling one and two target models. These models are representative for any target which may be considered as a random assembly of scatterers of which no one ever contributes more than a small fraction of the reflected power, and which have random relative phases [33].

Swerling case three and four models are represented by Chi-square distributions with four degrees of freedom. These models are representative for a target which consists of one large dominant scatterer combined with an assembly of many small scatterers of which the combined RCS is of the same order of magnitude as the single dominant scatterer. In general, the degree of the Chi-square distribution becomes higher as the coherent component of the target becomes larger.

A special class of fluctuation models is formed by Chi-square distributions where the number of degrees of freedom is less than two. This class of RCS models (Weinstock models) has been fitted to objects consisting of long cylinders and cylinders with fins.

b. The Rice family of target models is given by:

(4.3-2)

$$w(x,<x>) = \frac{1}{x} (1+a^2) * \exp[-a^2 - \frac{x}{<x>} * (1+a^2)] *$$

$$I_o[2*j*a*\sqrt{\{1+a^2 * \frac{x}{<x>}\}}]$$

where:

x is the radar cross-section

$<x>$ is the average radar cross-section

a^2 is the ratio of the dominant scatterer radar cross-section to the total radar cross-section of the smaller scatterers

I_o is the zero-order Bessel function.

Swerling [46] has shown that the Rice family of models can be approximated by the Chi-square distribution with the number of degrees of freedom given by:

$$2k \quad = \quad 2\,[1 + a^2/(1+2a)\,] \qquad (4.3\text{-}3)$$

As with the Swerling target models three and four, the physical interpretation of the Rice target models leads to a mechanism with one dominant scatterer and an assembly of many small scatterers. The ratio between the dominant scatterer RCS and the sum of all the small scatterer cross sections is given by a^2.

c. A log-normal family of target RCS models has been defined as [33]:

$$w(x,s) = \exp\left[\frac{-\{\ln(x) - <\ln(x)>\}}{2*s^2}\right] * \frac{1}{x*s*\sqrt{(2\pi)}} \qquad (4.3\text{-}4)$$

where:

s is the standard deviation of $\ln(x)$

x is the radar cross-section.

The physical interpretation of this class of targets leads to a set of highly directive scatterers such as large flat plates viewed at random aspects [46]. Nathanson states that targets which exhibit a large mean-to-median RCS ratio such as ships will tend to exhibit a log-normal distribution.

While each of the mentioned targets RCS families describe the statistical distributions of the radar cross section, they do not detail the correlation properties of the distributions. In his original work, Swerling proposed two categories of correlation behaviour:

a. Pulse to pulse independence as assumed for models two and four i.e. no correlation between consecutive pulses.

b. Perfect correlation from pulse to pulse within a scan, but independence from scan to scan (models one and three).

However, often more detailed assumptions than those used by Swerling are necessary when considering the correlation properties of real target returns. In general, the returned radar signal may be de-correlated due to motion of the scatterer relative to the line of sight, change of radar frequency or internal motion. The frequency spectrum of the RCS fluctuation and its corresponding correlation function are dependant on [21]:

- Target dimensions related to the radar wavelength
- Target slenderness and surface structure
- Target motion relative to the radar
- Rotating parts

For an object with uniformly distributed scatterers, the correlation time describing the interval between samples regarded as uncorrelated is given by [2]:

$$t_c = \frac{\lambda}{2 * w_a * L_x} \qquad (4.3\text{-}5)$$

where:

λ is the radar wavelength

w_a is the rotation rate of the scattering object relative to the radar

L_x is the object span perpendicular to the radar line of sight.

The frequency spectrum will be rectangular with width

$$f_{max} = 1/t_c \qquad (4.3\text{-}6)$$

and the associated correlation function will be:

$$\rho(\tau) = \frac{\sin(\pi * f_{max} * \tau)}{\pi * f_{max} * \tau} \qquad (4.3\text{-}7)$$

The scatterer distribution of a reflecting object is also represented in the literature by gaussian or Markoffian distributions which lead to gaussian and exponential correlation functions respectively. Barton [2] states that Markoffian spectra have proven useful in describing targets which are subject to internal motion. Further, many aircraft targets whose physical span limit the rotation induced spectra are satisfactorily described by a Markoffian spectrum with a half-power spectral width equal to the rotation-induced maximum spectral component:

$$\pi * f_3 = 1/t_c \qquad (4.3\text{-}8)$$

$$W(f) = \frac{W_o}{1 + (f/f_3)^2} \qquad (4.3\text{-}9)$$

$$\rho(\tau) = \exp(-2 * \pi * f_3 * \tau) \qquad (4.3\text{-}10)$$

The process of envelope detection applied in many radars tends to increase the spectral width and decrease the correlation time of RCS fluctuations. A gaussian spectrum will increase in spectral width by a factor 1.4, while the Markoffian spectrum will double for envelope detectors [2]. A further increase in spectrum may occur due to propellor modulation and skin vibration.

The modelling of a target RCS via statistical means when the target dimension is small relative to the radar resolution cell (point target) can be achieved with the previously mentioned models. A greater degree of sophistication can be introduced for simulations which require the targets to traverse a specific trajectory by describing the average target RCS as a function of aspect angle, and superimposing the statistical model on this average [32]. However, for targets whose dimensions extend beyond the radar resolution cell, the point target assumption is not valid. Swerling [46] has postulated statistical models for the portions of the target in a resolution cell assuming a specific statistical characteristic for the target when it may be regarded as a point target. In his paper, Swerling postulates that for targets exhibiting Rayleigh characteristics as point targets, consistent statistical models for the portions of the target within the resolution cell for the extended target could be:

a. A model in which each portion of the target within each resolution cell also exhibits Rayleigh characteristics.

b. A model in which the portion of the target in some or all cells exhibit Rice or Chi-square characteristics when the cells become small.

c. A model in which, for sufficiently small cell sizes, the portion of the target in each cell is non-fluctuating.

The fluctuation rate of the contents of each cell is postulated to be less than or equal to the rate of fluctuation for larger cells. Targets exhibiting Rician fluctuation characteristics are postulated to exhibit similar characteristics to those of Rayleigh targets in the event of extended targets, except that at least one of the resolution cells would always contain a Rice target. For simulation purposes, Mitchell states that "the larger the target is in relation to the resolution cell, the less important are the details of any particular resolution cell". It is therefore assumed in the simulations that the statistical models applied to each portion of the target for extended targets will be the same as that of a point target, except for log-normal target models. For these models, Swerling concluded that no consistent models could be postulated for each portion. The fluctuation rate for the extended models has been assumed to be equal to that of a point target.

4.4 LAND CLUTTER

4.4.1 Land Clutter Modelling

Radar clutter may be defined as echoes which are undesirable in a specific radar application. These echoes may originate from scattering objects distributed over a surface (land clutter), scattering objects distributed within a particular volume (weather or chaff) or discrete point scattering objects (urban areas). In practice, the unwanted echoes serve as an additional source of noise against which desired signal echoes must compete. In order to establish the effect of clutter returns on the radar performance parameters such as detection probability and positional accuracy, clutter models have been developed which aim to represent the clutter process as closely as possible. These clutter models attempt to address both the intrinsic effects which are due to inherent properties of the reflecting scatterers and are primarily influenced by wind-driven motion of the scatterers, as well as induced effects which are primarily influenced by antenna scanning, platform motion and transmitter instability characteristics of a radar [39].

In characterizing clutter, important parameters which need to be considered are [5]:

a. Clutter RCS or reflectivity over the surface or volume.

b. Numbers of discrete sources.

c. Spatial extent and distribution of sources.

d. Velocity extent and distribution (spectrum).

e. Wavelength dependance of RCS.

f. Amplitude probability distribution.

g. Spatial correlation of amplitudes.

h. Polarization properties.

Clutter models may be categorized into three broad categories [25]:

1. Simple clutter models in which the backscatter coefficient σ^0 is taken as an average dependant on the terrain, or described analytically as a function of frequency, angle of incidence and terrain type.
2. Statistical models in which the clutter median or mean may be varied with frequency, incidence angle and terrain as with the simple model, but where the instantaneous backscatter coefficient is described as a statistical parameter belonging to a particular probability density function and exhibits a particular spectrum. These statistical models generally cater for a statistical behaviour of the backscatter coefficient within a resolution cell, as well as a spatial probability distribution and auto correlation function.
3. Scattering models in which the average backscatter coefficient σ^0 is calculated as a function of surface characteristics via mathematical or computer analysis.

Elementary to all clutter models is the concept of a backscatter coefficient. The equivalent radar cross section of an area or volume of distributed scatterers is defined by the product of the intersected area or volume within the radar resolution cell and the backscatter coefficient. In general, the mean value of the backscattering coefficient is specified (this mean representing a temporal and spatial mean [38]), and an extensive database has been accumulated in the literature for different terrains. An alternative to the backscatter coefficient, known as the constant Gamma model, has also been published in the literature. The constant Gamma parameter γ is dependant on the radar grazing angle ψ, and relates to the backscatter coefficient according to:

$$\sigma^0 = \gamma \sin(\psi) \qquad (4.4.1\text{-}1)$$

For ground based radars, the grazing angle is usually less than one degree, and even though an extensive database exists for average backscatter coefficients, most of the data is applicable to higher grazing angles [3], and a very limited amount of measurements are applicable to the low grazing angle situation. Various simple clutter models exist which predict the backscatter coefficient as a function of range. One such model is defined by:

$$\sigma^{o} = K \qquad \text{for } R < R_h$$

$$\sigma^{o} = K (R_h/R)^4 \qquad \text{for } R > R_h \qquad (4.4.1\text{-}2)$$

A continuous curve approximation is given by:

$$\sigma^{o} = K * \frac{R^4}{(R_h^4 + R^4)} \qquad (4.4.1\text{-}3)$$

where:

$K = -25$ dB worst case

$K = -30$ dB heavy clutter

$K = -45$ dB average clutter [25].

A disadvantage of the above model is that it assumes the specified clutter to be present for the complete radar range. A more accurate model predicts how rapidly the clutter will disappear for different antenna heights, terrain types and radar wavelengths. Such a model recognizes that the clutter reflectivity as viewed by a ground-based radar is the product of a backscatter coefficient and a two-way power propagation factor F_c^4. The clutter area is subdivided into three regions, the boundaries being defined by the horizon range R_h and a critical range R_c:

a. Short range region:

In this region the grazing angle is above a defined critical angle, and the propagation factor is approximately unity. The critical angle is defined by:

$$\sin(\psi_c) = \lambda/(4*\pi*\sigma_h) \qquad (4.4.1\text{-}4)$$

where:

σ_h is the rms surface roughness.

The short range boundary is defined by:

$$R_c = \frac{4*\pi*h_r'*\sigma_h}{\lambda} \qquad (4.4.1\text{-}5)$$

where:

h_r' is the antenna height defined as a height h_r above the local surface. The local surface is at a height $2\sigma_h$ above the average terrain.

The backscatter coefficient for this region may be approximated by:

$$\sigma^o = \gamma * (h_r + 2*\sigma_h) / R \qquad (4.4.1\text{-}6)$$

b. Medium range region:

In this region the propagation factor F_c is influenced by reflection and interference phenomena, and may no longer be assumed constant. The boundaries to this region are formed by the horizon range and the critical range, and the backscatter coefficient may be approximated by:

$$\sigma^o*F_c^4 = \gamma * (h_r'/R) * (R_c/R)^4 \qquad (4.4.1\text{-}7)$$

c. Long range region:

In this region propagation is determined by diffraction. Depending on the type of terrain, a choice is made between smooth-sphere and knife-edge diffraction. Knife-edge diffraction tends to occur when the radar horizon is established by an isolated object separated from its surroundings. The criterion for an object to create a knife-edge diffraction is that the object should receive free-space illumination. For an object with a height $2\sigma_h$, an intervening points of σ_h, the criterion for full illumination translates to [3].

$$2\sigma_h > 64 * \sqrt{\phi} * 4\sqrt{h_r} \qquad (4.4.1\text{-}8)$$

Smooth-sphere diffraction allows σ^o to be estimated as:

$$\sigma^o = \gamma * h_r'/R \qquad (4.4.1\text{-}9)$$

Statistical clutter models characterize the non-homogeneous nature of the backscatter coefficient σ^o resulting from the random nature of ground terrain. The general approach in describing land clutter is to state its properties in terms of:

a. An average backscatter coefficient $<\sigma^o>$.

b. An amplitude probability distribution.

c. A power spectral density.

d. A spatial distribution.

Experimental data has enabled the determination of an average backscatter coefficient for different terrain categories. For low-resolution ground data this average represents a composite temporal and spatial average [38]. The properties of surface clutter in general do allow some broad characteristics to be deduced. For smooth terrain, the backscatter coefficient will tend to adhere to the three regions defined in the simple clutter model (4.4.1-3). However, with increasing surface roughness, the regions tend to merge into one for which the backscatter coefficient is given by (4.4.1-1). In order to categorize smooth and rough terrain, a Rayleigh criterion may be applied. According to this criterion, terrain features for which the rms height exceeds $\lambda/(8\sin\psi)$ constitutes rough terrain.

Two types of amplitude statistics are useful in describing land clutter:

1. Temporal amplitude statistics which characterize the returned clutter signal amplitude fluctuations resulting from relative motion of individual scatterers within a resolution cell (intrinsic effects).

2. Spatial amplitude statistics accounting for the spatial variability of land clutter. A possible measure of spatial variability is to consider the backscatter coefficient as a random variable which represents values of the coefficient that may be found in independent spatial cells. No clear

definition exists in the literature as to what constitutes independent cells for land clutter.

The simplest clutter model applicable to land clutter is the Rayleigh clutter model. This model is applicable to terrains where the scatterers are uniformly distributed, and no subset of scatterers predominates. Generally this model may be associated with weather clutter, chaff, sea clutter observed with low resolution radar or high resolution radar at high grazing angles, and land clutter observed from high grazing angles over undeveloped terrain. The clutter cross-section probability density function is given by:

$$p(\sigma) = \frac{1}{\sigma} * \exp\left(\frac{-\sigma}{<\sigma>}\right) \qquad (4.4.1\text{-}10)$$

where:

$$<\sigma> = <\sigma^{o}> * A_c \qquad (4.4.1\text{-}11)$$

$<.>$ denotes the ensemble average

A_c denotes the clutter cross-section.

The power spectral density associated with the Rayleigh clutter model is assumed to be gaussian, leading to:

$$S(f) = P_c * \frac{\lambda}{2\sigma_v\sqrt{(2\pi)}} * \exp\left[-0.5 \frac{c^2}{(2\sigma_v{}^2)}\right] \qquad (4.4.1\text{-}12)$$

where:

σ_v is the rms velocity spread of the clutter

P_c is the received clutter power.

The associated auto correlation function is given by:

$$R(\tau) = P_c * \exp\left[\frac{-\tau^2}{2\sigma_\tau^2}\right] \qquad (4.4.1\text{-}13)$$

where:

$$\sigma_\tau = \lambda/(4\pi\sigma_v) \qquad (4.4.1\text{-}14)$$

If a predominant scatterer is present within the distributed clutter, a Rician model may be assumed [38].

In general, however, a shadowing effect occurs at low grazing angles in which significant portions of the land clutter may be obscured from the radar at particular aspect angles. As the aspect angle changes, different parts of the ground clutter reflect signals to the radar, introducing larger amplitude fluctuations than predicted by a Rayleigh clutter model. Two alternative models are generally applied to accommodate the large amplitude fluctuation behaviour: The log-normal and the Weibull clutter models. In applying these models, two interpretations are possible [39]:

1. The clutter process is regarded as a wide-sense stationary process in which the radar cross-section values are samples of either of the alternative clutter models.

2. The clutter process is regarded as a time-varying process in which the statistical parameters are regarded as stationary within the radar observation period over a specified correlation distance. The probability density function of the clutter signal envelope is regarded as Rayleigh within the correlation distance. The value of the backscatter coefficient with each correlation block varies statistically according to the log-normal or Weibull distributions.

The log-normal clutter model has been used to characterized ground clutter at low grazing angles, as well as urban areas. The model yields a relatively high probability of large amplitudes, and tends to over-estimate the dynamic range of real clutter. The clutter cross-section probability density function is given by [39]:

$$p(\sigma) = \frac{1}{\sigma_p \sigma \sqrt{(2\pi)}} * \exp\left[\frac{-\ln^2(\sigma/\sigma_m)}{2\sigma_p^2}\right] \qquad (4.4.1\text{-}15)$$

where:

$$\sigma_p = 2\sigma_v \qquad (4.4.1\text{-}16)$$

σ_v is the rms velocity spread of clutter

σ_m is the median clutter cross-section.

The mean clutter cross-section is related to the median value according to:

$$<\sigma> = \sigma_m * \exp(2\sigma_v^2) \qquad (4.4.1\text{-}17)$$

The Weibull clutter model enables a more accurate representation of clutter distribution over a wider range of conditions than the Rayleigh and log-normal models. The clutter cross-section probability density function is given by [39]:

$$p(\sigma) = \beta \ln(2)\ \sigma_c^{\beta-1} * \exp[-\sigma_c^{\beta} * \ln(2)] \qquad (4.4.1\text{-}18)$$

where:

$$\sigma_c = \sigma/\sigma_m \qquad (4.4.1\text{-}19)$$

$$\beta = a/2 \qquad (4.4.1\text{-}20)$$

a = distibution skewness.

The mean clutter cross-section is given by:

$$<\sigma> = \frac{\sigma_m \Gamma(1 + 1/\beta)}{[Ln2]^{1/\beta}} \qquad (4.4.1\text{-}21)$$

4.4.2 *Spectral Characteristics*

The clutter spectrum for Rayleigh clutter is assumed gaussian, with an rms spectral spread determined by internal clutter motion. In surveillance radar, however, the scanning motion of the antenna introduces a spectral spread to the clutter spectrum due to the added velocity component induced by the antenna motion. The rms width of the spectral component due to scanning is given by [5]:

$$\sigma^o_{sc} = 2\surd(Ln2) * w/(f_3\theta_3) \qquad (4.4.2\text{-}1)$$

Further spectral spreading may result from transmitter instabilities and platform motion. Assuming a stationary system, the primary cause for spectral spreading will be antenna scanning. The variance of the complete spectrum will be given by the sum of variances of the individual components:

$$\sigma_c^2 = \sigma_f^2 + \sigma_{scan}^2 \qquad (4.4.2\text{-}2)$$

where:

$$\sigma_f' = 2\sigma_v/\lambda \qquad (4.4.2\text{-}3)$$

4.4.3 *Land Clutter Simulation*

Although the cross-section distribution of land clutter may be more accurately modelled by non-gaussian distributions such as log-normal and Weibull, an accurate representation of a non-gaussian clutter model requires the complete multi-dimensional probability density function to be specified. For a Rayleigh clutter model, the underlying statistics are gaussian, and the multi-dimensional probability density function is specified by its mean and covariance functions.

The non-gaussian process, however, requires higher order moments to be determined. In order to overcome this, the clutter process is modelled as a Rayleigh distribution with a variable mean backscatter coefficient $<\sigma^{o}>$. Within a radar scan, the mean backscatter coefficient is assumed to be constant, and the cross-section fluctuation described by an exponential distribution. However, on a scan-to-scan basis the mean value $<\sigma^{o}>$ is determined by a non-gaussian distribution with a correlation time in the order of five to ten seconds. Further sophistication may be introduced into the clutter model by including the simple clutter model (4.4.1-3) to modify the average backscatter coefficient applicable to a given terrain as a function of range. The thus calculated value of $<\sigma^{o}>$ is used in the non-gaussian distribution to determine the scan-to-scan values of the variable average backscatter coefficient as used in the within-scan exponential distribution.

The received clutter power from a radar resolution cell can be related to the radar parameters according to:

$$P_c = \frac{P_T\, G_T\, G_R\, \lambda^2\, \sigma_o\, A_c\, F_c^4}{(4\pi)^3\, R^4\, L_c} \qquad (4.4.3\text{-}1)$$

where:

σ^{o} is the backscatter coefficient

F_c is the propagation factor

L_c is a loss factor

A_c is the clutter cross-sectional area.

Assuming that the ensemble average power $< \| U(\theta,\tau_m) \| >$ is representative of the returned clutter power for a resolution cell, the average power will consist of a number of spectral contributors such that:

$$\sum_n \| < U(\theta,\tau_m,f_{dn})^2 > \| = \| < U(\theta,\tau_m)^2 > \| \qquad (4.4.3\text{-}2)$$

The statistical fluctuation of the received clutter power will be reflected in the amplitudes of the contributing spectral component phasors. A gaussian approximation is used to represent the spectral components of the clutter signal [32].

4.5 VERIFICATION OF THE SIMULATION PROCESS

In order to establish confidence in the results of the simulation process, the simulation results were compared to published data in three specific areas:

- False alarm probability versus threshold.
- Detection probability versus signal-to-noise ratio.
- Azimuth accuracy for specific estimators.

4.5.1 False Alarm Probability

The probability of false alarm is defined in the literature as the probability that a noise fluctuation is mistaken as a signal return. In the original work by Marcum [30] a false alarm time is defined as the time in which the probability (P_o) is 0.5 that the noise will not exceed a bias level. In his original work Marcum described the method and provided numerical results for the determination of the bias level under the assumption that the noise was of a thermal nature. Marcum has also defined a false alarm number, n', which defines the number of independent opportunities for a false alarm during the false alarm time. The false alarm probability P_f is related to the false alarm number via

$$P_o = 0.5 = (1-P_f)^{n'} \qquad (4.5.1\text{-}1)$$

which for large false alarm numbers can be approximated by:

$$P_f = 1/n' * \ln(1/P_o) \qquad (4.5.1\text{-}2)$$

The bias level applied to the thermal noise is a function of the number of independent pulses integrated, the detector law and integrator law and whether the integration performed is analogue or binary.

The original work by Marcum provided the mathematics and results for analogue integrated data using a linear detector. Extensive tables were later published by Pachares [34] for the square law detector and linear analogue integration.

The bias levels applied to the simulated data for linear and square law detectors and linear (equally weighted samples) analogue integration were determined by an approximate expression as described by V Gregers-Hansen [23]. In the approximation the bias Yb is expressed in terms of a mean value m_N and a standard deviation together with a threshold constant:

$$Y_b \quad = \quad m_N + k_b\sigma_N \qquad (4.5.1\text{-}3)$$

Tables 4.5.1-1 and 4.5.1-2 summarize the expressions applied in calculating the bias level.

Table 4.5.1-1: Linear detector bias levels

m_N	1.2533 N
σ_N	$0.65514\sqrt{N}$
k_b	$(k_{b1}-k_{b\infty})[0.8(N-1)+1]^{-0.39} + k_{b\infty})$
$k_{b\infty}$	$g - [(2.515517 + 0.802853g + 0.01033g^2)/$
	$(1.0 + 1.432788g + 0.1889269g^2 + 0.001308g^3)]$
g	$\sqrt{[-2\ln(P_f)]}$
k_{b1}	(g - 1.2533) / 0.65514

Table 4.5.1-2: Square law detector bias levels

m_N	N
σ_N	$\surd N$
k_b	$(k_{b1}-k_{b\infty})[1.1(N-1)+1]^{-0.51} + k_{b\infty})$
$k_{b\infty}$	$g - [(2.515517 + 0.802853g + 0.01033g^2)/$
	$(1.0 + 1.432788g + 0.1889269g^2 + 0.001308g^3)]$
g	$\surd[-2\ln(P_f)]$
k_{b1}	$-\ln(P_f) - 1$

Similarly, the bias levels applied for binary integration were determined by the equations summarized in table 4.5.1-3.

Table 4.5.1-3: Binary integration bias levels Yb

Linear Law	Square Law
$\surd[-2\ln(P_f)]$	$-\ln(P_f)$

Fundamental to the bias level calculations is the assumption that the noise is white. In order to ensure that this assumption is valid, the simulated noise was examined for distribution and spectral characteristics. A Chi-square test was performed on batches of 100 noise samples to ascertain the validity of the hypothesis that the noise generated complies with a gaussian distribution.

The spectral characteristics of the generated noise samples was determined using the Wiener-Kninchine theorem. According to this theorem, the auto-correlation function and the power spectral density are related by the Fourier transform. For a white spectrum, the power spectral density is a constant defined as:

$$S_n(w) = N_o \qquad (4.5.1\text{-}4)$$

The auto correlation function of the noise shall then be:

$$R(\tau) = F^{-1}[S_n(w)] \\ = N_0\,\delta(\tau) \qquad (4.5.1\text{-}5)$$

For a stationary random signal a(n), the auto correlation sequence is defined to be [26]:

$$r(m) = E[\,a(n)\,a^*(n+m)\,] \qquad (4.5.1\text{-}6)$$

Given a finite set of data samples [a(0), a(1),...,a(N-1)], an unbiased estimate of the auto correlation sequence is given by:

$$r'(m) = \frac{1}{N - \|m\|} * \sum_{n=0}^{N-1-\|m\|} [\,a(n)\,a^*(n+m)\,] \qquad (4.5.1\text{-}7)$$

However, due to the large variance in values obtained as m approaches N, a biased estimator is normally applied:

$$r'(m) = \frac{1}{N} * \sum_{n=0}^{N-1-\|m\|} [\,a(n)\,a^*(n+m)\,] \qquad (4.5.1\text{-}8)$$

For different batches of noise samples the auto correlation sequence was determined and the impulse nature of the sequence verified. Figure 4.5.1-1 illustrates the results of one such run.

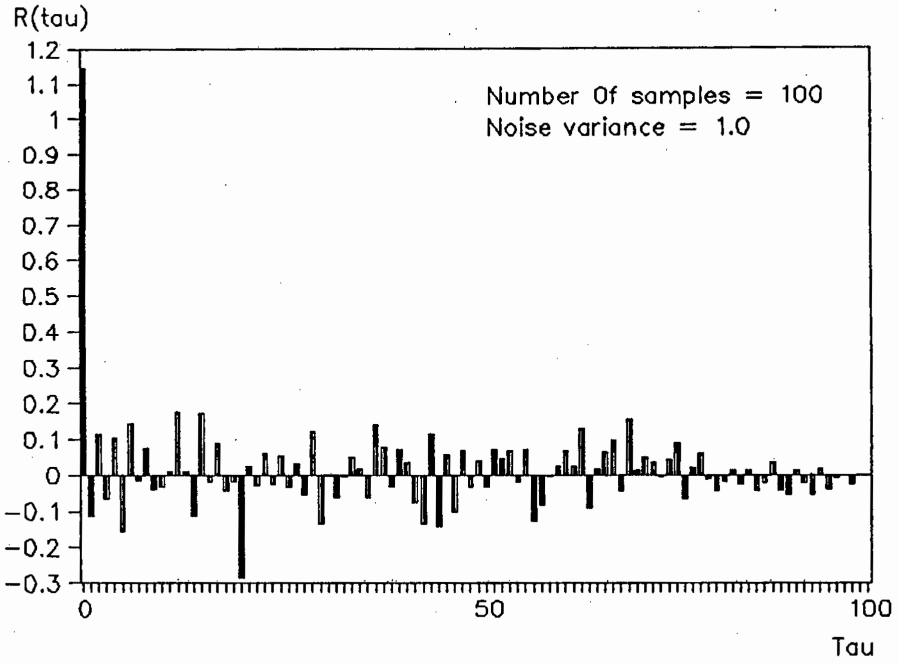

Figure 4.5.1-1: Noise autccorrelation sequence

The probability of false alarm was determined via direct Monte Carlo methods. The relative simulation error is related to the required number of iterations and the probability being estimated according to [40]:

$$N = 9(1-p)/(pd^2) \qquad (4.5.1\text{-}9)$$

where:

N is the required number of iterations

p is the event probability

d is the relative simulation error (p'-p)/p

p' is the estimated probability.

The number of iterations were limited to 10^5 for practical reasons, thereby increasing the relative simulation error for very small false alarm probabilities. Table 4.5.1-4 indicates the different probabilities estimated, the number of iterations performed and the results achieved.

Table 4.5.1-4: Estimated false alarm probabilities

Pf	d	N	Linear law	Square law
True	Error	Samples	P_f Estimate	P_f Estimate
0.3	0.1	2100	0.308	0.309
0.1	0.1	8100	0.094	0.105
0.03	0.1	29100	0.029	0.031
0.01	0.1	89100	0.010	0.010
0.003	0.2	74775	0.0029	0.00295
0.001	0.3	99900	0.00097	0.00096

4.5.2 Probability of Detection

In 1962, L. F. Fehlner [19] published an extensive set of curves based on the original work by Marcum and Swerling. In the publication Fehlner recalculated the probability of detection as a function of the ratio of signal energy to noise energy at the output of the matched filter. Di Franco and Rubin [16] published a similar set of curves in 1968.

The curves were calculated for the non-fluctuating as well as fluctuating (Swerling) target models assuming square law detection and linear analogue integration. However, as a result of different definitions for signal-to-noise ratio (both of which are used in the radar literature), a 3 dB discrepancy between the curves published by Fehlner and those published by Di Franco and Rubin exist.

In order to verify the correct detection characteristics of the simulation process, Monte Carlo simulations were performed for a specific false alarm number (which relates to the false alarm probability according to 4.5.1-1) and the resulting curves were compared to those published by [19] and [16] (Appendix B).

As with the false alarm iterations, the number of samples required for the detection probabilities were determined by equation (4.5.1-9). The limitation imposed on the number of iterations due to practical reasons resulted in a reduced accuracy at lower signal-to-noise ratios.

4.5.3 Azimuth Accuracy

The application of specific detector and estimator techniques with the aid of the simulation program has enabled comparison of the achieved positional estimates in azimuth with curves published in the literature. However, the number of articles which study the problem of angular position estimation are limited, and sufficient information is not always provided to enable the simulation parameters to be defined, or to distinguish whether any additional processing was applied in the determination of the estimate statistics.

The estimation of azimuth position employing a linear detector and linear analogue integration was examined by V. Gregers-Hansen [22]. In the article, curves indicating the normalized standard deviation of the azimuth estimate for the non-fluctuating and fast-fluctuating case have been plotted assuming a sinx/x antenna pattern. Furthermore, Gregers-Hansen applied a resolution criterion in the article in which additional target detections which occurred within a beamwidth of the initial detection were rejected. The results of simulations applying the same rules and system parameters as indicated in the article yielded a set of graphs as illustrated in figures 4.5.3-1 and 4.5.3-2.

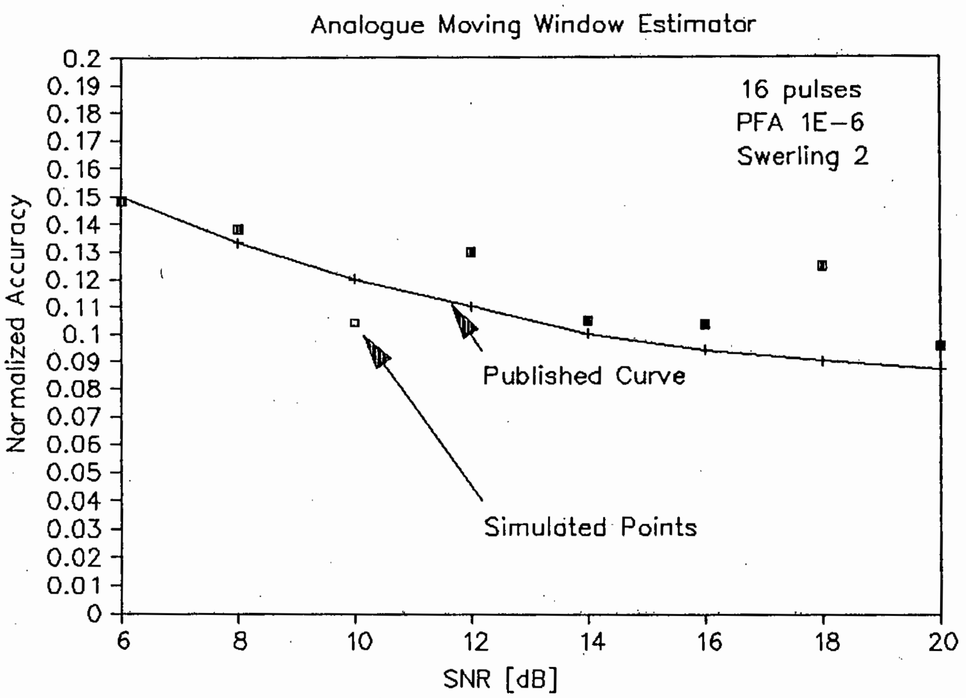

Figure 4.5.3-1: Analogue moving window estimator for Swerling model 2

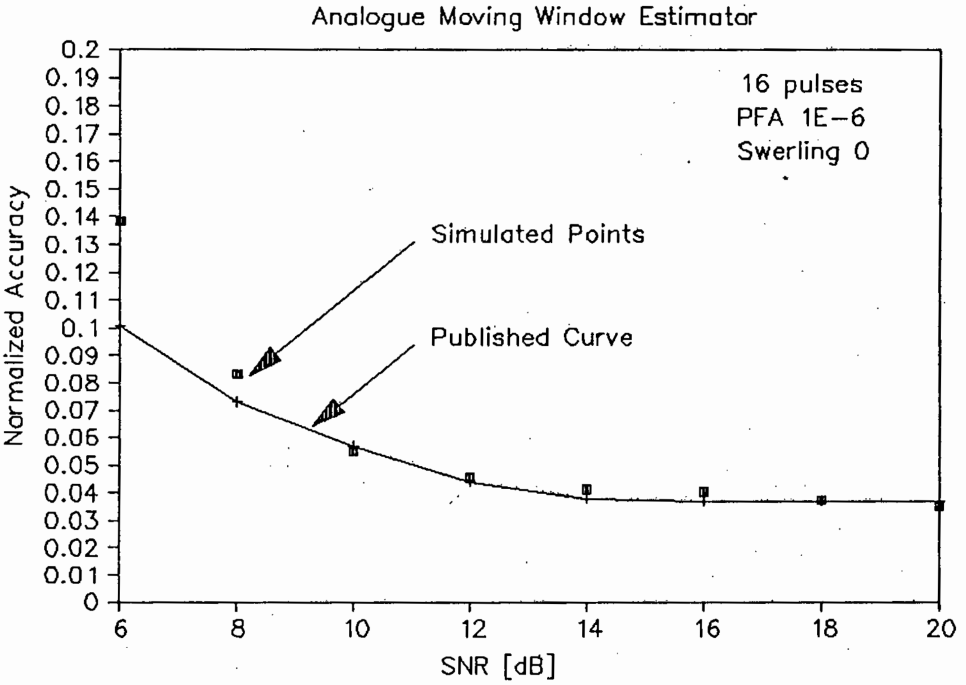

Figure 4.5.3-2: Analogue moving window estimator for Swerling model 0

It should be pointed out here that the results presented by Gregers-Hansen indicate a wide spread in the simulated points, and that the curves shown in figures 4.5.3-1 and 4.5.3-2 represent the curves fitted to the data points in the article.

Performance evaluation of the binary processing simulation was achieved by comparing the results of the simulations for Swerling models 0, 1 and 2 with curves published in an article authored by G. Galati and F. Studer [20]. Figures 4.5.3-3 through 4.5.3-5 illustrate the achieved results in relation to the published graphs. Initial work indicated reasonable similarity for the Swerling 1 and 2 models, as indicated in figures 4.5.3-4 and 4.5.3-5. The simulated results tend to indicate a slightly worse normalized accuracy than those published by the authors. The cause of this may be found in the fact that the authors do not appear to have included the effect an asynchronous pulse transmission relative to the antenna rotation (figure 4.3.5-6). The pulse transmitted at the beam centre may vary $\pm\theta/2$ about the nose of the beam, resulting in the signal-to-noise ratio not always reaching an optimum. Furthermore, the results presented by the authors consist of curves fitted to the simulation results. No indication is given regarding the spread of the results or the accuracy of the curves fitted.

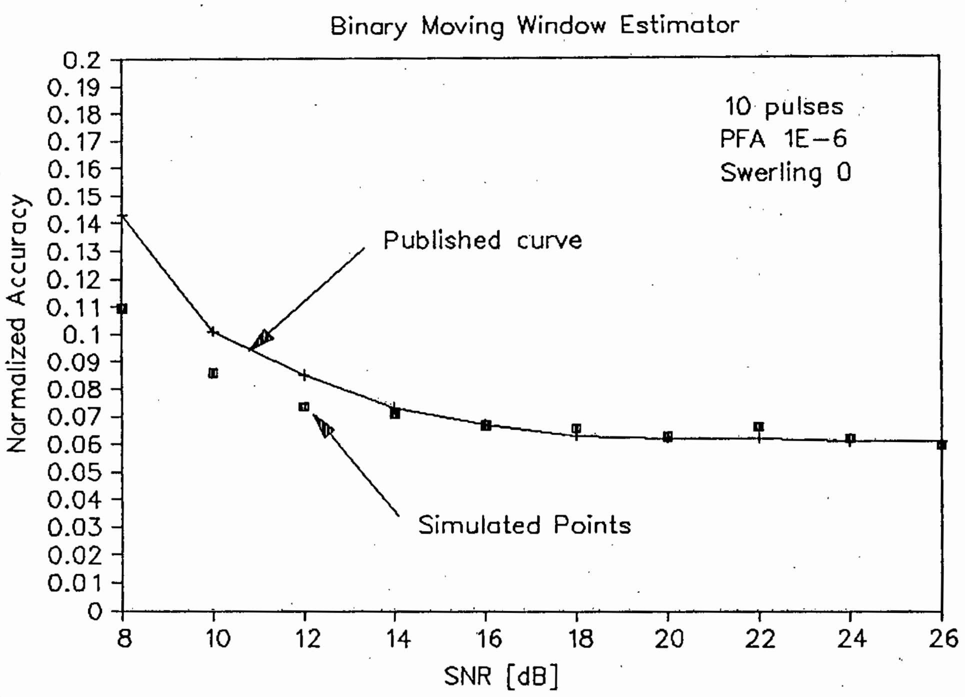

Figure 4.5.3-3: Binary moving window estimator Swerling 0

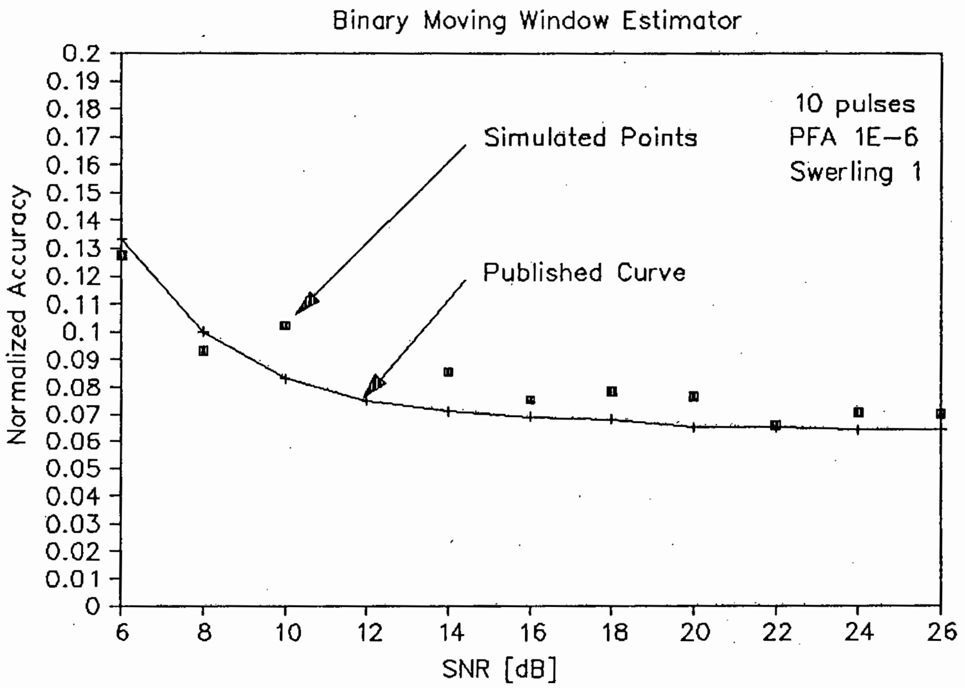

Figure 4.5.3-4: Binary moving window estimator Swerling 1

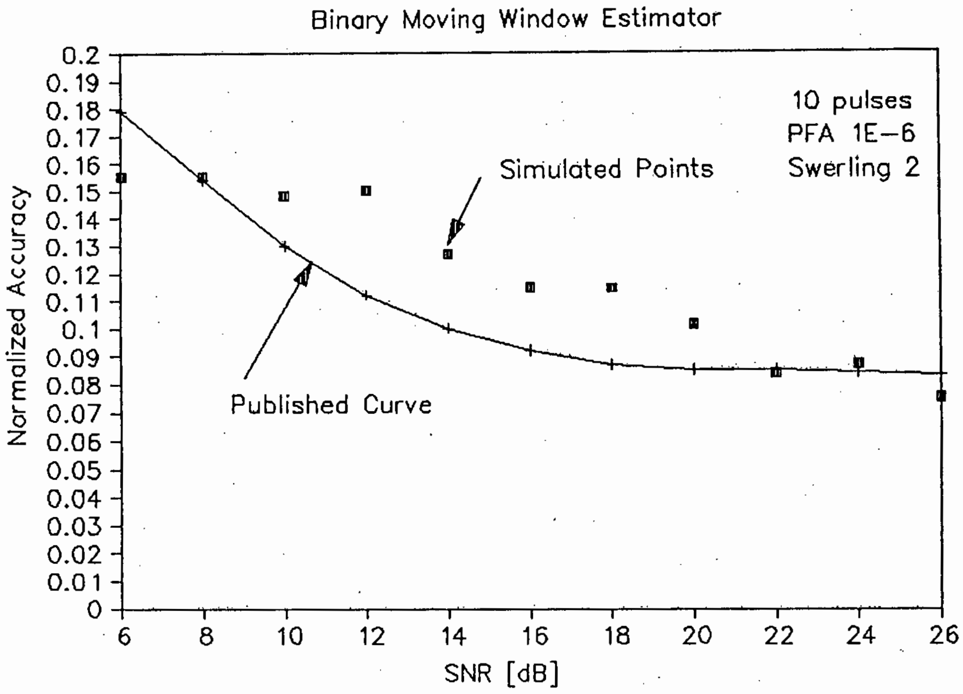

Figure 4.5.3-5: Binary moving window estimator Swerling 2

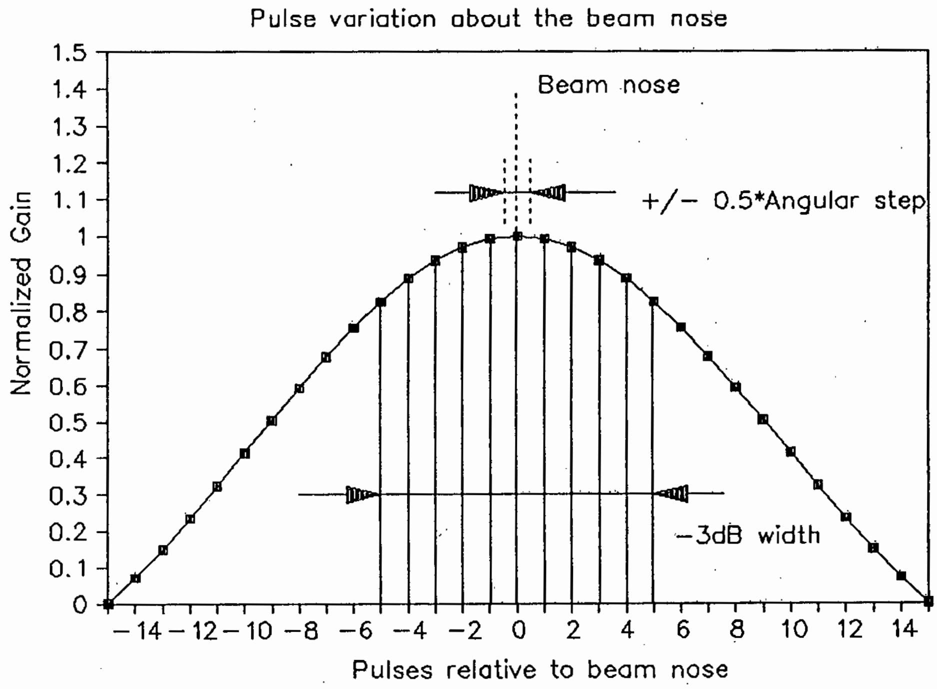

Figure 4.5.3-6: Variation of the pulse transmission

Results achieved with the Swerling 0 model indicate a discrepancy between the achieved accuracy and those found by the authors (figure 4.5.3-3). To establish the cause of this discrepancy, the probability of detection curves depicted in the article for the case of 10 pulses integrated were compared with curves published by D. K. Barton [5]. According to the curves published by Galati and Studer, the integration of 10 pulses will yield a 25% single scan probability of detection at a single-pulse signal-to-noise ratio of 5 dB [20]. Application of standard detection probability curves [5] show that a 25% probability of detection for the non-fluctuating case is achieved with an equivalent single-pulse signal-to-noise ratio of 10 dB. The equivalent single-pulse signal-to-noise ratio for n-pulse integration may be calculated according to [5]:

$$Do(1) = \frac{nX_1^2}{X_1 + 2.3} * [\, 0.5 + 0.5\sqrt{ 1 + \frac{9.2}{nX_1^2}(X_1 + 2.3) } \tag{4.5.3-1}$$

where:

X_1 represents the signal-to-noise ratio at the intermediate frequency

n represents the number of pulses integrated.

Application of equation 4.5.3-1 for 10 pulses integrated and the single-pulse ratio of 5 dB yields an equivalent single-pulse signal-to-noise ratio of 13 dB as opposed to the 10 dB [5]. Taking into account a 1.5 dB loss due to the binary integrator [6], an equivalent single-pulse signal-to-noise ratio of 11.5 dB results. A 1.5 dB discrepancy thus appears to exist between the detection probability curves published by Galati and Studer and standard detection curves. In order to establish whether this discrepancy may explain the difference in accuracy performance for the Swerling 0 model, the simulations were run with a 1.5 dB correction (reduction) applied to the signal-to-noise ratio in order to achieve the same detection probabilities. The results of this experiment are illustrated in figure 4.5.3-7. It is apparent from figure 4.5.3-7 that the achieved accuracy with the simulations correspond much closer to the curve published by Galati and Studer with the 1.5 dB correction applied. It may therefore be concluded that the curves published by Galati and Studer for the Swerling 0 case are incorrect. A similar examination of the detection probability curves for the Swerling 1 and 2 curves did not highlight any discrepancies. This is supported by the similarity in simulated to published results for these two models. Based on the previous results, no corrections have been applied to the signal-to-noise ratio in any of the simulations run for the accuracy evaluations.

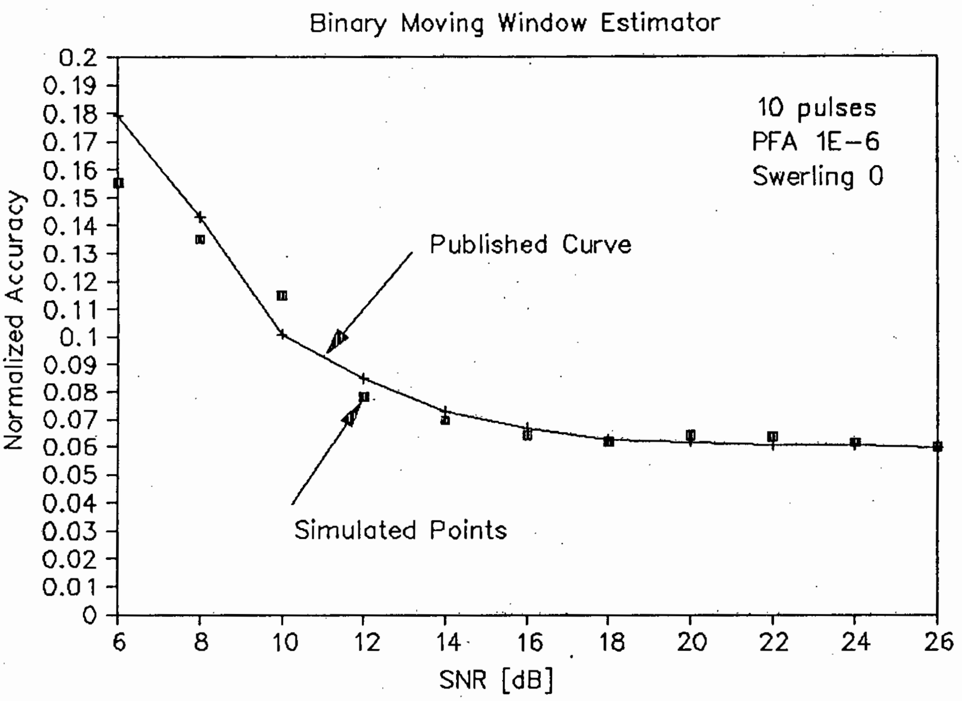

Figure 4.5.3-7: Corrected signal-to-noise accuracy curve

4.6 AZIMUTH ESTIMATORS

Azimuth estimators aim to establish the angular location of a scattering object within the radar resolution cell. Theoretically, if the antenna beam pattern were known exactly, and no noise entered the radar system from any source, the azimuth accuracy would be limited by the quantization of the antenna position encoder. In practice, however, the existence of receiver noise, scatterer radar cross-section fluctuation and other noise sources limit the achievable azimuth accuracy. The ideal estimator attempts to minimize the influence of noise as effectively as possible by sensing the system response function in the azimuth coordinate. For the pulsed scanning radar this is effectively the sequence of received pulse returns from the scatterer weighted by the antenna pattern. Broadly, practical estimators can be categorized into two classes:

- Unbiased estimators in which the expected value is equal to the parameter of interest. Examples of these are estimators which convolve the received pulse train with an odd-symmetrical pattern of weights and subsequently detect a zero-crossing.
- Biased estimators in which an offset is present between the expected value and the parameter of interest. This bias may be dependant on- or independent of signal-to-noise ratio, depending on the estimator applied.

Pulsed radar systems generally sample the returns from the transmitted pulses, thereby quantizing the detection range into discrete intervals (range bins). Envelope or square law detection allow the signal amplitude to be determined within each discrete range interval. A practical implementation of an estimator requires the train of pulse amplitudes received within the main beam of the antenna to be stored for each range interval.

4.6.1 Unbiased Estimators

The most well-known of the unbiased estimators is the maximum likelihood estimator [9]. With this type of estimator, the sequence of pulse amplitudes at a given range interval are multiplied with a set of odd-symmetrical weights, and the azimuth location determined by the point at which the weighted sum of amplitudes is zero (Figure 4.6.1-1).

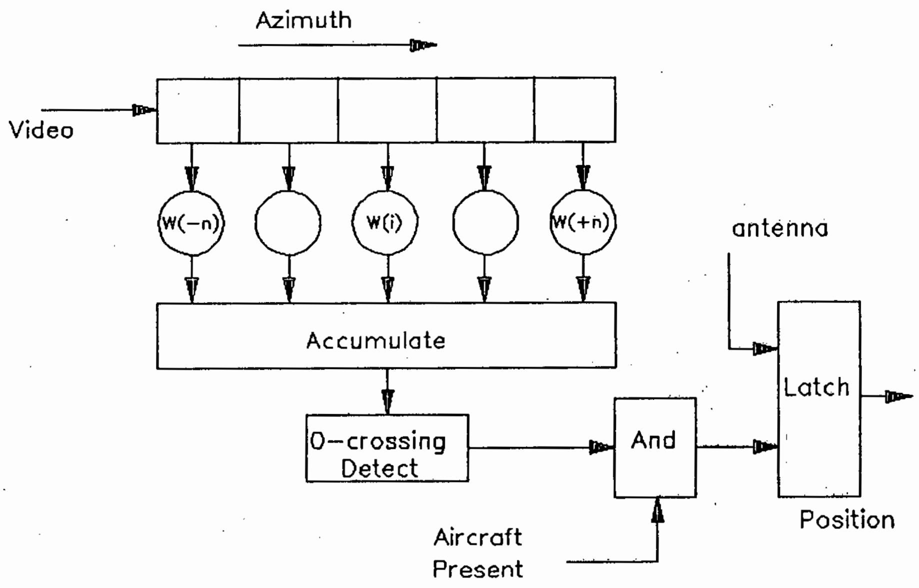

Figure 4.6.1-1: Maximum likelihood estimator

Bernstein [9] established that the optimum weights wi are given by:

$$w_i = \frac{B_3(\theta)}{[1 + K_m{}^2 B^4(\theta)]^2} * \frac{\partial B(\theta)}{\partial \theta} \qquad (4.6.1\text{-}1)$$

where:

$B(\theta)$ is the one-way antenna voltage pattern

K_m is the voltage signal-to-noise ratio on the beam axis.

For a symmetrical antenna pattern, any odd-symmetrical pattern of weights will yield an unbiased estimate. Other examples of weighting are rectangular weighting and pseudo-centre of gravity weighting (Figure 4.6.1-2). A reduction in storage requirements may be achieved by thresholding each signal amplitude and weighting the binary results. The azimuth location is still determined by establishing the zero-crossing point of the weighted sum. (Figure 4.6.1-3).

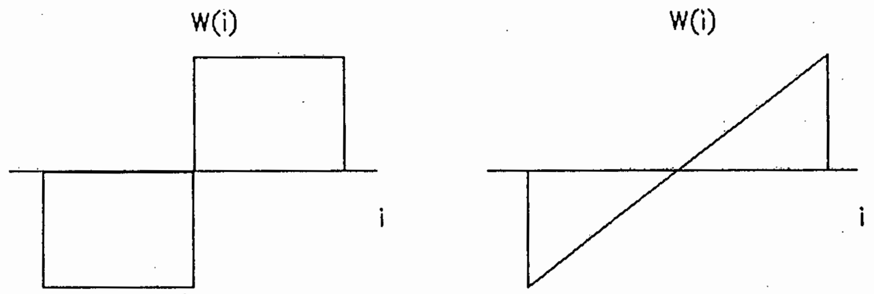

Figure 4.6.1-2: Odd-symmetrical weights

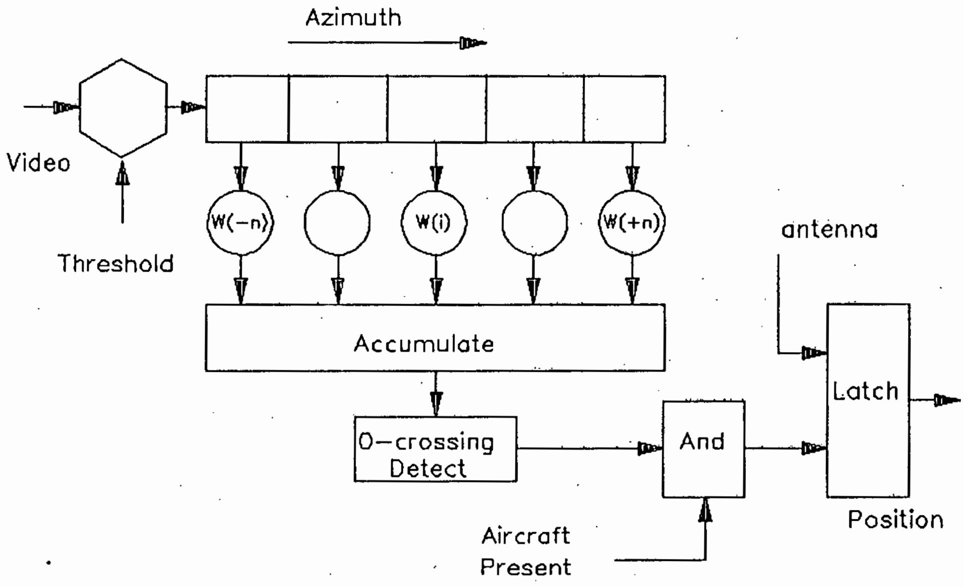

Figure 4.6.1-3: Weighted binary estimator

The optimum weights for this estimator as determined by Bernstein are given by [9]:

$$w_i = 2\,\tau^2 K_m{}^2 \frac{B_3(\theta)}{K_m{}^2 B^4(\theta)]^2} * \frac{\partial B(\theta)}{\partial \theta} \qquad (4.6.1\text{-}2)$$

where:

$$\tau = \surd[-2\mathrm{Ln}(P_f)] \qquad (4.6.1\text{-}3)$$

The availability of amplitude information enables the azimuth position to be established via alternative methods, such as establishing the angle at which the largest amplitude occurs. Improved accuracy may be achieved by establishing the angles at which the two largest returns within a received pulse train occur, and estimating the angle according to [43]:

$$\theta' = \theta + \delta\theta/2 + 1/(2a\delta\theta) * \ln(A_2/A_1) \qquad (4.6.1\text{-}4)$$

where:

θ_1 is the angle at which the largest amplitude occurs

θ_2 is the angle at which the second largest amplitude occurs

$\delta\theta = \theta_1 - \theta_2$

$a = 1.386/(\theta_3)^2$

θ' is θ_1 if $\theta' < \theta_1$

θ' is θ_2 if $\theta' > \theta_2$.

The application of the weighting and amplitude ratio estimators requires a separate detection mechanism to indicate target presence. Typically, a moving window integrator may be used, and consequently the detection performance is determined by the integrator.

A hybrid version of the weighting estimator may be found in the batch processor [48] (figure 4.6.1-4).

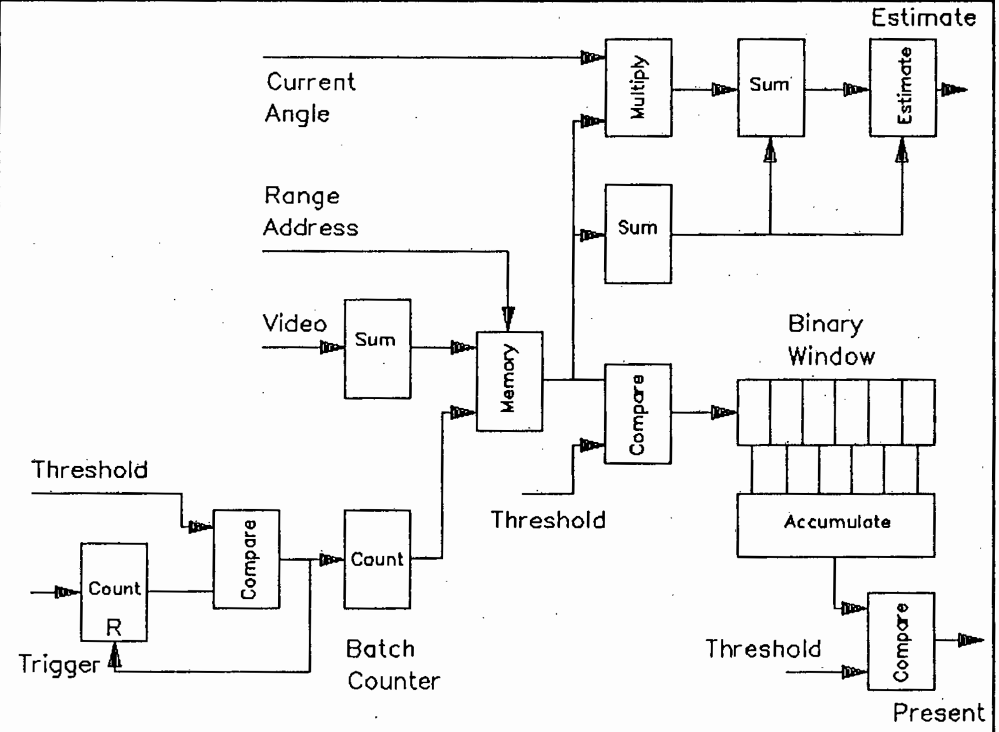

Figure 4.6.1-4: Batch processor estimator

This type of estimator operates on batches of pulses, and is really applicable to systems with a large number of pulses returned within a beam. Basically, the N returned pulses within the half-power beamwidth are grouped into k batches of n pulses, where $N=k*n$. The signal amplitudes in each batch are summed and the resulting sum thresholded to yield either a one (threshold crossed) or a zero. The resulting k binary values are subsequently summed and compared to a second threshold in order to establish target presence. An estimate of the azimuth location is formed by:

$$\theta' = \frac{\sum_{i=1}^{k} B_i\theta_i}{\sum_{i=1}^{k} B_i} \qquad (4.6.1\text{-}5)$$

where:

B_i is the amplitude of the n summed pulse amplitudes within a batch

θ_i is the angle corresponding to the centre of the batch.

The detection performance of the batch processor is approximately 0.5 dB worse than that of the analogue moving window for a large number of pulses. Calculation of the threshold settings for a given false alarm probability require the false alarm probability per binary sample into the binary integrator to be determined according to:

$$M = 1.5\sqrt{K} \qquad (4.6.1\text{-}6)$$

$$P_{fa\text{-}out} = \sum_{j=M} \binom{K}{j} (P_{fa\text{-}in})^{j} * (1-P_{fa\text{-}in})^{K-j} \qquad (4.6.1\text{-}7)$$

where:

K is the number of batches within the half-power beamwidth

M is the binary window second threshold

$P_{fa\text{-}in}$ represents the false alarm probability of the binary pulses input into the binary integrator

$P_{fa\text{-}out}$ represents the false alarm probability out of the binary integrator.

The threshold setting for the summed pulse amplitudes within a batch is then determined according to Table 4.5.1-1 or 4.5.1-2 for a probability of false alarm equal to that calculated for the input to the binary integrator.

4.6.2 Biased Estimators

The group of biased estimators yield an azimuth estimate which is offset from the true azimuth position. Generally, these estimators attempt to establish the start- and the end angle of an object as the antenna beam scans past. The simplest form of this is given by the analogue moving window integrator. The start angle of the object is signified by the angle at which the sum of the video amplitudes within the half-power beamwidth exceeds a particular threshold, while the end angle is signified by the angle at which the summed video falls below the threshold. The azimuth position is then taken as the centre between the start- and end angle (beamsplitting). The binary integrator uses the same principle, but rather that integrating the signal amplitudes, the individual amplitudes are compared to a given threshold, and the binary results are summed and thresholded (figure 4.6.2-1).

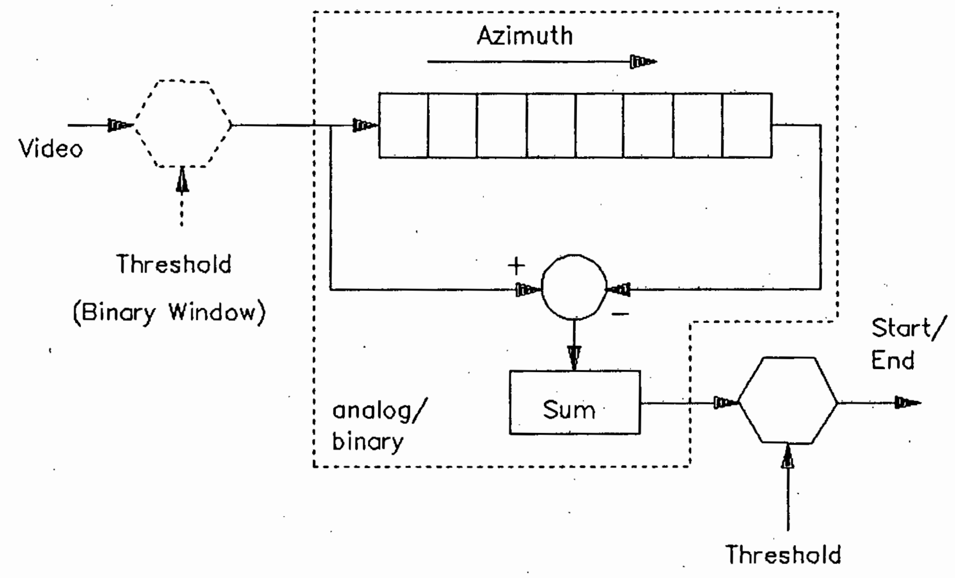

Figure 4.6.2-1: Analogue and binary moving window

The detection performance and threshold settings for the analogue and binary integrators are well documented in the literature. Skolnik [43] states that for large numbers of pulses, the detection performance of the binary integrator is approximately 2 dB less than that of the analogue integrator. Variations to the analogue moving window integrator are the feedback integrator [48] and the two-pole filter. The feedback integrator is given by (figure 4.6.2-2)

$$S_i = a S_{i-1} + x_i \qquad (4.6.2\text{-}1)$$

where:

x_i is the pulse amplitude

α is the feedback factor.

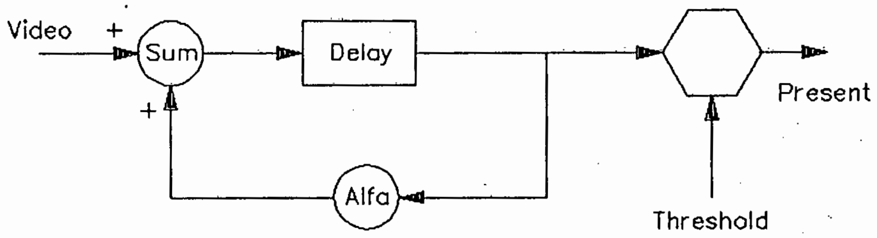

Figure 4.6.2-2: Feedback integrator

The two-pole filter is given by (figure 4.6.2-3):

$$y_i = x_i - k_2 z_{i-1} \tag{4.6.2-2}$$

$$z_i = y_{i-1} + k_1 z_{i-1} \tag{4.6.2-3}$$

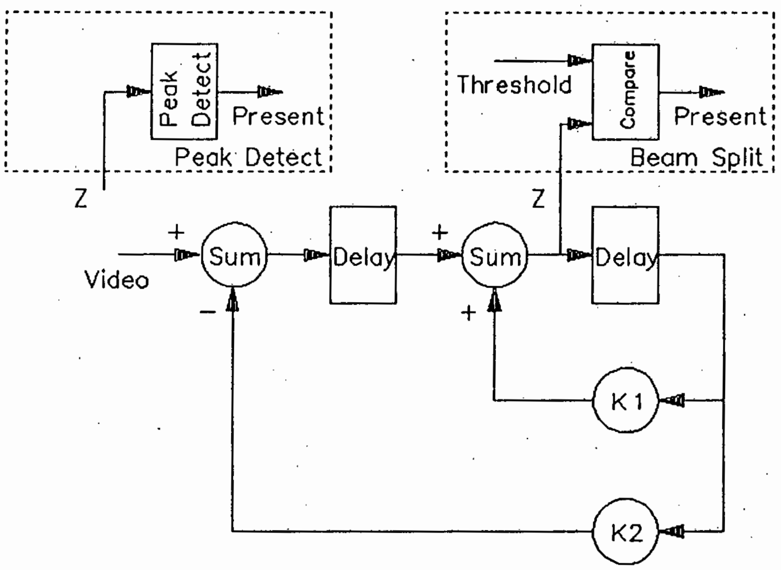

Figure 4.6.2-3: Two-pole filter

Both integrators allow the azimuth position to be estimated by either thresholding the integrator output and applying a beamsplitting technique, or by determining the angle at which the maximum value occurs. The detection performance of the feedback integrator is given by the detection performance of an analogue integrator with an equivalent number of pulses integrated:

$$M_{eq} = 1/(1-\alpha) \qquad (4.6.2\text{-}4)$$

Maximum detection probability is achieved if:

$$M_{eq} = 0.63N \qquad (4.6.2\text{-}5)$$

where:

N is the number of pulses within the half-power beamwidth.

For the two-pole filter, maximum detection probability is achieved with feedback factors:

$$k_1 = 2 * \exp[\frac{\xi w_d \tau}{\sqrt{[1-\xi^2]}}] \cos(w_d \tau) \qquad (4.6.2\text{-}6)$$

$$k_2 = 2 * \exp[\frac{-2 \xi w_d \tau}{\sqrt{[1-\xi^2]}}] \qquad (4.6.2\text{-}7)$$

where:

$\xi = 0.63$

$N w_d \tau = 2.2.$

For large numbers of pulses, the probability density function of the filter becomes nearly gaussian, and threshold settings may be determined from normal curves to achieve a given probability of false alarm.

Binary azimuth estimation methods have introduced different variations to the binary integrator. Basically, counters are driven up or down by the binary quantized signal amplitudes according to specific rules. Examples of counter rules are:

1. Success-run detector [17]: The success-run detector establishes the presence of a target by measuring the recurrence time of some event.

The simplest application measures the recurrence time by counting the number of pulse repetition intervals between events. If the count value exceeds a given threshold, a target is declared and its azimuth position estimated by (figure 4.6.2-4)

$$pri_{centre} = pri_{current} - counter/2 \qquad (4.6.2\text{-}8)$$

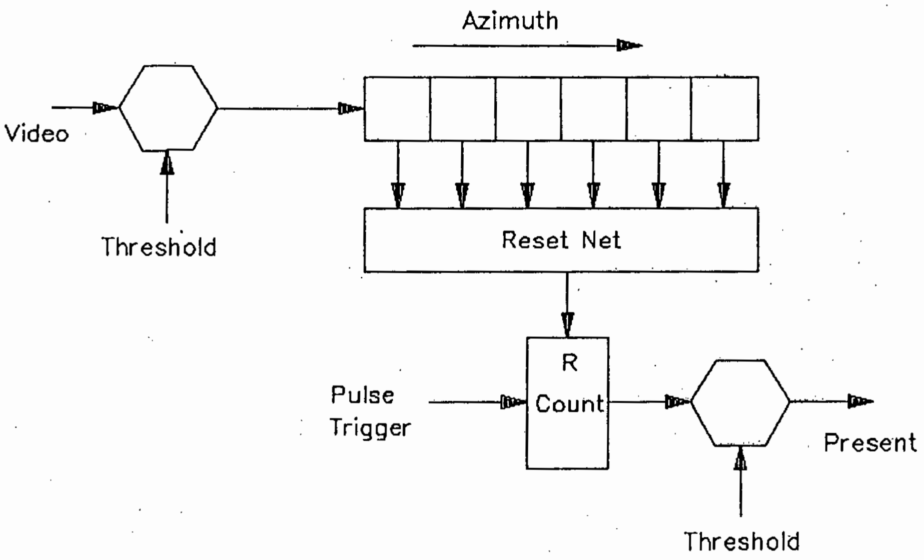

Figure 4.6.2-4: Success-run estimator

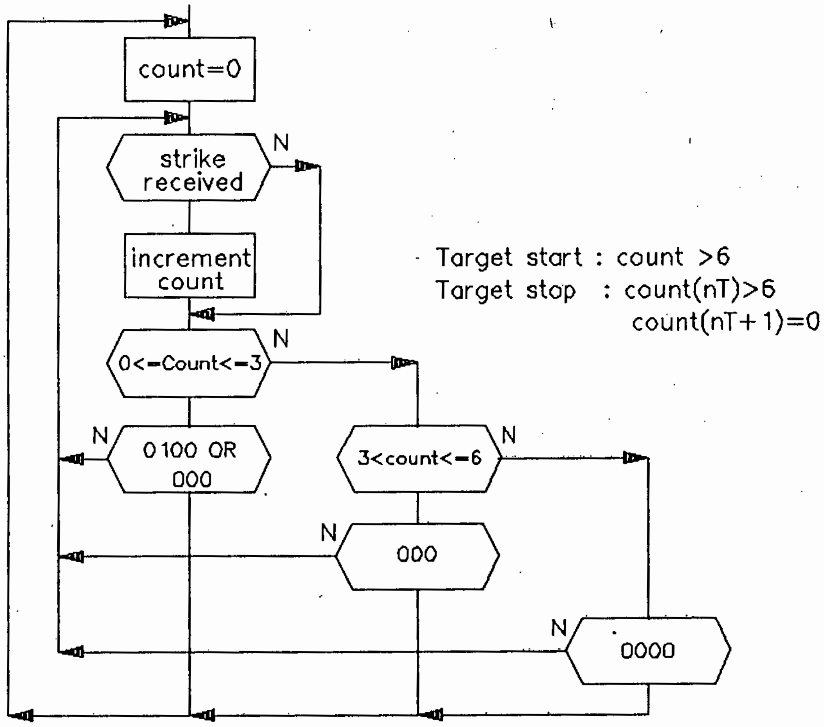

Figure 4.6.2-5: Alternative success-run estimator rules

A more elaborate configuration may detect on the basis of the recurrence of one of several events, as shown in figure 4.6.2-5. The azimuth position is estimated by determining the centre between the start and end declarations of the target. The false alarm threshold setting for this type of detector may be determined from the event probabilities for the counter. For the success-run detector of figure 4.6.2-5, Dinneen and Reed [17] have shown that the probability of the counter assuming a zero value, xo, is given by:

$$xo = \frac{(1-p)^4}{1-p(1-p)^2-p(1-p)^3-2p^2(1-p)^3-p^3(1-p)^3-p^3(1-p)^4} \qquad (4.6.2\text{-}9)$$

where:

p is the probability of a single pulse threshold crossing.

The probability of detecting a false target with the illustrated success-run detector is given by the probability of the counter attaining a value of 7:

$$x^7 = px^6 + p(1-p)x^5 + p(1-p)^2x^4 \qquad (4.6.2\text{-}10)$$

2. Sequential observer: The sequential observer increments a counter by "r" steps each time the pulse amplitude exceeds the quantization threshold, while pulse amplitudes which do not exceed the quantization threshold decrement the counter by "s" steps. The start of the target is declared whenever the count exceeds a detection threshold, while the end occurs when the counter falls below the detection threshold (figure 4.6.2-6). A variation to this mechanism is found by counting the counter up and down with uniform steps, and resetting the counter on occurrence of two consecutive zero's (figure 4.6.2-7).

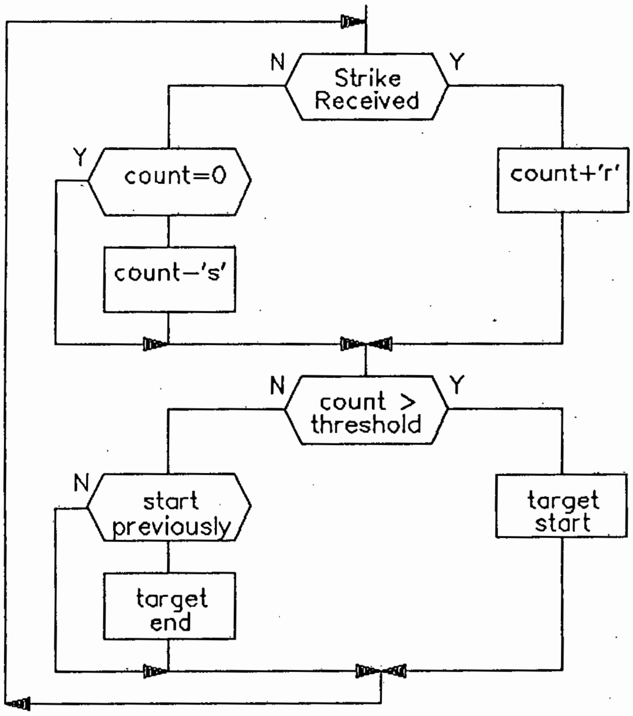

Figure 4.6.2-6: Sequential observer estimator1

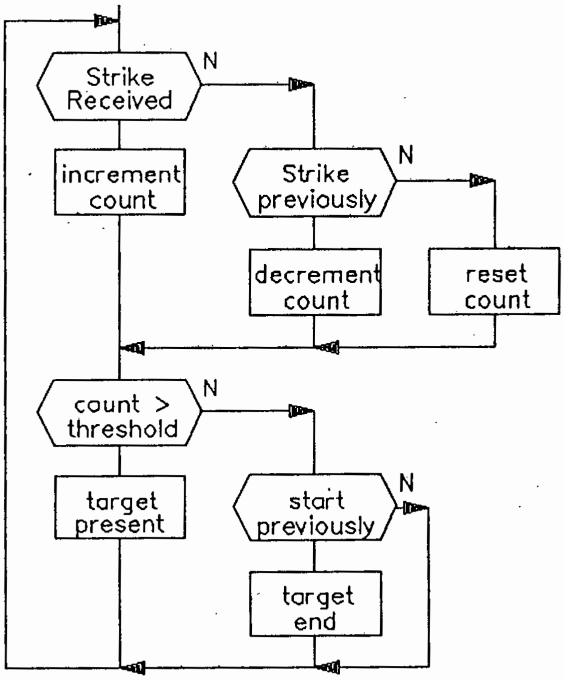

Figure 4.6.2-7: Sequential observer estimator2

The threshold settings for the two detectors have been determined by Blythe [12] and are given by:

Sequential observer 1: For small output false alarm probabilities (1E-6)

$$P_{fa} = q(1-2p/q)^2 \, Q_o(L) \tag{4.6.2-11}$$

Sequential observer 2:

$$P_{fa} = p \, q^2 \, [p(1+q)]^{L-1} \tag{4.6.2-12}$$

where:

p is the single pulse probability of false alarm

$$q = 1-p \tag{4.6.2-13}$$

L is the detection threshold

$$Q_o(m) = \sum_{r=}^{M} {}^{m-r}C_r \left(\frac{p}{q}\right)^{m-r} \tag{4.6.2-14}$$

5.0 EVALUATION METHOD AND RESULTS OBTAINED

5.1 EVALUATION METHOD

The evaluation of estimator accuracies has been achieved with the aid of a video signal simulation program developed in C. The primary components of the simulation program are illustrated in figure 5.1-1.

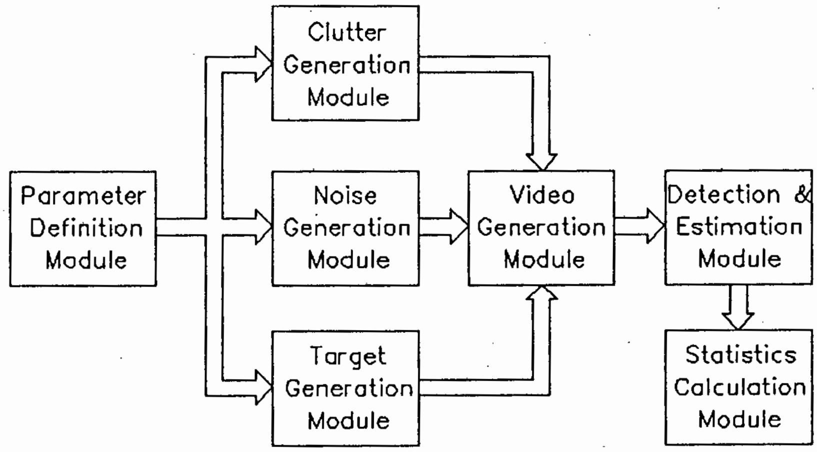

Figure 5.1-1: Simulation program primary components

A parameter definition module enables radar system-, target-, clutter parameters, data processing rules and simulation constraints to be defined (Appendix C). The clutter module generates the clutter return received at the radar utilizing a log-normal clutter model. Gaussian noise is generated by a noise generation module while the return from a target is generated in the target module. The composite return resulting from the noise, clutter and target sources is generated by the video signal module. Subsequent processing of the video signal is performed by the detection and estimation module, and the results are gathered in a statistics module to yield detection probabilities, false alarm probabilities and azimuth accuracies.

Figure 5.1-2 depicts a flowchart of the simulation program.

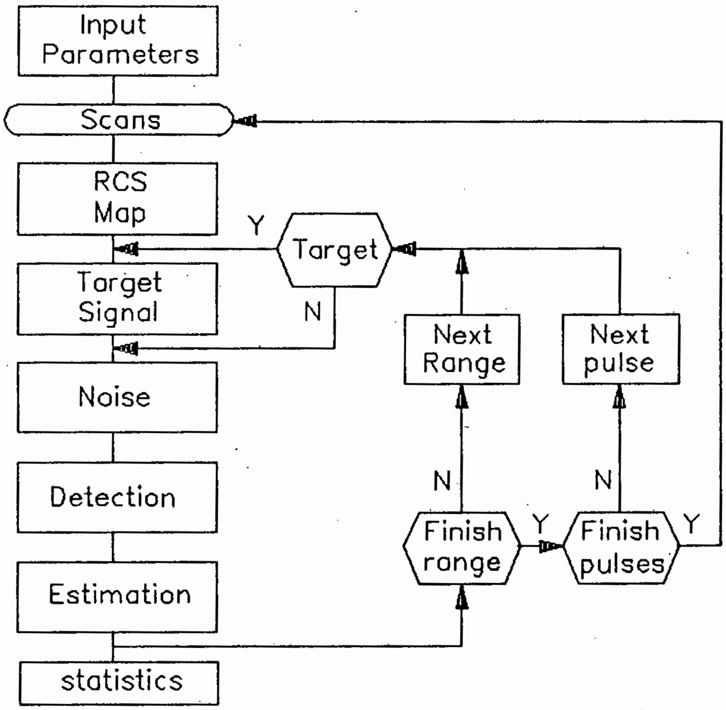

Figure 5.1-2: Simulation flowchart

The outer loop in the flow chart is repeated for 500 scans for each value of signal-to-noise ratio (trial) in order to establish the azimuth accuracy according to:

$$\sigma_h^2 = \frac{1}{N-1} \sum_{i=1}^{N} \sigma_i^2 * \left[\frac{1}{N} \sum_{i=1}^{N} \sigma_i \right]^2 \qquad (5.1\text{-}1)$$

where:

σ_i is the azimuth estimate for the i^{th} trial.

Within each scan, a total of 6n sweeps (pulse transmission and reception) are simulated, where n represents the number of pulses within the half-power beamwidth. The number of sweeps simulated within each scan allows the effect of antenna sidelobes to be included in the processing. During the reception period after each pulse transmission, the received signals are sampled at discrete time intervals such that at least one sample per -3 dB pulsewidth is obtained. These time samples are continually processed to establish the presence and location of a target.

5.2 RESULTS

The performance obtained with the different azimuth estimation techniques previously described is illustrated in the following figures. Each graph shows the normalized azimuth standard deviation as a function of the single-pulse signal-to-noise ratio with the false alarm probability at the output of detector/estimator set at 10^{-6}. Each curve has been calculated with 500 scans being performed for each 2 dB step in the signal-to-noise ratio. For each estimator the azimuth performance for Swerling models 0,1,2,3 and 4 have been determined assuming a gaussian antenna pattern. However, due to the lengthy computation times required and the limited practical value of the Swerling 3 and 4 models, further calculations have been limited largely to the models 0, 1 and 2. Specific aspects which have been considered for the different estimators may be itemized as:

1. Comparative evaluation between estimators assuming a gaussian antenna pattern.
2 The effects of the target model on each estimator.
3 The influence of quantization.
4. The utilization of a dynamic threshold typical to a constant false alarm system.
5. The influence of antenna pattern.
6. The influence of partial radar cross-section correlation.
7. The effects of clutter interference.

8. Number of pulses

9. Theoretical performance.

5.2.1 Estimator Performance

The different estimators evaluated may be grouped into two categories:

- Analogue processing estimators
- Binary processing estimators

The group of analogue processing estimators utilize the full amplitude information of the video signal to establish the centroid of a detected object. Examples of this type of estimator are the analogue moving window-, the maximum likelihood estimator and the two-pole filter. The group of binary processing estimators quantize the video signal into two binary levels prior to locating the object centroid. Examples of this type of estimator are the binary moving window-, the binary quantized weighted estimator, the sequential observer and the success-run estimator.

A hybrid type of estimator may be found in a batch processor, which utilizes both analogue and binary processing. In each estimator category, the estimators may be subdivided further into unbiased- and biased estimators. The class of unbiased estimators yields an azimuth estimate which is equal to the actual object position, while the class of biased estimators yield an estimate which is offset from the true value. Figure 5.2.1-1 illustrates the estimator classification.

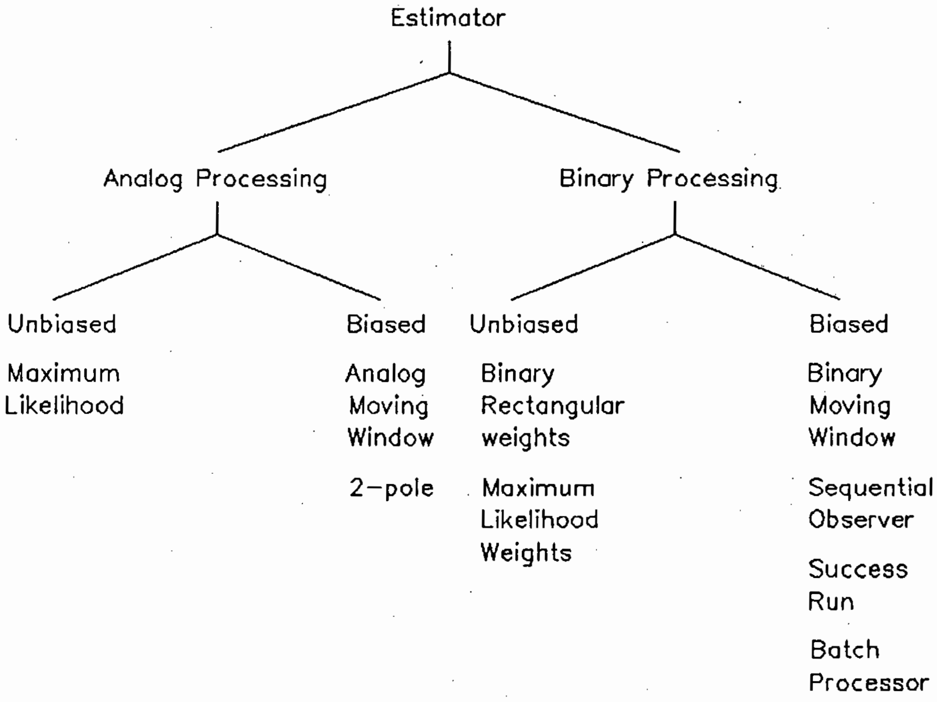

Figure 5.2.1-1: Estimator classification

5.2.1.1 Analogue Estimators

In order to facilitate comparative evaluation, the analogue moving window estimator has been used as a reference. Figure 5.2.1.1-1 illustrates the normalized azimuth estimate as a function of signal to noise ratio for each of the Swerling models. It is evident from the graphs of figure 5.2.1.1-1 that the azimuth estimate deteriorates as the radar cross-section fluctuation of the detected object becomes more severe. The azimuth centroid has been established by a beam-splitting mechanism. This approach yields a bias which is constant. A major limitation of the analogue moving window is its susceptibility to interference. The presence of a large spike may cause a false detection. The detection performance of the analogue moving window has been reported in the literature [22] to be approximately 0.5 dB worse than the optimum detector.

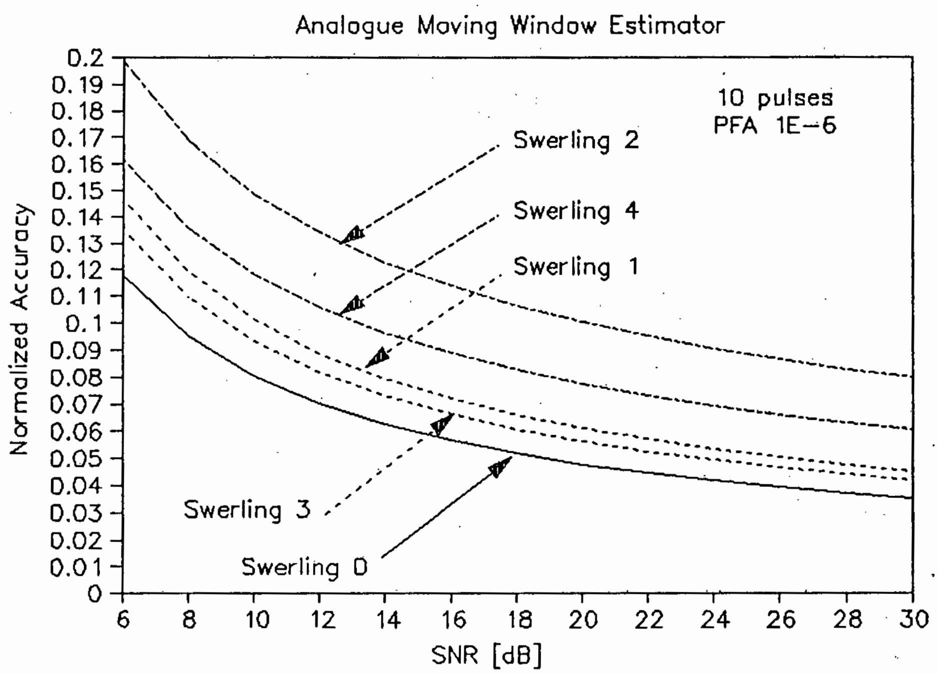

Figure 5.2.1.1-1: Analogue moving window estimator

The two-pole filter has the advantage over the analogue moving window estimator that it requires less storage. As with the analogue moving window, the two-pole filter yields a biased estimate. Two methods of establishing the azimuth centroid have been utilized:

- Peak amplitude detection.
- Beam-splitting.

The performance of the two-pole filter utilizing a peak detector to establish the azimuth centroid yields an estimate which is significantly worse (in the order of 100%) than that of the analogue moving window for the Swerling models 0,1 and 3 (figure 5.2.1.1-2).

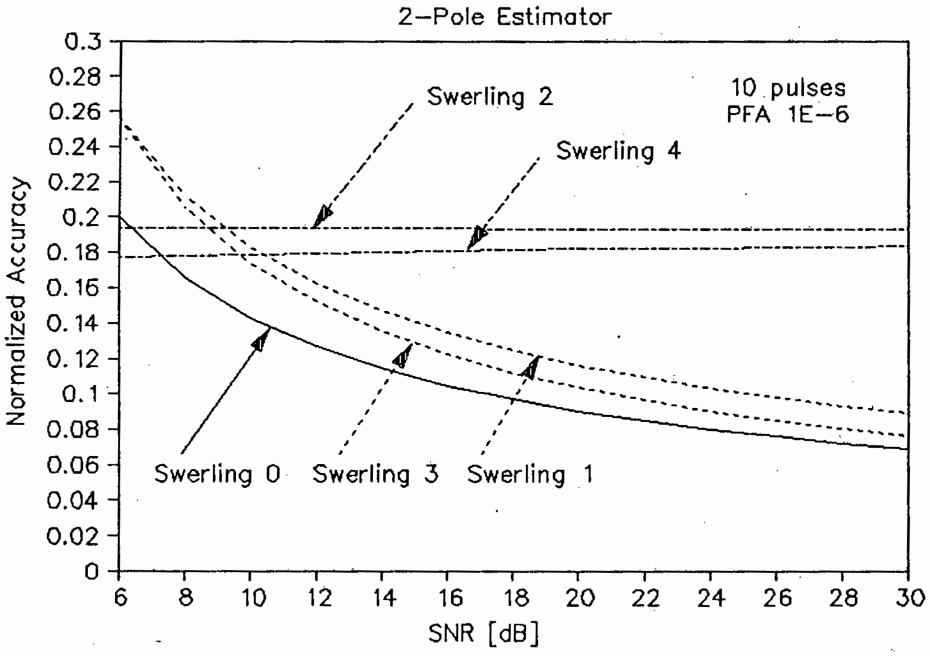

Figure 5.2.1.1-2: Two-pole estimator utilizing peak detection

For Swerling models 2 and 4, the two-pole filter yields very poor results. This may be attributed to the extreme sensitivity of this filter to interference due to its large inherent gain. For input samples with a large amplitude, as may be expected for the rapidly fluctuating models, a high output will result causing the peak detection mechanism to position the azimuth centroid at this peak. An alternative method may be achieved by utilizing a beam-splitting mechanism to establish the azimuth centroid (figure 5.2.1.1-3).

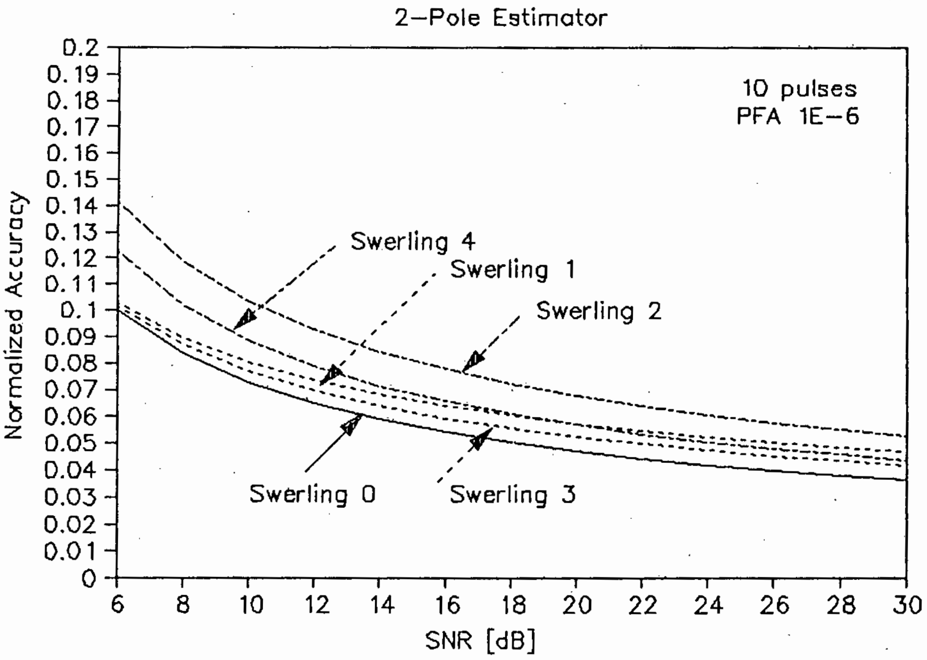

Figure 5.2.1.1-3: Two-pole estimator utilizing beam-splitting

Comparison of the achieved results for this situation with the analogue moving window indicates a better performance for models 2 and 4, while models 0, 1 and 3 yield an improvement at lower signal-to-noise ratios. These results are, however, somewhat misleading as the bias generated by the beam-splitting technique for the two-pole filter is not constant, but a function of the signal-to-noise ratio, increasing with lower ratios. Typically the bias normalized to the half-power beamwidth varies between 0.57 at low ratios to 0.53 at higher ratios. Taking this into account, the normalized rms estimate of the two-pole filter utilizing a beam-splitting technique comes very close to that of the analogue moving window. The detection performance of the two-pole filter is 0.15 dB worse than the optimum detector [13], yielding a better detection performance than the analogue moving window. Figures 5.2.1.1-2 and 5.2.1.1-3 illustrate the performance of the two-pole filter.

In contrast to the analogue moving window and two-pole filter, the maximum likelihood estimator yields an unbiased estimate of the detected object centroid

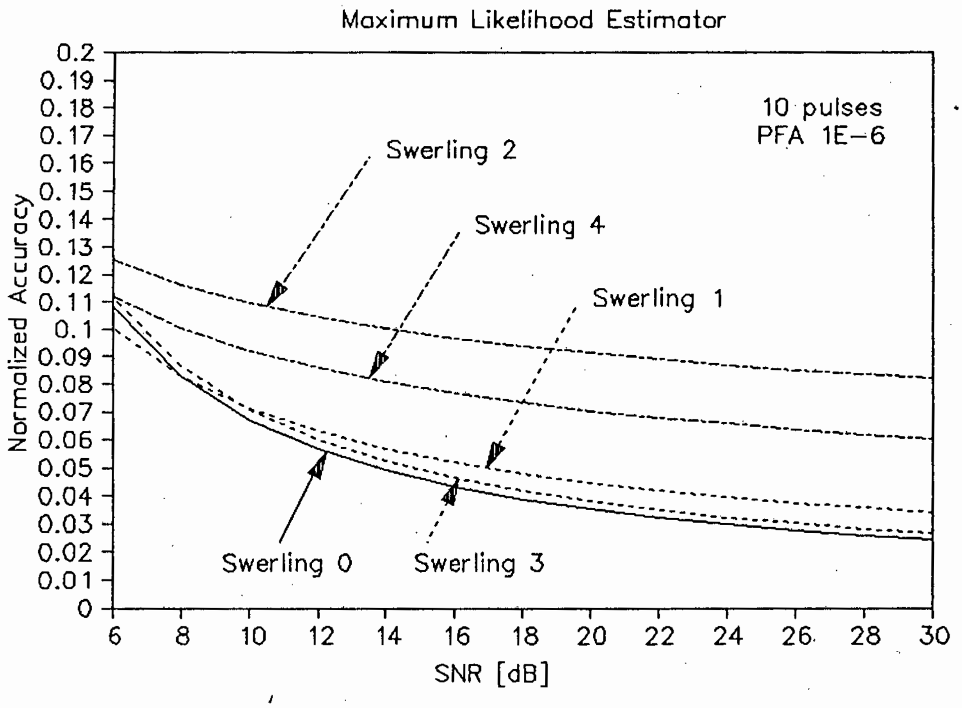

Figure 5.2.1.1-4: Maximum likelihood estimator

Performance comparison of the maximum likelihood estimator with that of the analogue moving window shows that the former yields an improved estimate for the Swerling models 0, 1 and 3. For the models 2 and 4, the maximum likelihood estimator yields an improved performance at low signal-to-noise ratios, but similar performance at the high ratios. This may be attributed to the optimization of the maximum likelihood weight to a low signal-to-noise ratio (10 dB). This effectively accentuates the information received near the beam centre. At higher ratios, the influence of the radar cross-section fluctuation and noise will be more pronounced away from the beam centre, and this will not be utilized by the optimized weights. The detection performance of the maximum likelihood estimator is determined by the detector mechanism used. In the evaluation, the analogue moving window was utilized as a detector.

5.2.1.2 Binary estimators

As with the evaluation of the analogue estimators, a particular binary estimator has been used as a reference. For the class of binary estimators, the binary moving window has been applied as a reference. Figure 5.2.1.2-1 shows the normalized azimuth estimate as a function of the signal-to-noise ratio.

As illustrated by the graph, the binary estimator is relatively insensitive to the fluctuation of radar cross-section. This is largely due to the amplitude quantizing which reduces the relative importance of the signal amplitude. The detection performance of the binary moving window for large numbers of pulses is approximately two dB worse than the optimum detector [43].

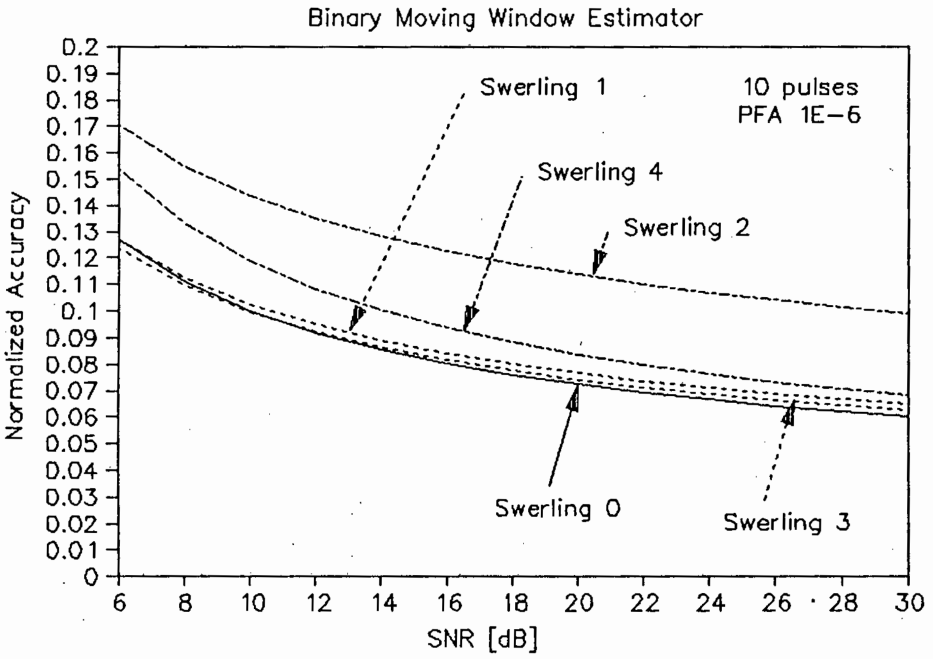

Figure 5.2.1.2-1: Binary moving window estimator

Related estimation techniques which, as with the binary moving window, yield biased estimates are the success-run estimator and sequential-observer estimator. The performance of the sequential-observer (figure 5.2.1.2-2) is very similar to that of the binary moving window. This may be expected, as the two estimators differ only in the criteria used to establish the trailing edge of the detected object.

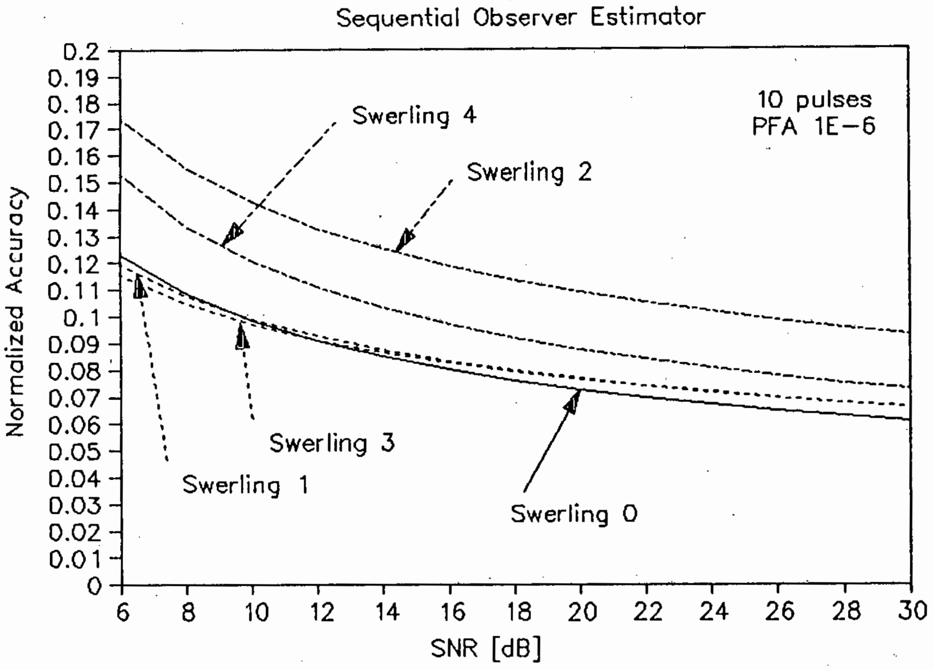

Figure 5.2.1.2-2: Sequential observer estimator

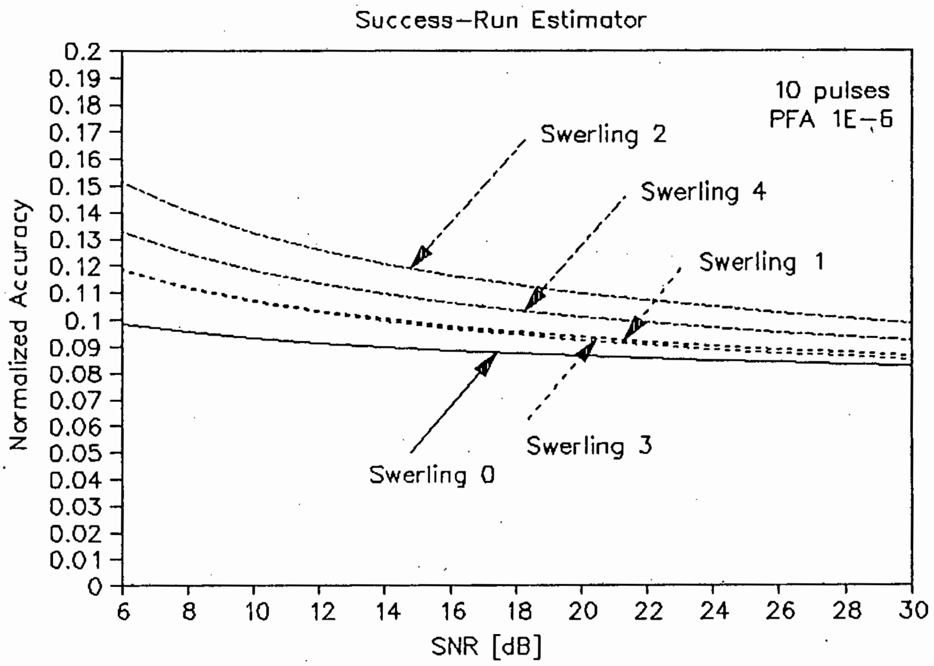

Figure 5.2.1.2-3: Success-run estimator

Both estimators increment or decrement a counter in uniform steps for each strike or miss returned from the detected object, but in contrast to the end angle being determined by the counter falling below a fixed threshold as with the binary window, the end azimuth of the sequential-observer is determined by the occurrence of three consecutive misses.The success-run (figure 5.2.1.2-3) estimator yields improved accuracy at lower signal-to-ratios, but a reduced performance at higher signal-to-noise ratios.

This may be attributed to the effective pattern recognition approach which the estimator applies. At lower ratios, the noise is the more dominant influence and the probability of the pattern occurring is very small, thereby reducing the occurrence of false centroids. At higher ratios, this advantage is lost as noise of thermal nature is less relevant here. The detection performance of the success-run estimator is worse than that of the binary moving window.

The batch processor may be regarded as a hybrid of analogue and binary processing. Batches of pulses are integrated with an analogue integrator. These integrated batches are thresholded to yield binary results. These binary values are integrated in a binary integrator, and a beam-splitting mechanism is utilized to establish the azimuth centroid. Figure 5.2.1.2-4 illustrates the results achieved with the batch processor integrating five batches of two pulses per batch.

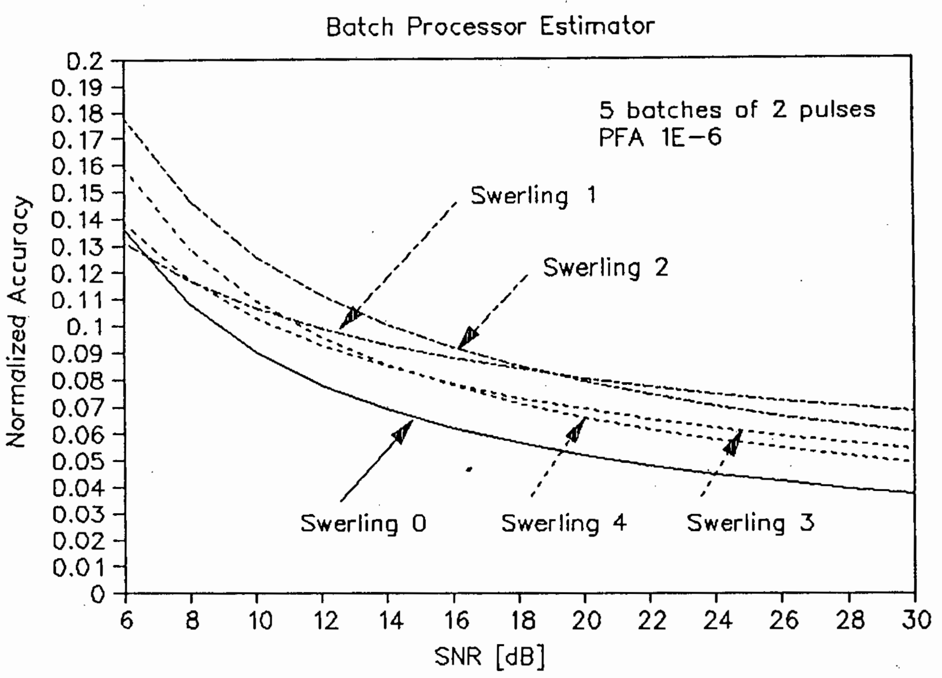

Figure 5.2.1.2-4: Batch processor estimator

Comparison with the binary moving window shows a similar performance at low signal-to-noise ratios, but improved performance at higher ratios.

This is largely due to the fact that the batch processor performs analogue integration yielding the gain of the analogue moving window, but also the reduced sensitivity to interference due to the binary integration. The detection performance for the batch processor for large numbers of pulses is better than the binary moving window, and is approximately 0.5 dB worse than the optimal detector [48].

The class of unbiased binary estimators employ a set of weights similar to the analogue unbiased estimators, but the video input is quantized into two levels prior to weighting. For a symmetrical antenna pattern, any odd-symmetrical set of weights yield an unbiased estimator. Two sets of weights have been applied in the evaluation: rectangular weights and maximum likelihood weights. The binary rectangular weights yield a slightly improved azimuth estimate at low signal-to-noise ratios, and a slightly deteriorated performance at higher ratios (figure 5.2.1.2-5).

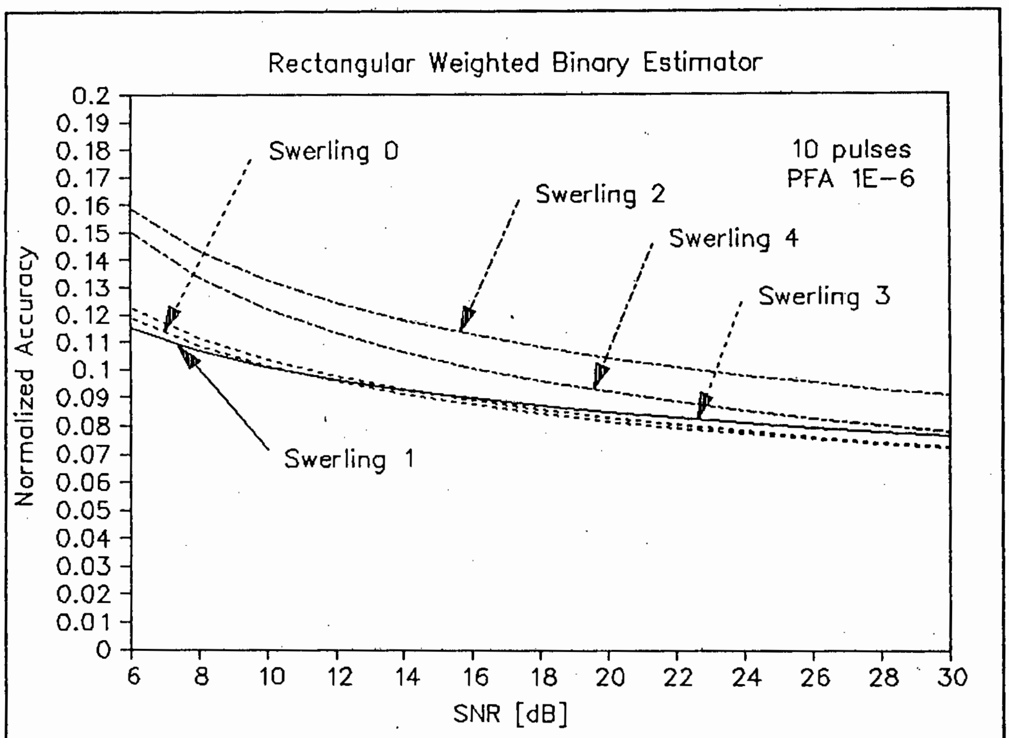

Figure 5.2.1.2-5: Binary estimator with rectangular weights

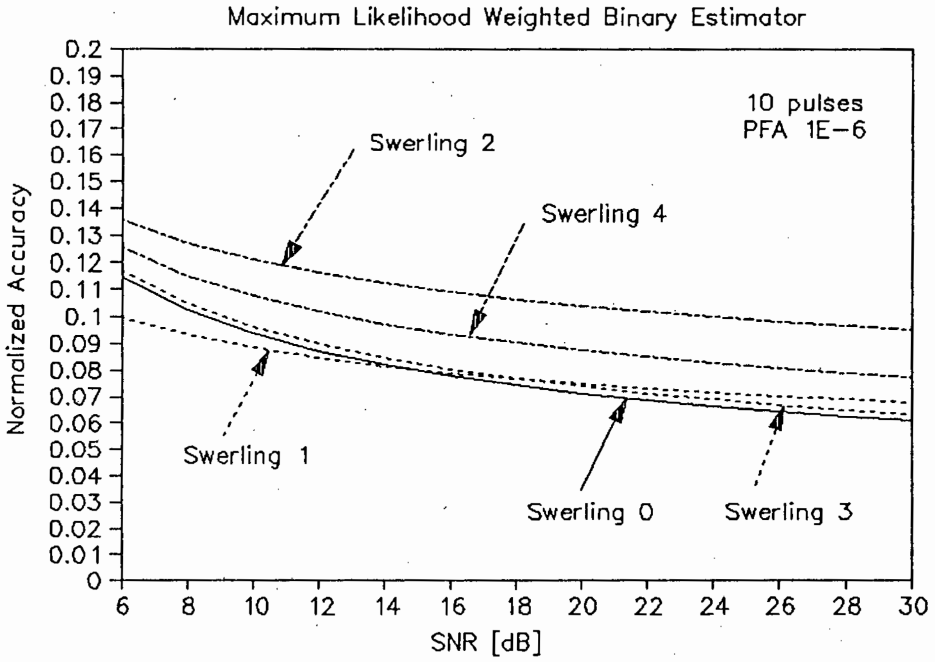

Figure 5.2.1.2-6: Binary estimator with maximum likelihood weights

Use of maximum likelihood weight yields a similar behaviour, but with a larger improvement at low ratios (figure 5.2.1.2-6). This is largely due to the maximum likelihood weights accentuating the strikes received near the beam centre. The detection mechanism utilized is a binary moving window.

5.2.1.3 Comparative Evaluation

For each of the two classes of estimators, binary- and analogue, a comparison has been performed relative to a reference estimator. It is of interest to compare the two reference estimators: the binary moving window and the analogue moving window. Figures 5.2.1.3-1 through 5.2.1.3-5 show the relative performances for each of the Swerling models.

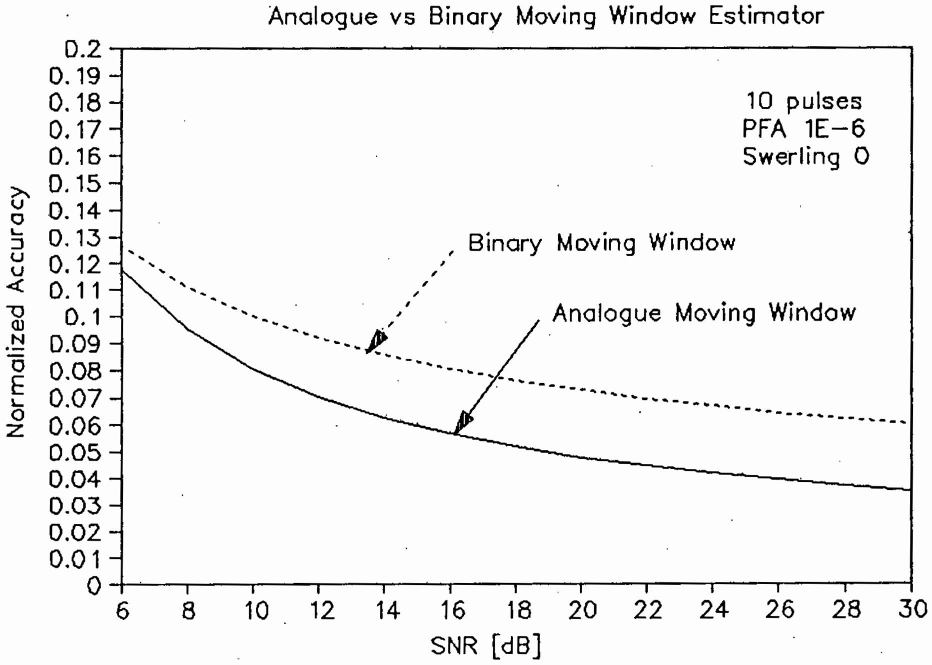

Figure 5.2.1.3-1: Analogue vs binary moving window Swerling 0

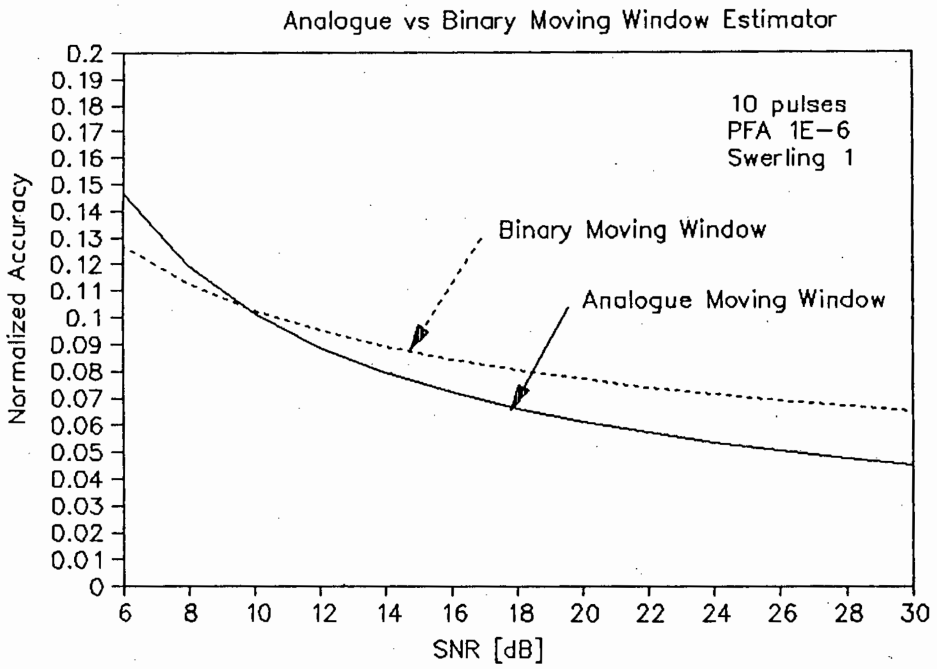

Figure 5.2.1.3-2: Analogue vs binary moving window Swerling 1

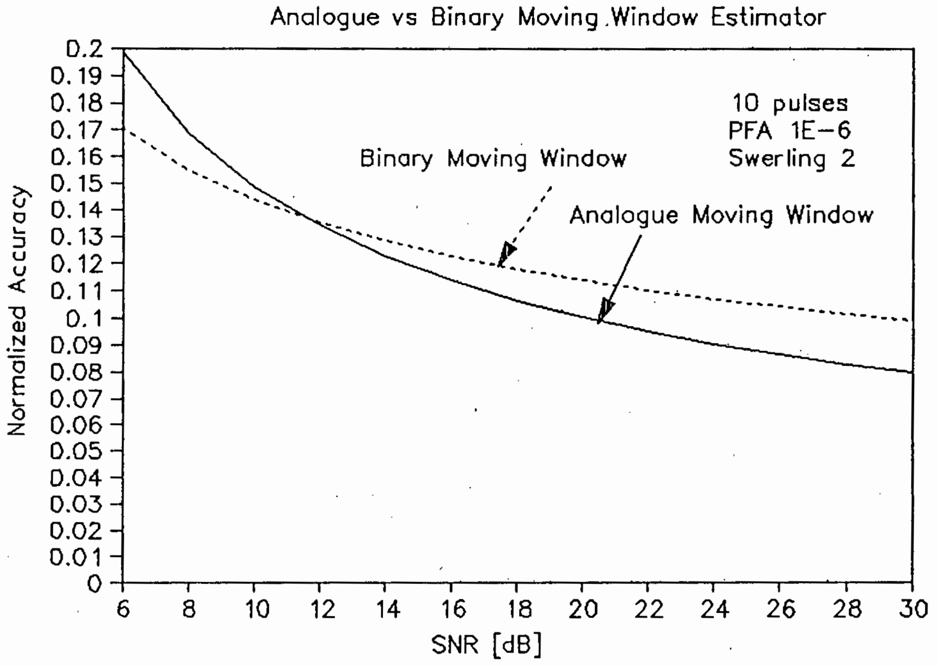

Figure 5.2.1.3-3: Analogue vs binary moving window Swerling 2

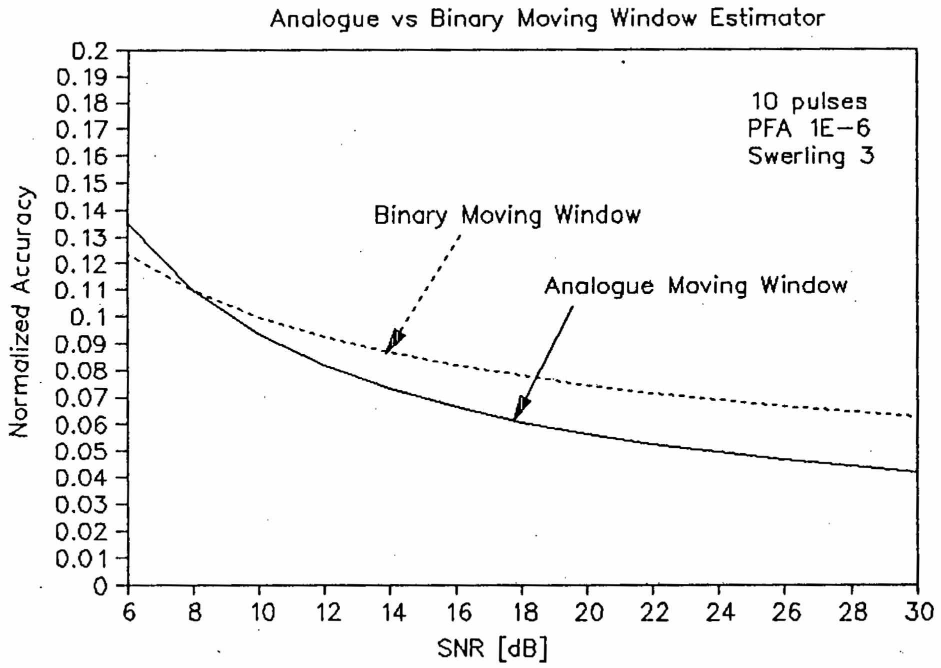

Figure 5.2.1.3-4: Analogue vs binary moving window Swerling 3

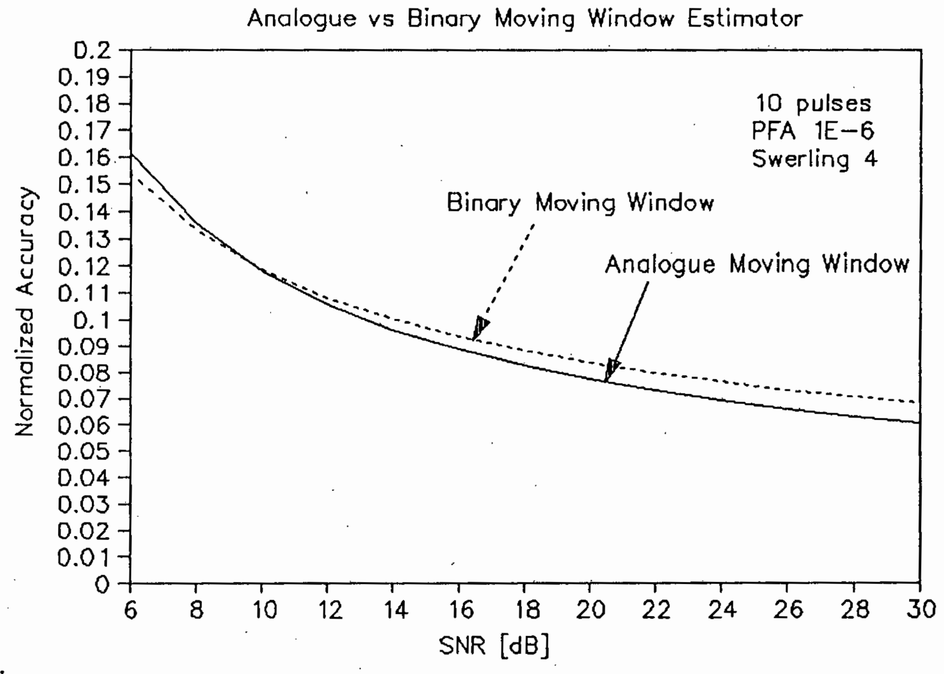

Figure 5.2.1.3-5: Analogue vs binary moving window Swerling 4

From these figures it is apparent that the binary window yields a better performance at lower signal-to-noise ratios while the analogue window yields better performance at higher ratios. This may be explained by the fact that at lower ratios, the relative influence of noise is larger, and the analogue moving window which is more susceptible to interference will be affected more severely. At higher ratios, the relative importance of noise is reduced and the use of amplitude information results in a better azimuth performance. Furthermore, the graphs illustrate a relative insensitivity of the binary window to radar cross-section fluctuation.

5.2.2 Influence of target model

The influence of the target model on the accuracy performance can be visualized intuitively by considering the effect of a varying radar cross-section on the amplitudes of the received pulse train (figure 5.2.2-1).

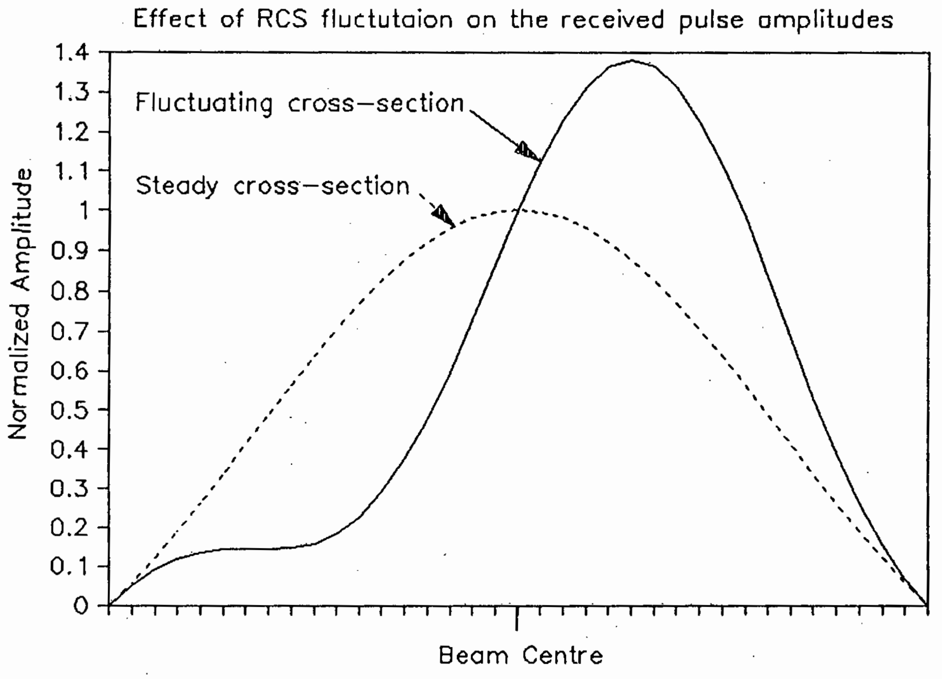

Figure 5.2.2-1: Effect of varying radar cross-section on received pulse amplitudes

The variation in cross-section will cause a distortion in the beam-modulated pulse train. This will effectively cause the start- and end position of the detected object to vary for beam-splitting type estimators, while for zero-crossing and peak detectors the criteria will be met at different points depending on the distortion introduced. A more quantitive understanding of the influence of target model may be obtained by considering the effect of detection probability on the theoretical azimuth estimate. Walter [50] has shown that for a given probability of detection, and false alarm probability, the azimuth estimate variance will be given by:

$$\sigma^2 = \frac{\sigma_o^2 + \dfrac{(T-2B_o)^3}{24B_o} * \dfrac{P_F}{P_D}}{1 + \dfrac{(T-2B_o)}{2B_o} * \dfrac{P_F}{P_D}} \qquad (5.2.1\text{-}1)$$

where:

σ_o^2 is the minimum estimate variance

$2B_o$ is the beamwidth in radians

P_D is the single pulse probability of detection

P_F is the probability of a false threshold crossing.

An increase in detection probability will result in an improved azimuth estimate standard deviation. Considering the results for the Swerling models 0 through 4 (figures paragraph 5.2.1), the general tendency for all estimator types is that the fixed radar cross-section yields the best results at higher signal-to-noise ratios. This is expected as only thermal noise is of influence here. At very low signal-to-noise ratios, the Swerling 1 model tends to yield slightly better results than the Swerling 0 model. This can best be explained by the fact that the Swerling 1 model yields the highest detection probability at low signal-to-noise ratios.

The performance for Swerling models 1 and 3 are very similar, with model 3 yielding slightly better results. Intuitively this could be expected as both models exhibit the same fluctuation rate (scan-to-scan independence), but model 3 is characterized by a dominant scatterer, similar to model 0. Model 1 is characterized by uniformly distributed scatterers, similar to Swerling 2. Quantitively, Swerling model 3 yields a better detection performance in the lower signal-to-noise region. At higher ratios, model 1 yields a better probability, but here the detection probabilities of both models approach unity, and the performance becomes very similar.

The fast fluctuation models 2 and 4 yield the worst result. This may be attributed largely to the added noise in the azimuth measurement introduced by the radar cross-section fluctuation. As with models 1 and 3, model 4 yields better results than model 2. Intuitively this may also be attributed to the fact that the model 4 is represented by a dominant scatterer model.

Consideration of the performance achieved with the log-normal fluctuation model assuming a scan-to-scan independence shows a slightly deteriorated performance compared to the Swerling 1 model. A mean-to-median ratio of four has been assumed for the log-normal model. The log-normal target is characterized by a relatively large fluctuation loss. At low signal-to-noise ratios, the achieved detection probability for 10 pulses integrated is approximately the same as the Swerling 1 model [46]. At higher signal-to-noise ratios, however, the detection probability for the log-normal target is less than that for the Swerling 1 model, resulting in the reduced accuracy performance.

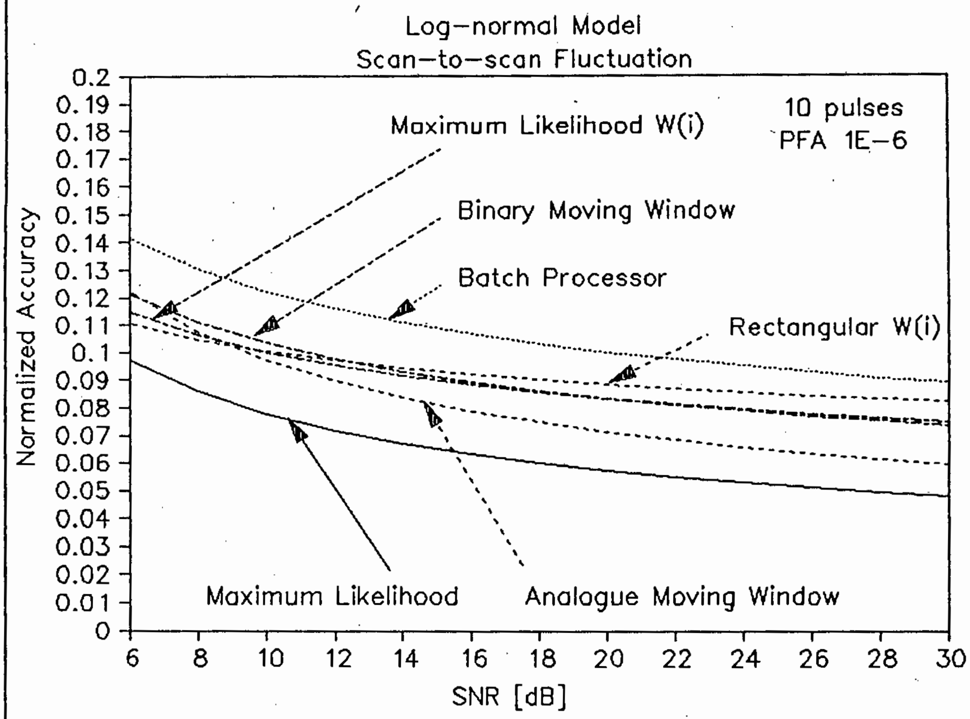

Figure 5.2.2-2: Comparative performance with a log-normal target

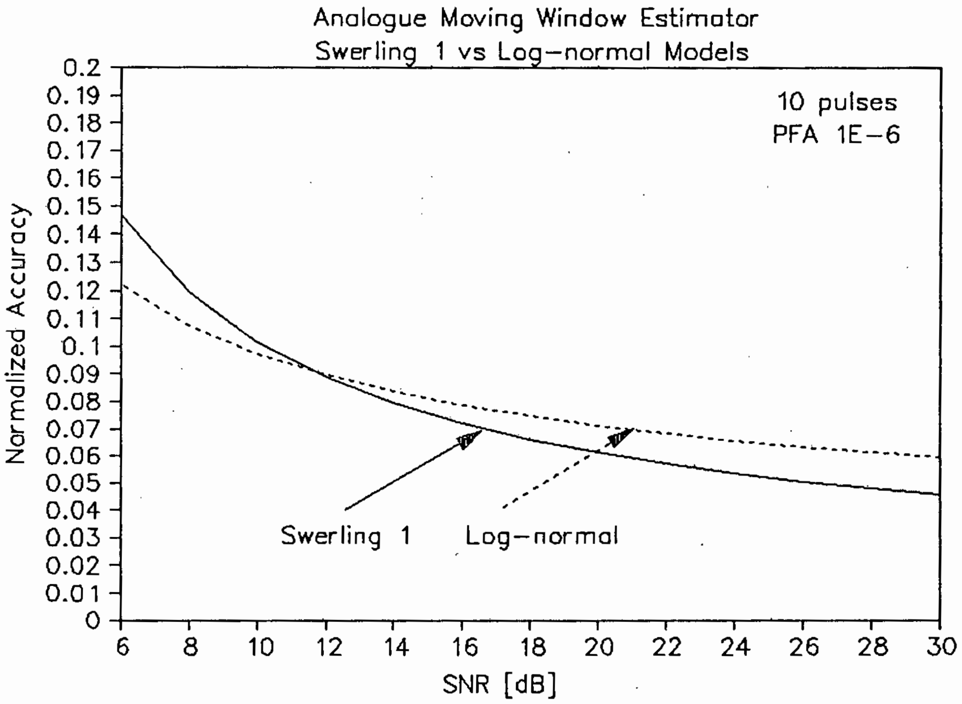

Figure 5.2.2-3: Analogue moving window estimator with a log-normal target

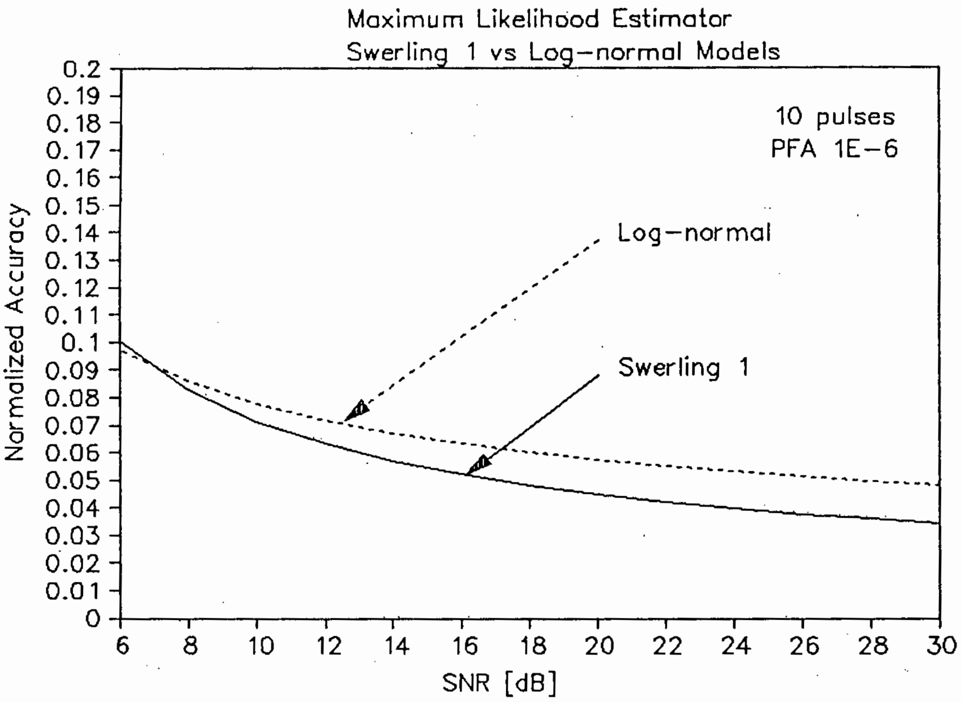

Figure 5.2.2-4: Maximum likelihood estimator with a log-normal target

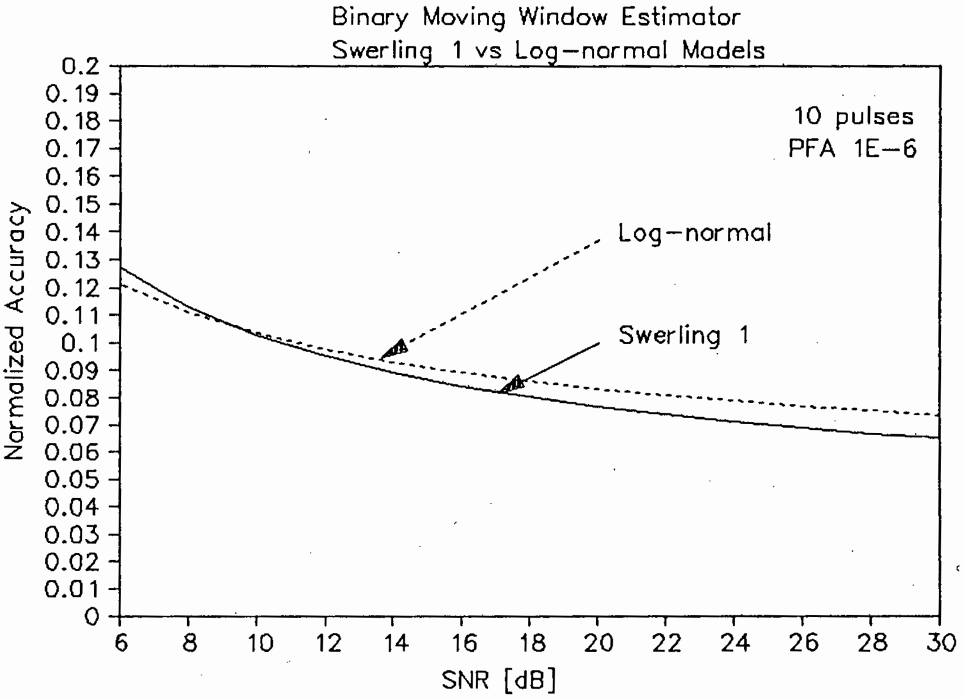

Figure 5.2.2-5: Binary moving window estimator with a log-normal target

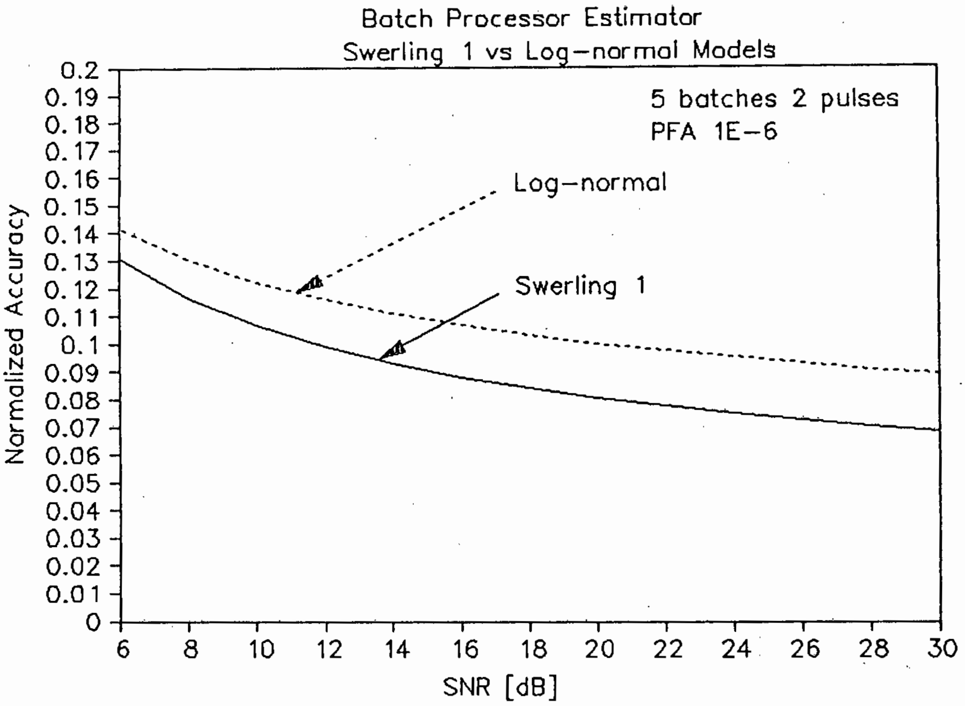

Figure 5.2.2-6: Batch processor estimator with a log-normal target

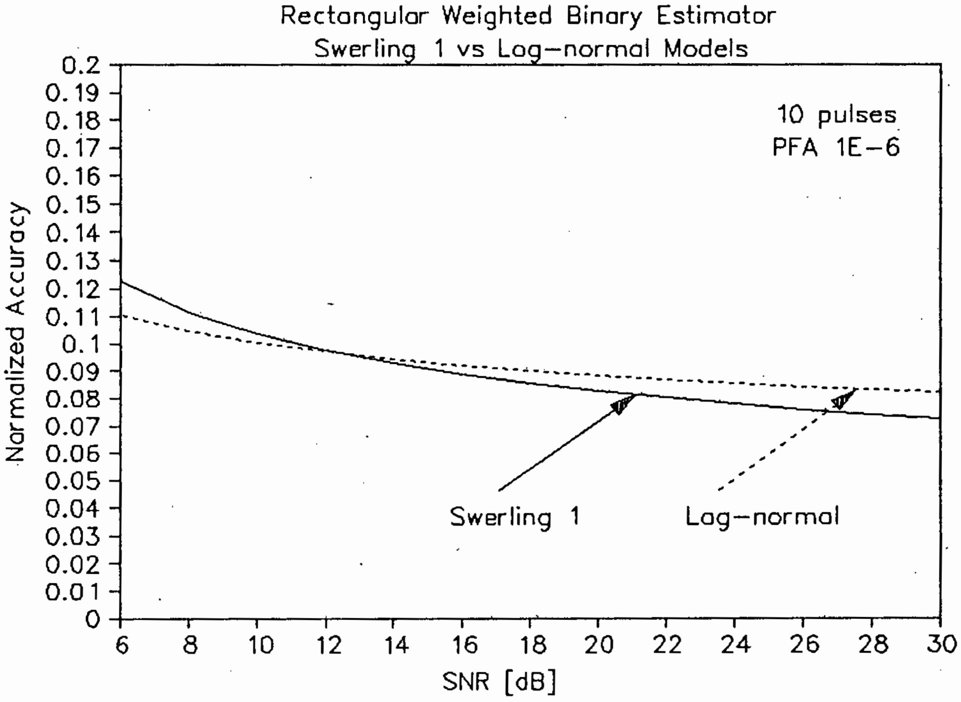

Figure 5.2.2-7: Rectangular weighted estimator with log-normal target

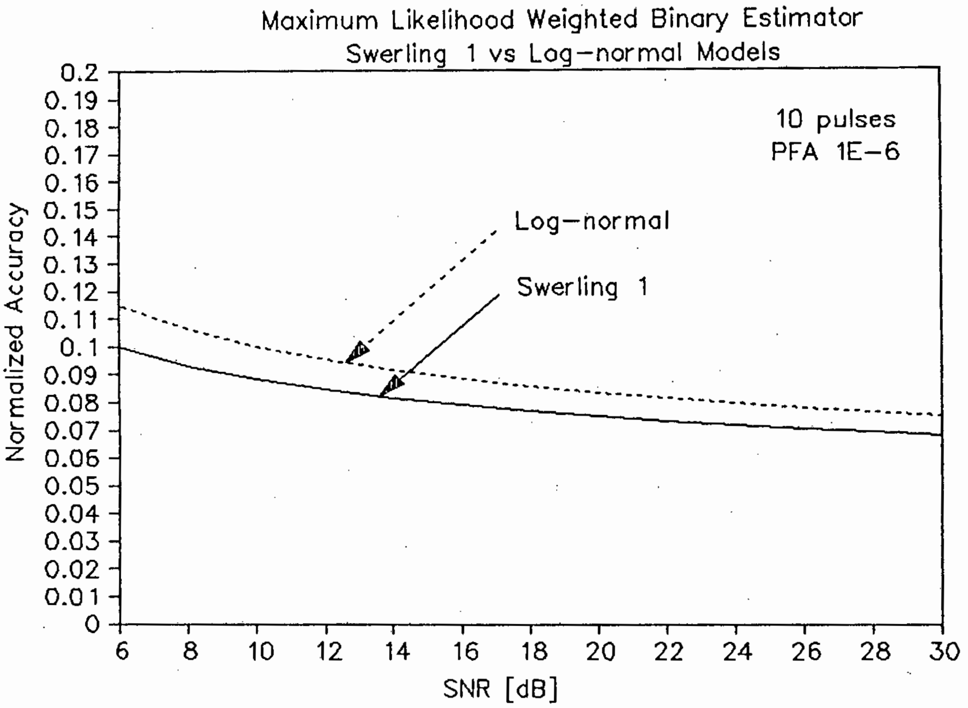

Figure 5.2.2-8: Maximum likelihood weighted estimator

5.2.3 Quantization

The performance of the various azimuth estimators is influenced by quantization noise. Two sources of quantization noise may be identified:

1. Quantization of the antenna position by the position encoder.

2. A finite angular step between consecutive pulses.

Estimator types which are capable of determining the scatterer centroid accurately, such as the weighting type of estimators which can determine the precise instant at which a zero-crossing occurred by interpolation, suffer the quantization noise introduced by the antenna position encoder. Estimator types which determine the centroid by establishing the start and end position of the scatterer, suffer an additional quantization noise due to the finite angular step rotated by the antenna during each pulse repetition interval. The quantization noise will add in an rms fashion to the azimuth estimate variance. The noise standard deviation introduced will be:

$\partial\theta/\sqrt{12}$ (5.2.3-1)

For the case of the quantization noise being dominated by the angular step size between pulses, the normalized quantization standard deviation will be:

$1/[n\sqrt{12}]$ (5.2.3-2)

It is evident that the larger the number of pulses within the half-power beamwidth, the less the quantization noise will be. For small signal-to-noise ratios, the azimuth estimate variance will be dominated by the estimator inaccuracy, but at higher ratios, the quantization noise becomes an important contributor. Figure 5.3-1 illustrates this effect for the analogue sliding window estimator utilizing 10 pulses. Without quantization, the normalized estimate variance approaches 0.027. The quantization noise variance will be 0.0008, resulting in a total estimate standard deviation of 0.039, as the graph of figure 5.3-1 confirms.

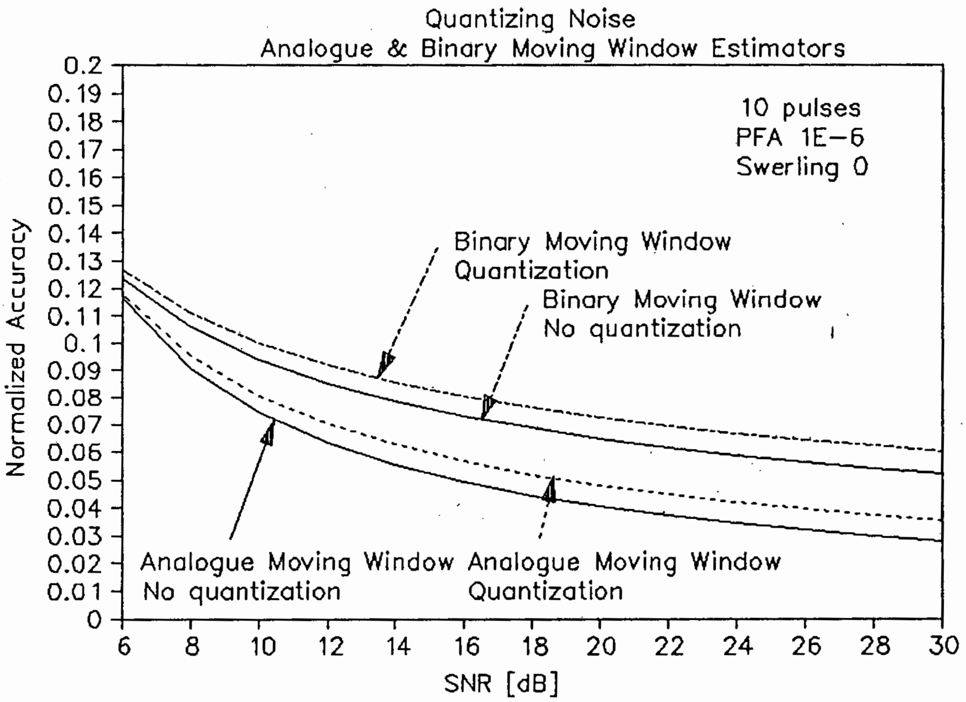

Figure 5.2.3-1: Quantization effects with the analogue and binary moving window estimators

5.2.4 Adaptive Thresholding

In the previous evaluations, the threshold setting for the estimators was determined by the required false alarm probability (1E-6), and maintained constant during all simulations. In practical systems, however, the threshold is adapted to suit the environment with a constant false alarm rate mechanism. Essentially, two CFAR mechanisms are applied in radar processors:

- Range-acting CFAR
- Temporal-acting CFAR.

The range acting class of CFAR processors establish an estimate of the average returned noise power on a pulse-to-pulse basis. This estimate is scaled with a margin and utilized to threshold the video. Typical examples of parametric CFAR circuits are the cell-averaging (CA-CFAR) and cell-averaging with greater-of selection (CAGO-CFAR) [37]. Temporal CFAR mechanisms establish an estimate of the returned noise power on a scan-to-scan basis by subdividing the radar cover into temporal cells (range by beamwidth cells), and updating each cell on a scan-to-scan basis. Within a temporal cell, the threshold is maintained at the previous scan value, and is only updated with the current scan information once the cell has passed. This effect is similar to the fixed threshold applied in the evaluations. A consideration here, however, is the occurrence of transitions between neighbouring temporal cells. For purposes of evaluation, it is more informative to establish the effect of varying threshold on the azimuth performance by using a range-acting CFAR. Six estimators representative for the different classes have been considered, specifically:

- analogue moving window estimator (figure 5.2.4-1)
- Maximum likelihood estimator (figure 5.2.4-2)
- binary moving window estimator (figure 5.2.4-3)
- batch processor estimator (figure 5.2.4-4)
- rectangular weighted binary estimator (figure 5.2.4-5)
- maximum likelihood weighted binary estimator (figure 5.2.4-6).

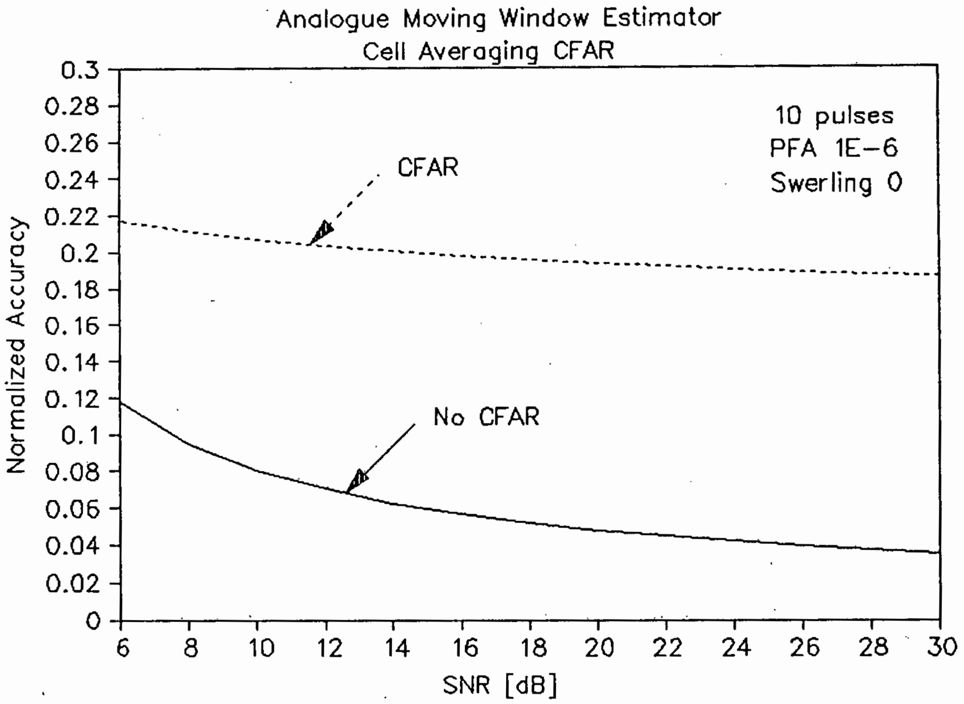

Figure 5.2.4-1: Analogue moving window estimator with adaptive threshold

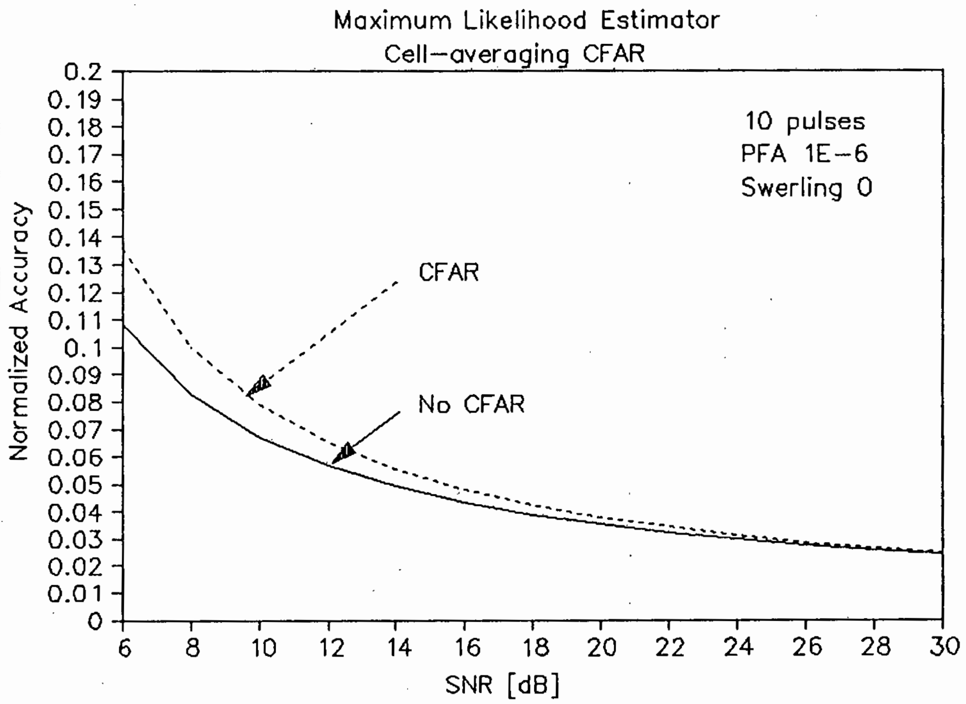

Figure 5.2.4-2: Maximum likelihood estimator with adaptive threshold

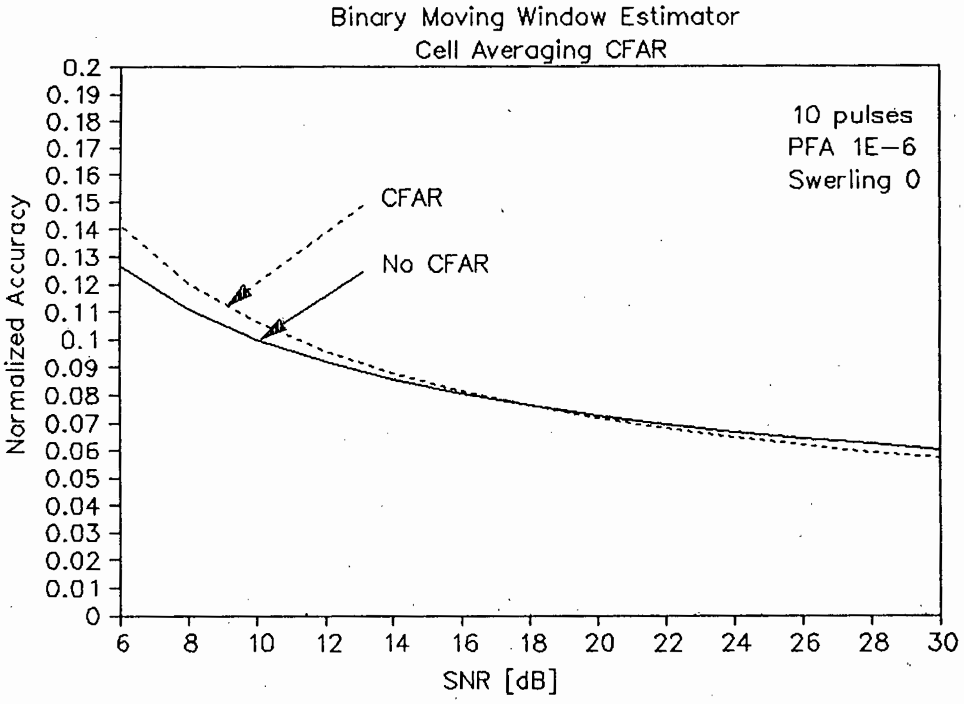

Figure 5.2.4-3: Binary moving window estimator with adaptive threshold

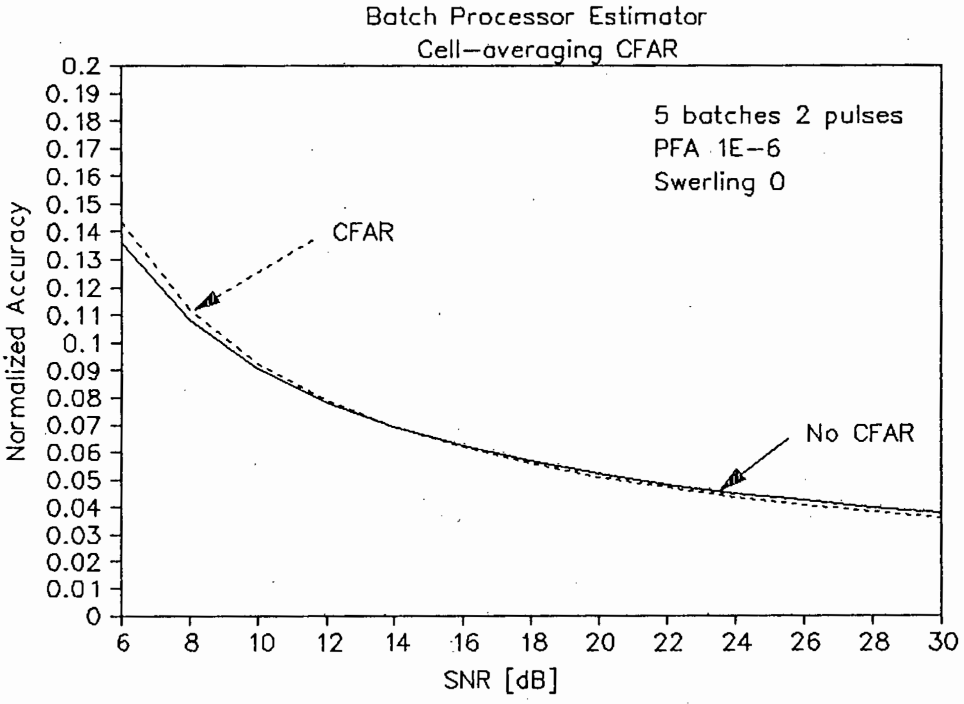

Figure 5.2.4-4: Batch processor estimator with adaptive threshold

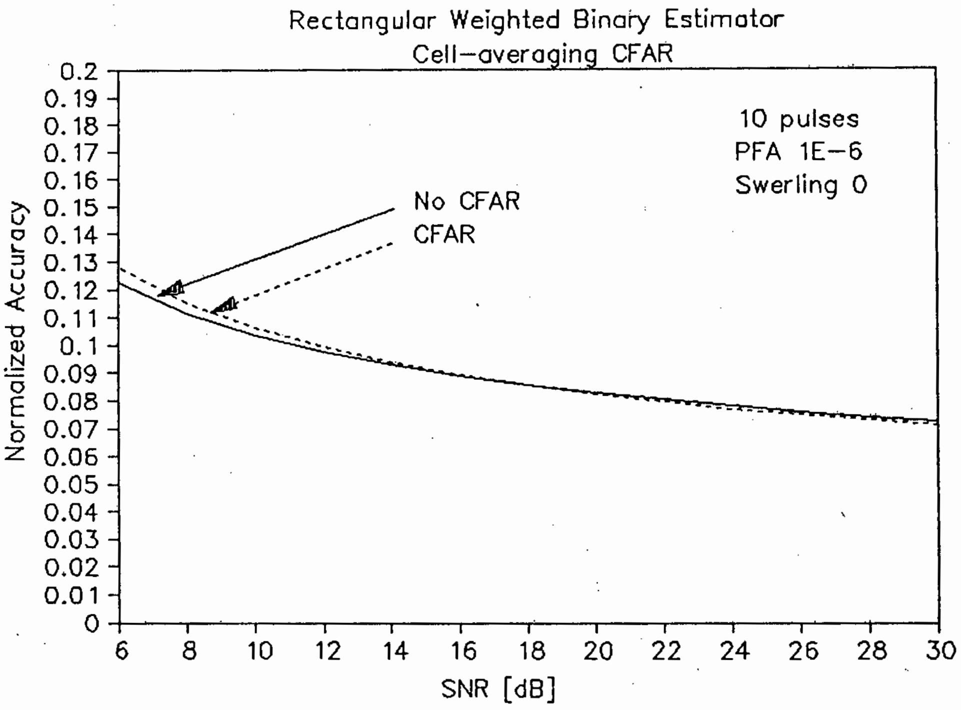

Figure 5.2.4-5: Rectangular weighted binary estimator, adaptive threshold

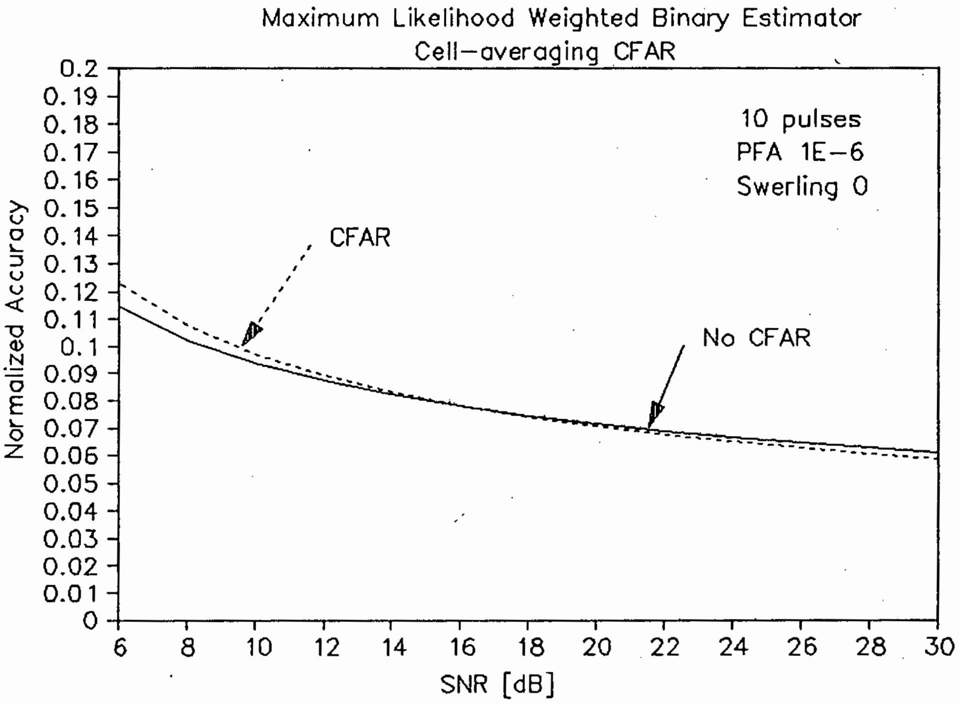

Figure 5.2.4-6: Maximum likelihood weighted estimator,adaptive threshold

For each of the estimators, the threshold was established with a cell-averaging CFAR. Sufficient range samples preceded and succeeded the range containing the test target in order to allow the CFAR to establish a threshold. The cell-sizes were set to 10 range cells, and the margin adjusted to obtain a false alarm probability of 1E-6. The graphs of figures 5.2.4-1 through 5.2.4-6 illustrate the results achieved for a fixed radar cross-section. It is evident from the graphs that the analogue moving window is severely affected. The effect of threshold quantization has not been considered in this evaluation. A slightly reduced performance may result due to the false alarm probability not being maintained at 1E-6, but further simulations are required to substantiate this assumption.

5.2.5 Antenna Pattern

The theory of angular accuracy relates the performance of the optimum estimator to a slope factor K_p according to:

$$\sigma_0 = \frac{\sigma_3}{K_p \sqrt{(E/N_0)}} \qquad (5.2.5\text{-}1)$$

The optimum estimator is in this case an estimator which senses the derivative of the antenna pattern and establishes the zero-crossing point. Practical estimators, however, utilize different methods to establish the azimuth centroid, and a generalization based on the different slope factors for the antenna patterns is therefore not necessarily valid. Six (figures 5.2.5-1 through 5.2.5-6) different estimators were evaluated with a gaussian and sin x/x pattern. A constant radar cross-section scatterer was assumed in order to evaluate only the effects of thermal noise and antenna pattern.

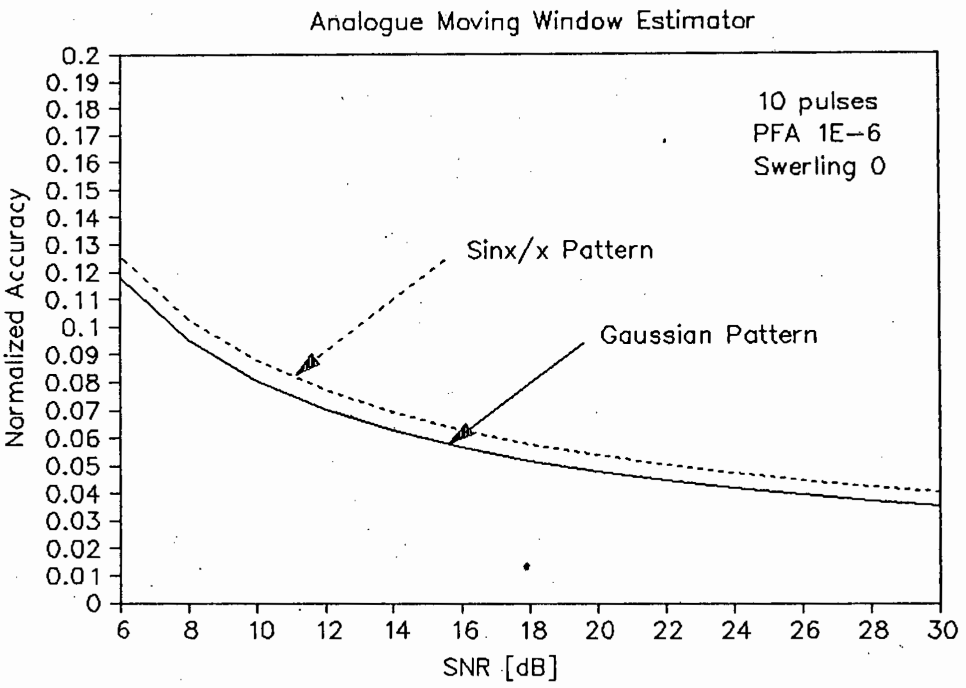

Figure 5.2.5-1: Analog estimator, gaussian and sinx/x patterns

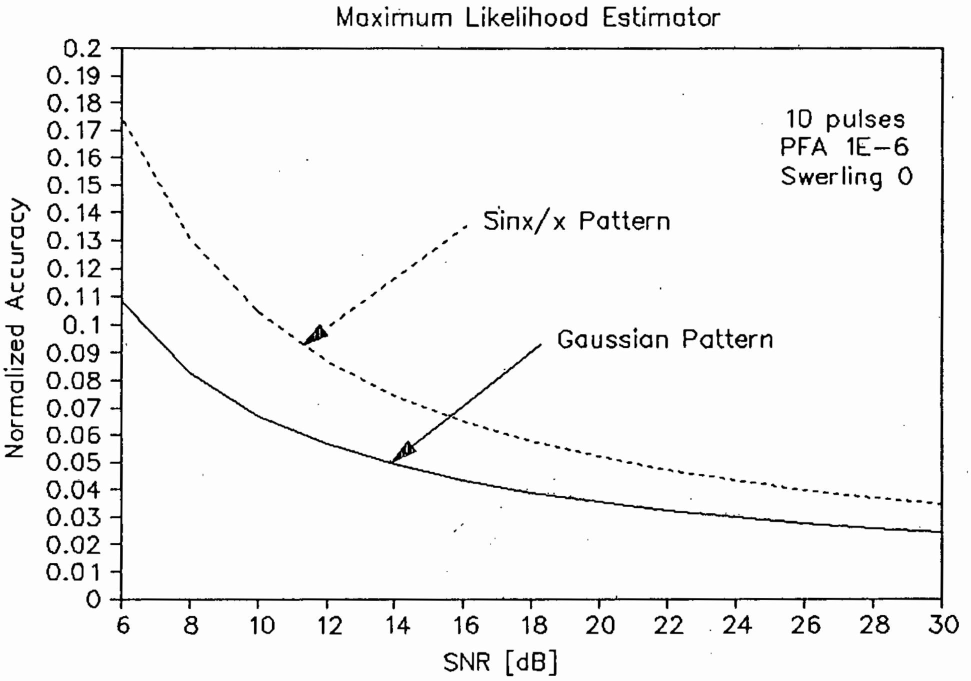

Figure 5.2.5-2: ML estimator, gaussian and sinx/x patterns

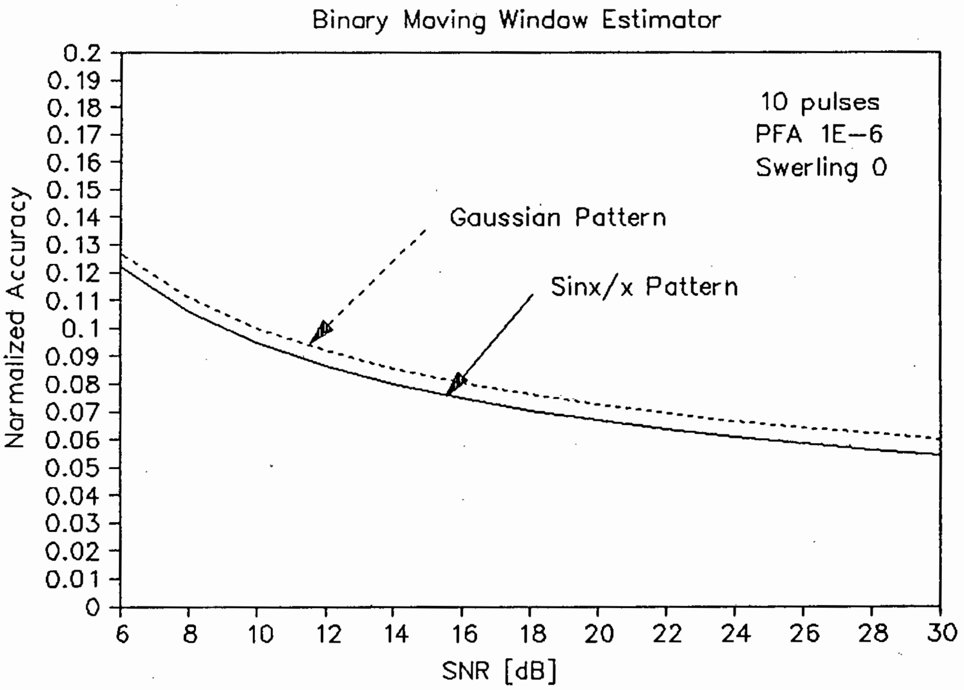

Figure 5.2.5-3: Binary moving window estimator with gaussian and sinx/x patterns

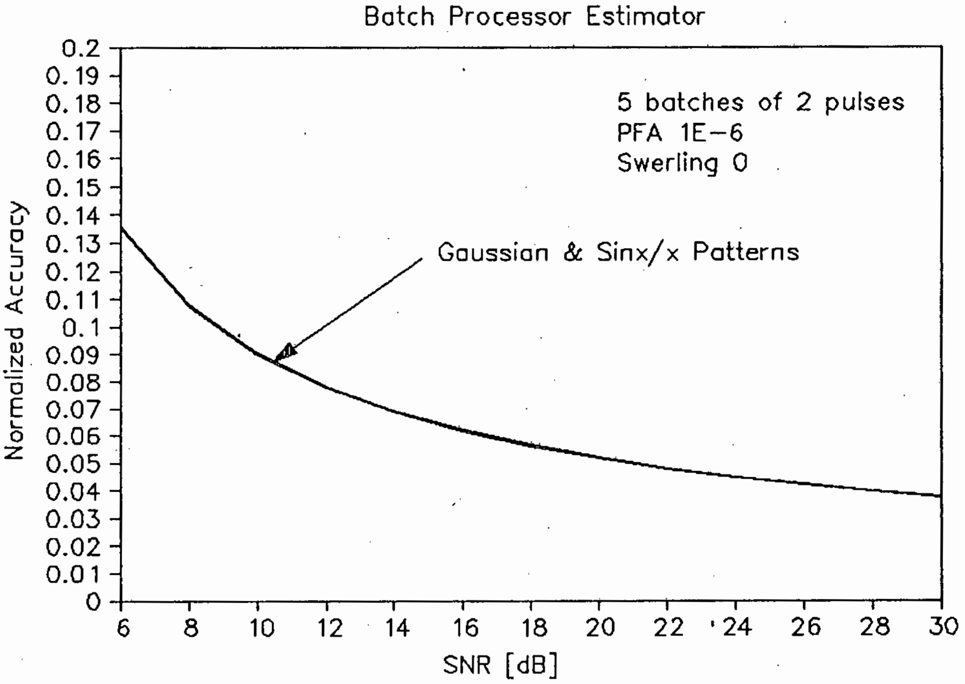

Figure 5.2.5-4: Batch processor estimator with gaussian and sinx/x patterns

From the graphs of figure 5.2.5-1 and 5.2.5-2 it is evident that for the analogue estimators the gaussian pattern yielded a better performance than the sin x/x pattern even though the latter has a slightly higher slope factor. The binary estimator (figure 5.2.5-3), however, indicated a slightly improved performance for the sin x/x pattern.

The batch processor (figure 5.2.5-4) which utilizes both analogue and binary processing indicated no significant difference.

Finally, the weighted binary estimators (figures 5.2.5-5, 5.2.5-6) tended to yield better results for the gaussian pattern at low signal-to-noise ratios, while at higher ratios the sin x/x pattern yielded better results.

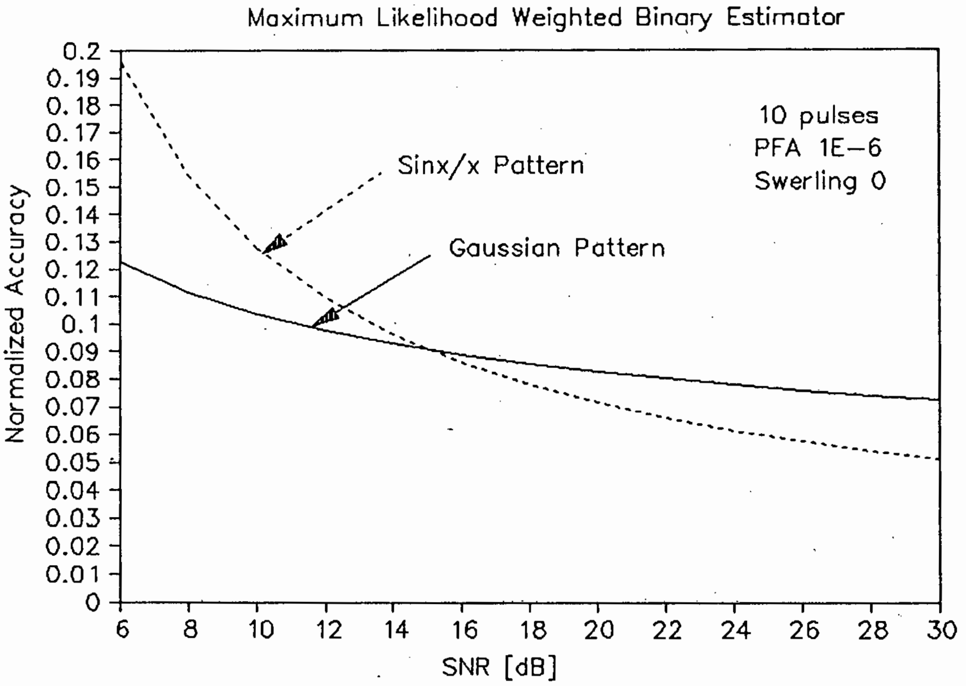

Figure 5.2.5-5: Rectangular weighted, gaussian and sinx/x patterns

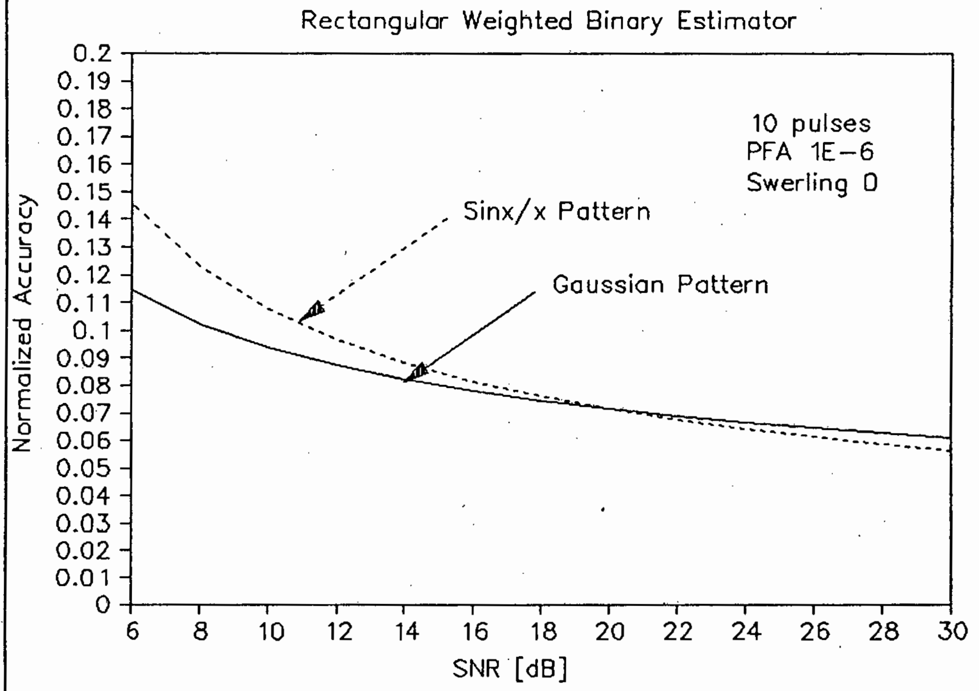

Figure 5.2.5-6: Maximum likelihood weighted, gaussian and sinx/x patterns

The effect is more pronounced for the maximum likelihood weights. This is primarily due to the maximum likelihood weights for the gaussian beam accentuating the information nearer to the beam centre than those for the sin x/x pattern.

5.2.6 Partially Correlated Objects

In order to establish the effects of intermediate radar cross-section fluctuation on the azimuth accuracy, simulations were performed with different estimators assuming a given signal-to-noise ratio and false alarm probability, but with varying degrees of fluctuation. The degree of fluctuation is characterized by the ratio of observation time (the time during which the detected object is within the radar beam) to object correlation time, to/tc. Barton [2] has defined this as a parameter n_e-1, which signifies the number of independent samples received by the radar. Figures 5.2.6-1 through 5.2.6-6 illustrate the results achieved. As was first identified by Walter [50], the azimuth performance for estimators with partially correlated scatterers may be significantly worse than predicted by the boundary cases of scan-to-scan and pulse-to-pulse independence. These boundary cases are identified by the number of independent pulses being less than one reflecting the scan-to-scan fluctuation case and the number of independent pulses being greater than one reflecting the pulse-to-pulse fluctuation case. The graphs of figure 5.2.6-1 and 5.2.6-2 also show that the analogue processing group of estimators are more severely affected than the binary processing group, largely due to the insensitivity of the binary processing schemes to radar cross-section scintillation.

In each of the curves, a Fourier curve fit has been applied to the data to achieve the smooth figures.

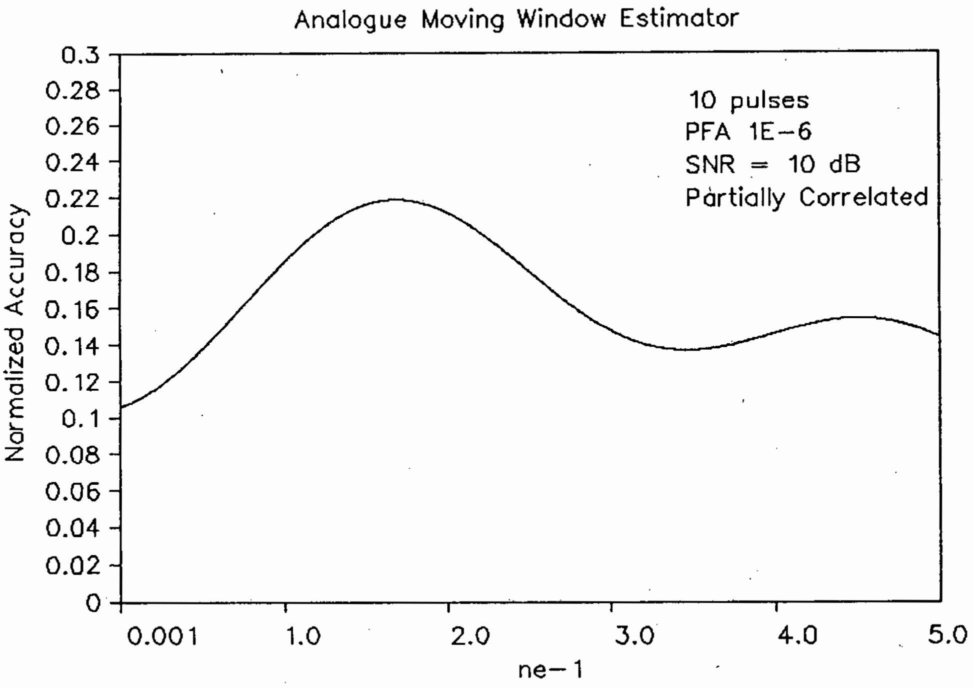

Figure 5.2.6-1: Analogue moving window estimator

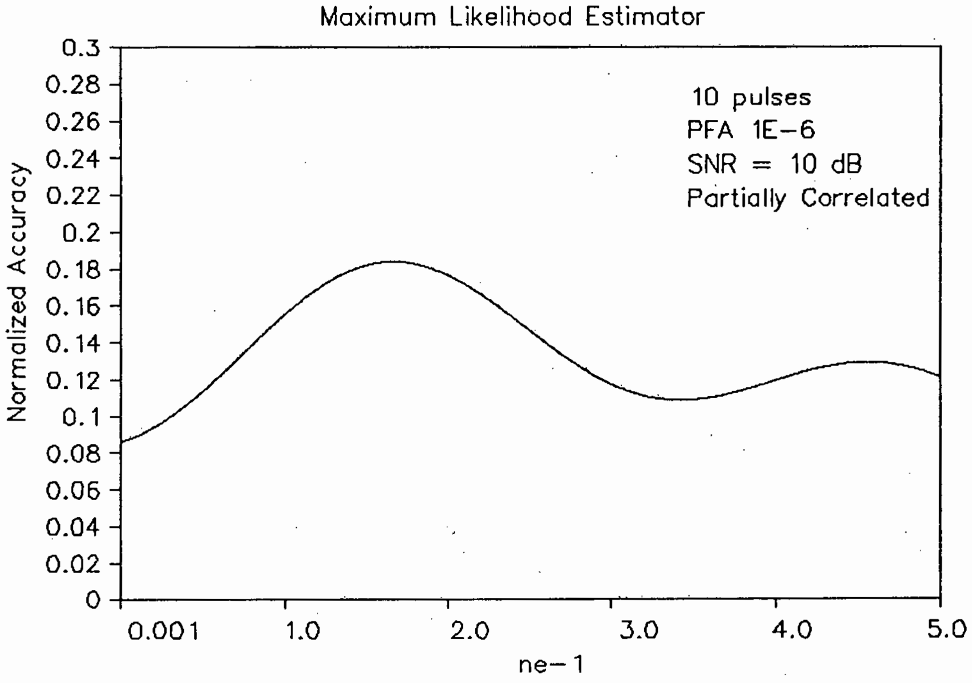

Figure 5.2.6-2: Maximum likelihood estimator

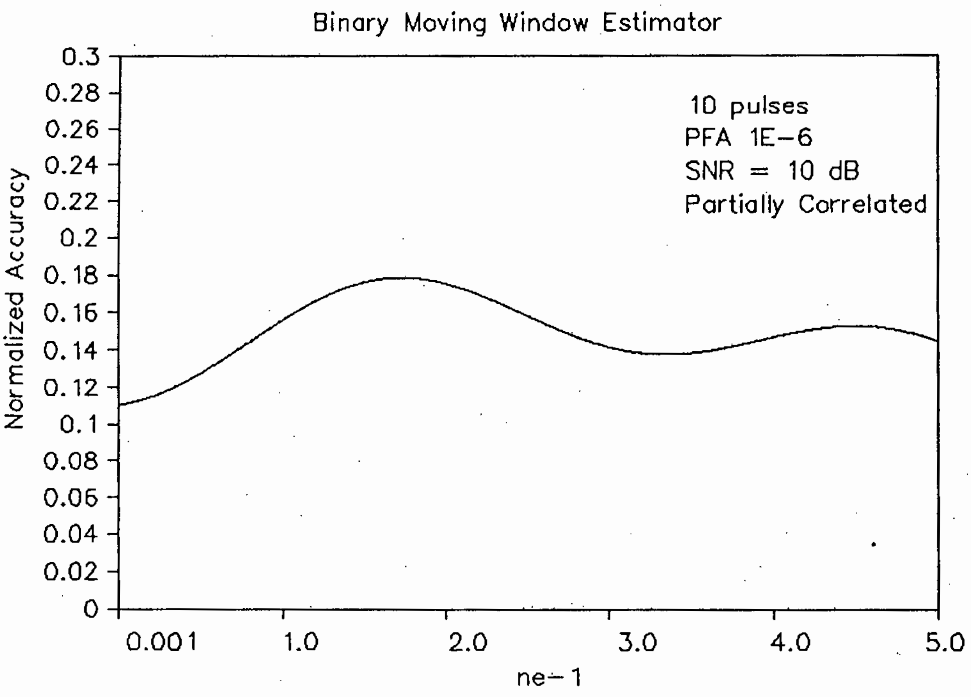

Figure 5.2.6-3: Binary moving window estimator

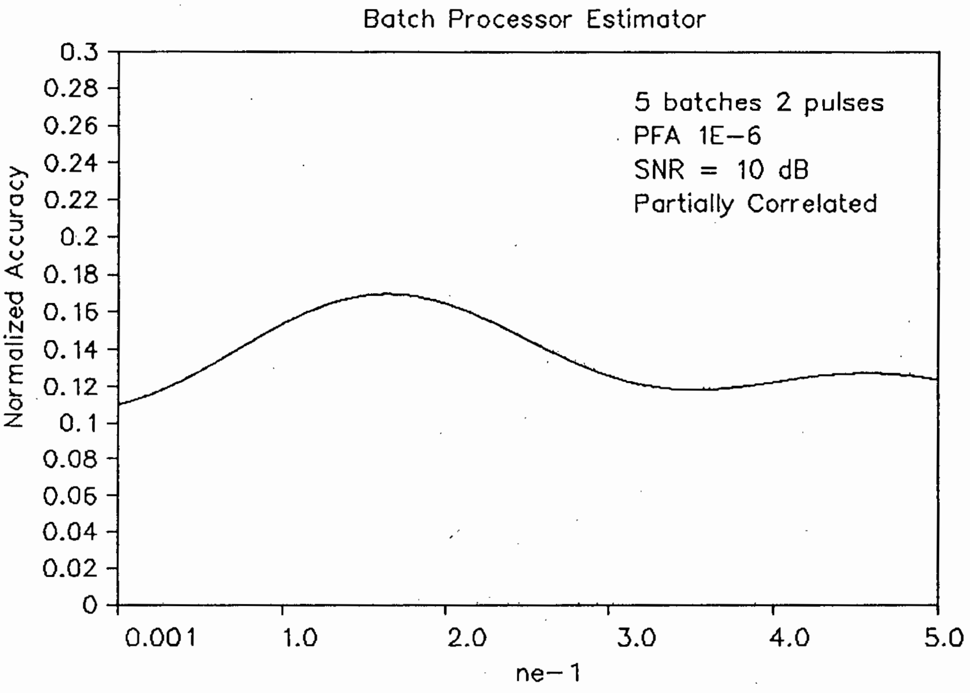

Figure 5.2.6-4: Batch processor estimator

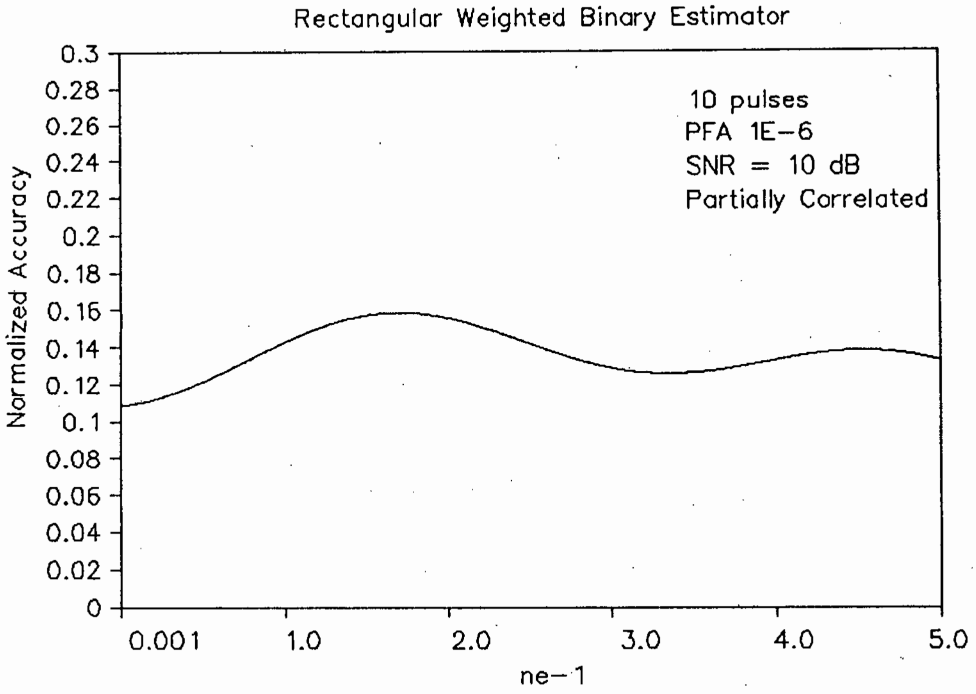

Figure 5.2.6-5: Rectangular weighted binary estimator

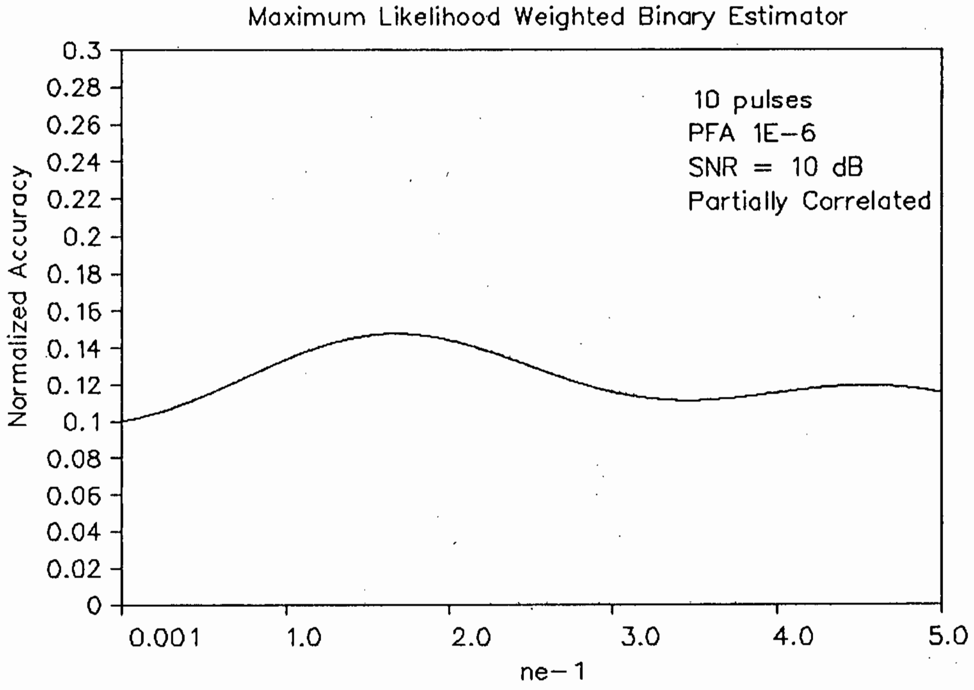

Figure 5.2.6-6: Maximum likelihood weighted binary estimator

5.2.7 Clutter Influence

Clutter affects the detection and estimation performance of a radar by reflecting incident energy which competes with the energy reflected by the detected object. The influence on the azimuth estimate is largely dependant on the magnitude of the received clutter power during the detection and estimation process. If the detected object is enclosed by clutter, as indicated in figure 5.2.7-1, the clutter power functions as an additional noise source, and the azimuth estimate deteriorates accordingly. This is illustrated in figure 5.2.7-2.

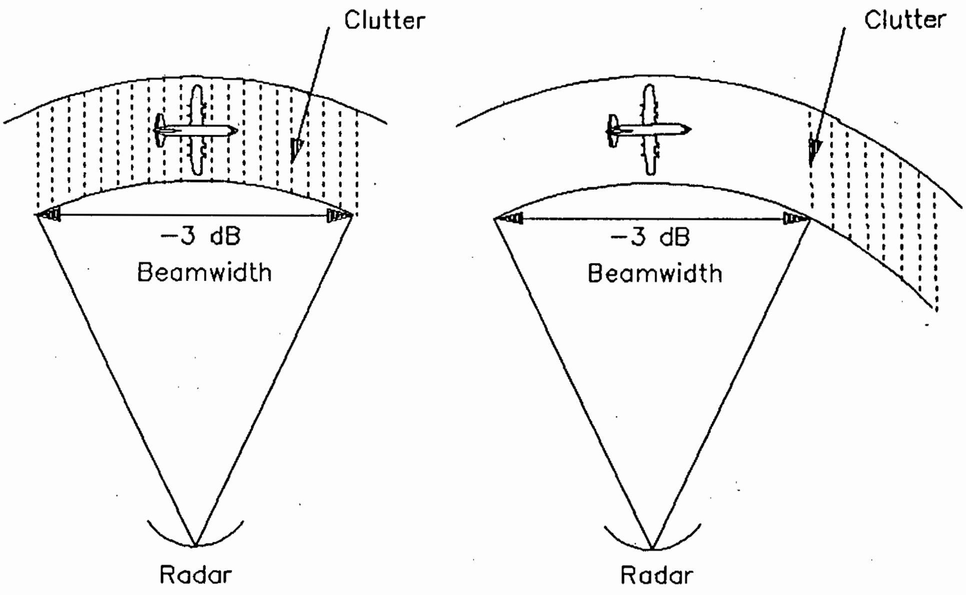

Figure 5.2.7-1: Clutter scenarios

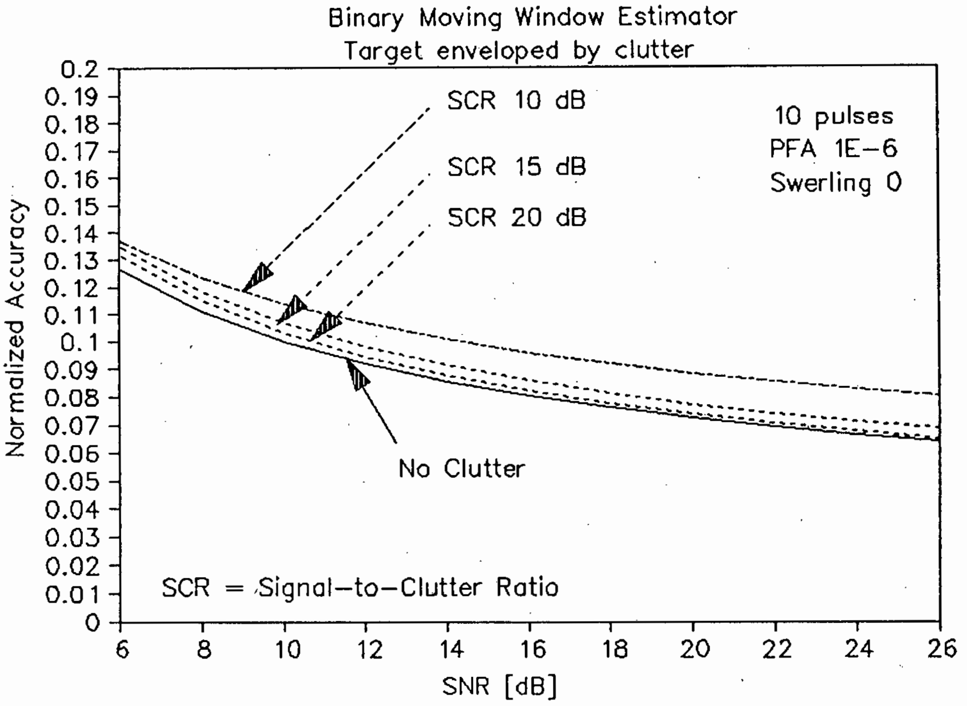

Figure 5.2.7-2: Target enclosed by clutter

The signal-to-clutter ratio has been maintained at a fixed value and the object is assumed to be enclosed in clutter. For clutter offset from the desired object (figure 5.2.7-3), the azimuth estimate is affected at large signal-to-noise ratios, but at small ratios the influence is less pronounced. This is largely due to the reduced antenna gain in the direction of the clutter when the nose of the beam is pointing at the detected object. At low ratios, the returned clutter power at the reduced antenna gain will be negligible in the scenario chosen (figure 5.2.7-3), and the estimator performance will be determined by the thermal noise. With increased ratios, however, due to the signal-to-clutter ratio being maintained constant the received clutter power will no longer be negligible, and the azimuth estimate will deteriorate. This behaviour supports the theory which states that the azimuth accuracy standard deviation will deteriorate as a function of signal-to-interference. Practical systems usually employ clutter rejection techniques such as moving target indicator processors to reduce the clutter power with which the detected object must compete.

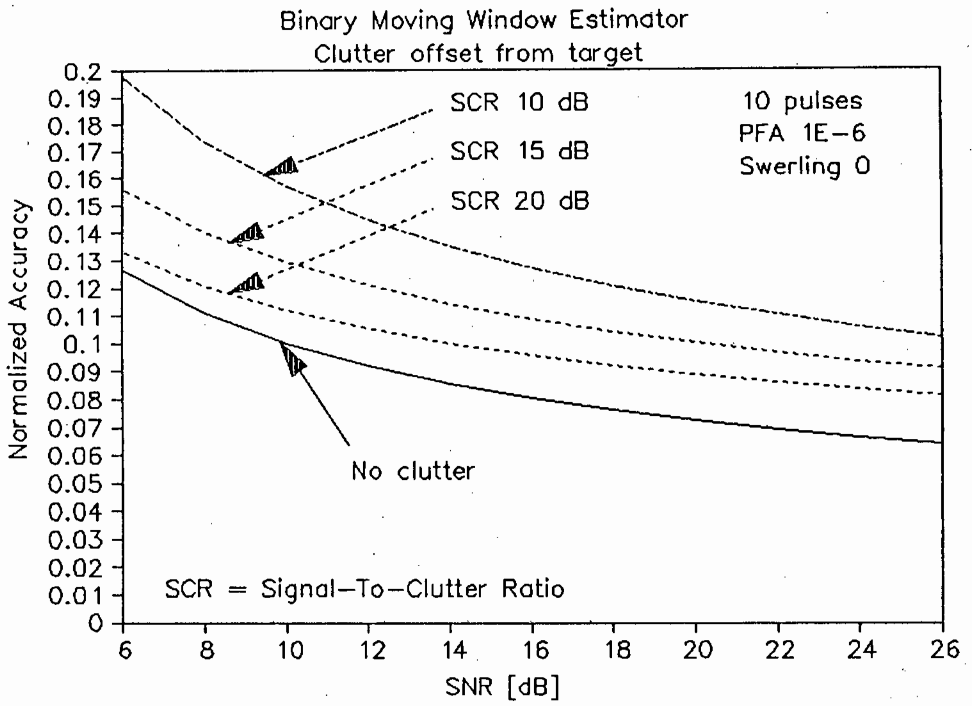

Figure 5.2.7-3: Offset clutter

5.2.8 Increased Number of Pulses

Figures 5.2.8-1 through 5.2.8-6 illustrate the achieved results for the case of 40 pulses integrated. The graphs illustrate an improvement with the number of pulses integrated, as is expected due to the improved probability of detection for a given signal-to-noise ratio (5.2.1-1). In his original work, Swerling [45] produced a single curve by scaling all the results with a normalization factor $\sqrt{N}/\beta$. With this, Swerling assumed that the quantization noise is negligible, and that the improvement in accuracy is directly related to the number of pulses integrated via a factor $\sqrt{N}$ (where N represents the number of pulses integrated with the antenna beamwidth). Whether this applies to the estimators simulated and to all target models is not clear from the limited number of simulation runs performed with increased numbers of pulses. Application of the normalizing factor to the curves of figure 5.2.8-1 through 5.2.8-6 did not yield a single curve per estimator, but more curves are required to establish whether a single curve could be applied per estimator.

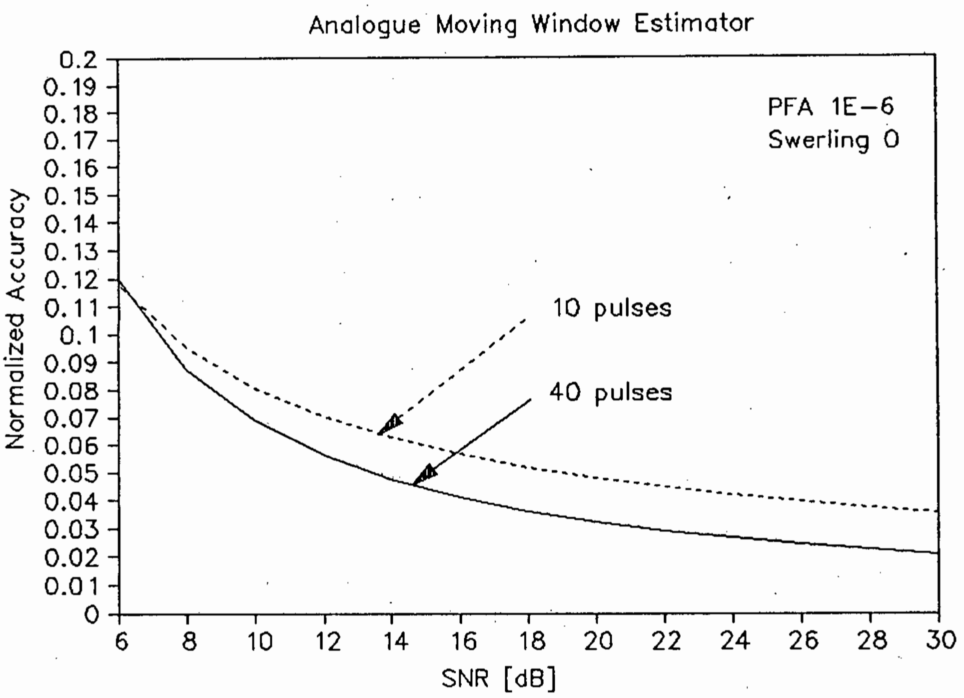

Figure 5.2.8-1: Analogue moving window estimator, 40 pulses

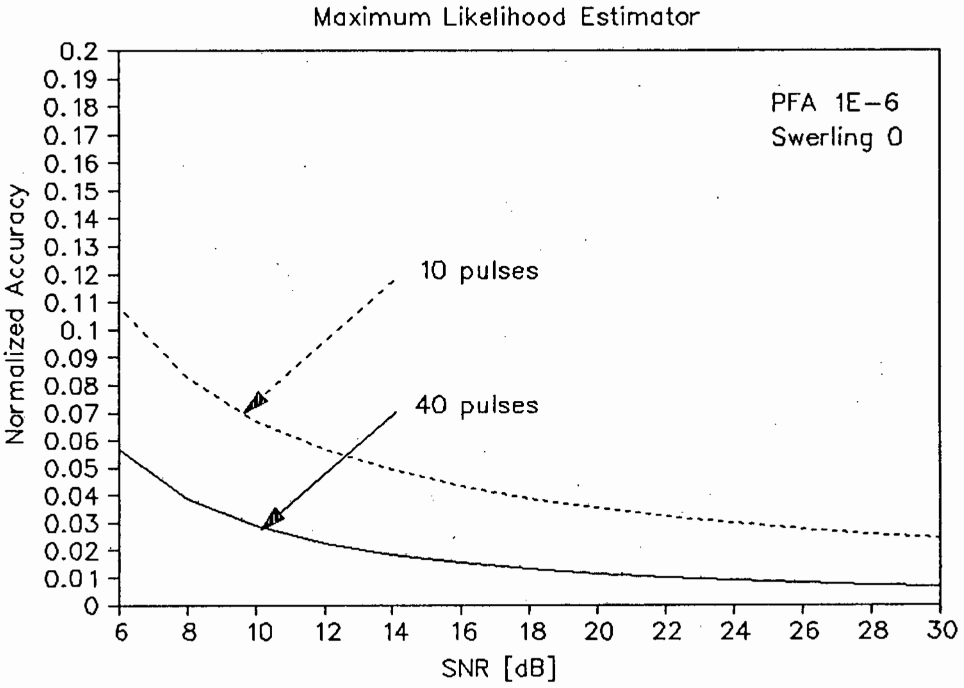

Figure 5.2.8-2: Maximum likelihood estimator, 40 pulses

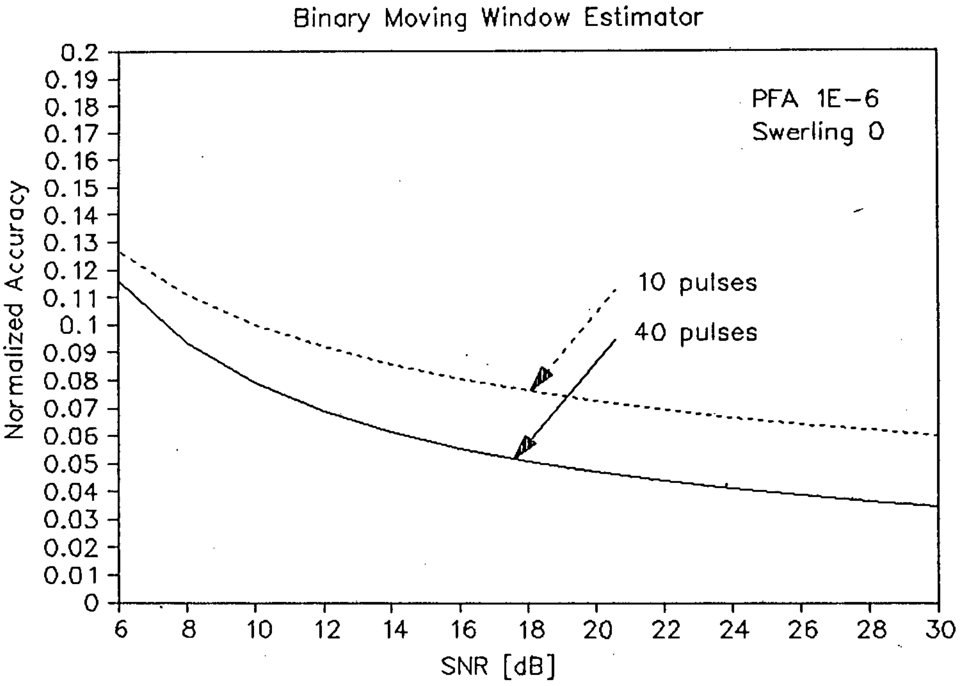

Figure 5.2.8-3: Binary moving window estimator, 40 pulses

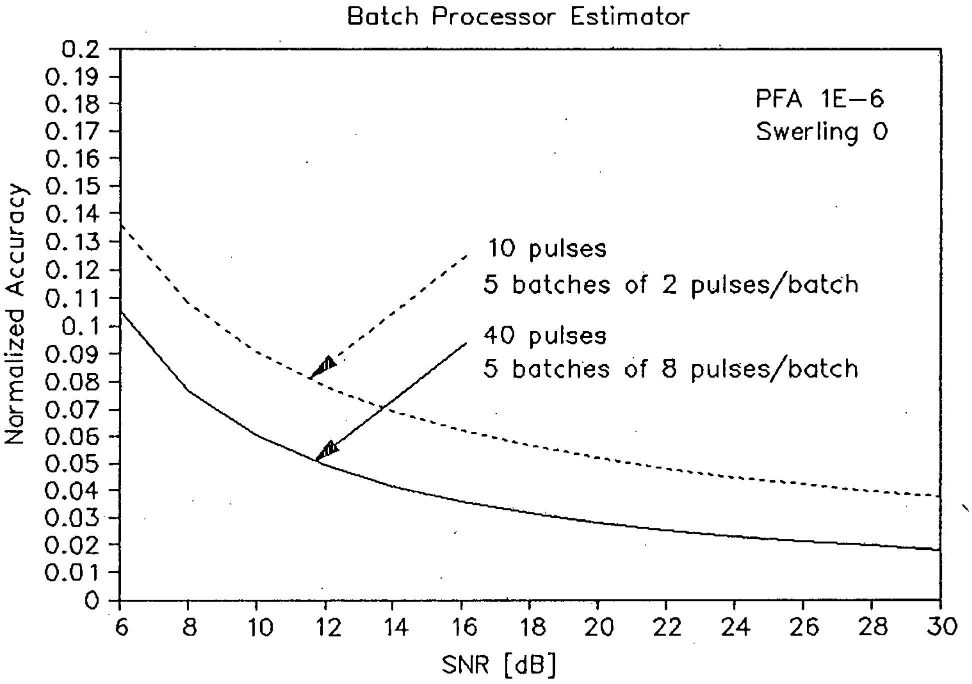

Figure 5.2.8-4: Batch processor estimator, 40 pulses

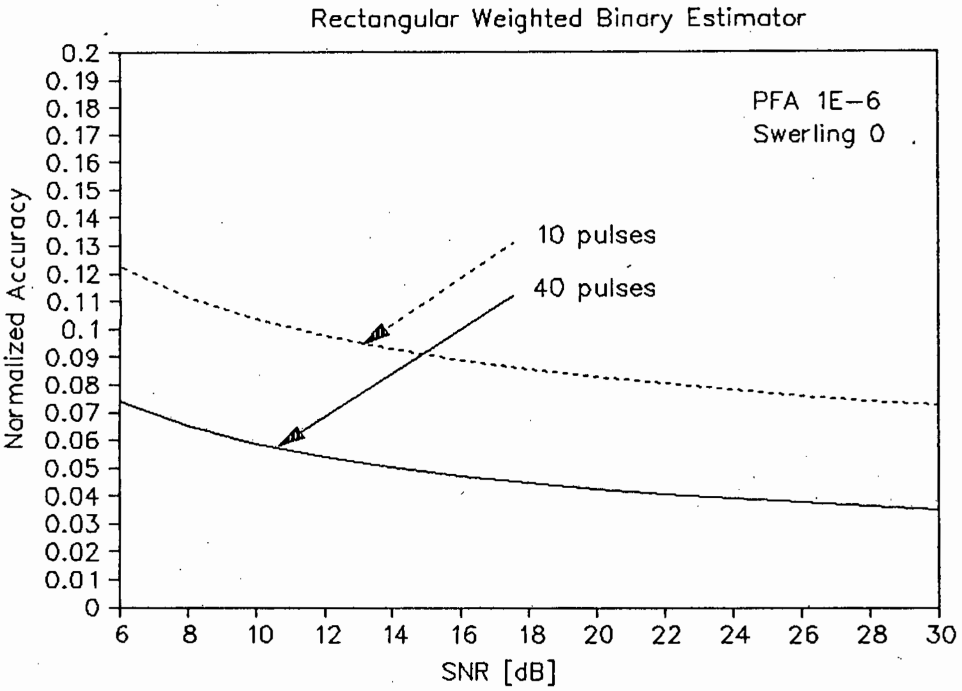

Figure 5.2.8-5: Rectangular weighted binary estimator, 40 pulses

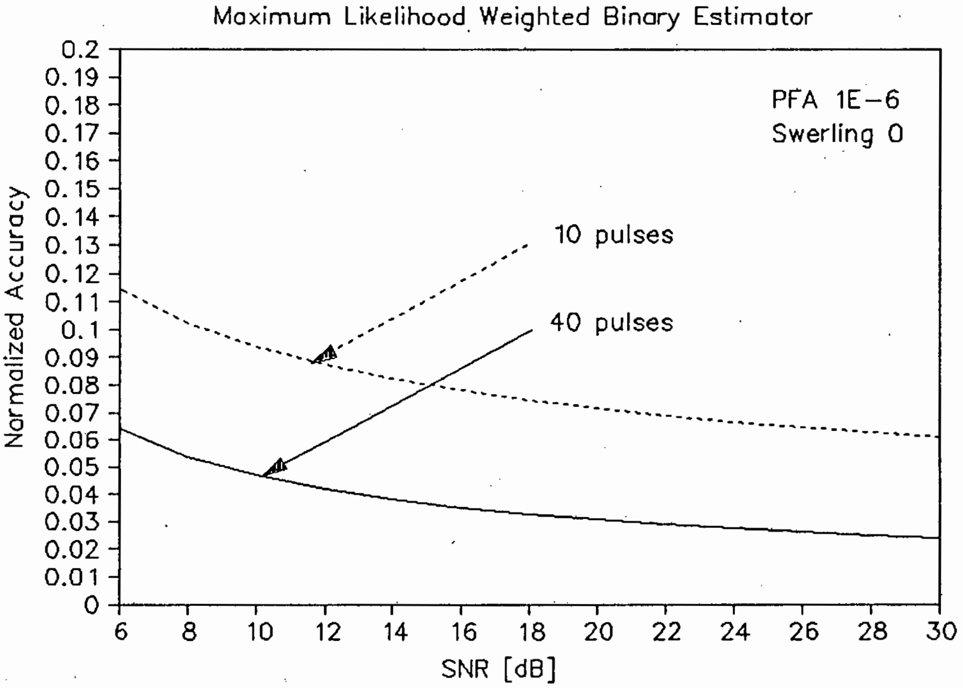

Figure 5.2.8-6: Maximum likelihood weighted binary estimator, 40 pulses

5.2.9 Theoretical Performance

In order to evaluate the performance of the simulations against theory, the generalized accuracy approach described in chapter 2 has been applied in determining the theoretical normalized accuracy for the maximum likelihood estimator and rectangular weighted unbiased estimator assuming a gaussian antenna pattern. The theoretical curves and the simulated results are illustrated in figures 5.2.9-1 and 5.2.9-2. In both cases, the simulations correspond to the theoretical curves to a large degree. At low signal-to-noise ratios the simulations produce a better result than the theory, which may be due to insufficient samples being available at these ratios to obtain sufficient accuracy with the results.

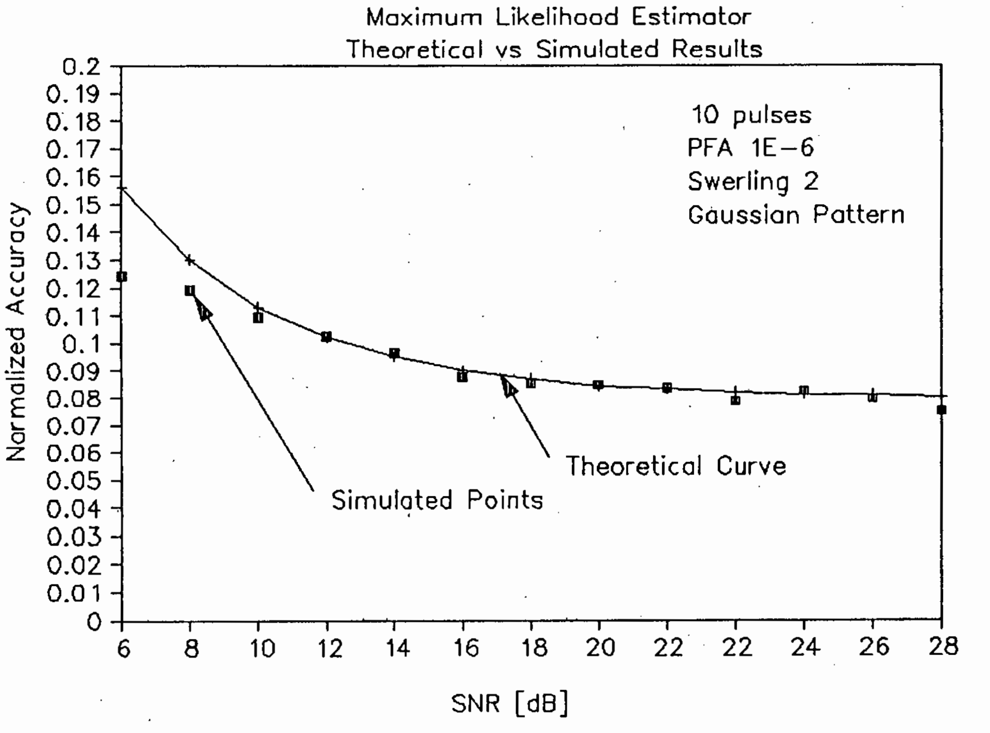

Figure 5.2.9-1: Maximum likelihood estimator theoretical vs simulated

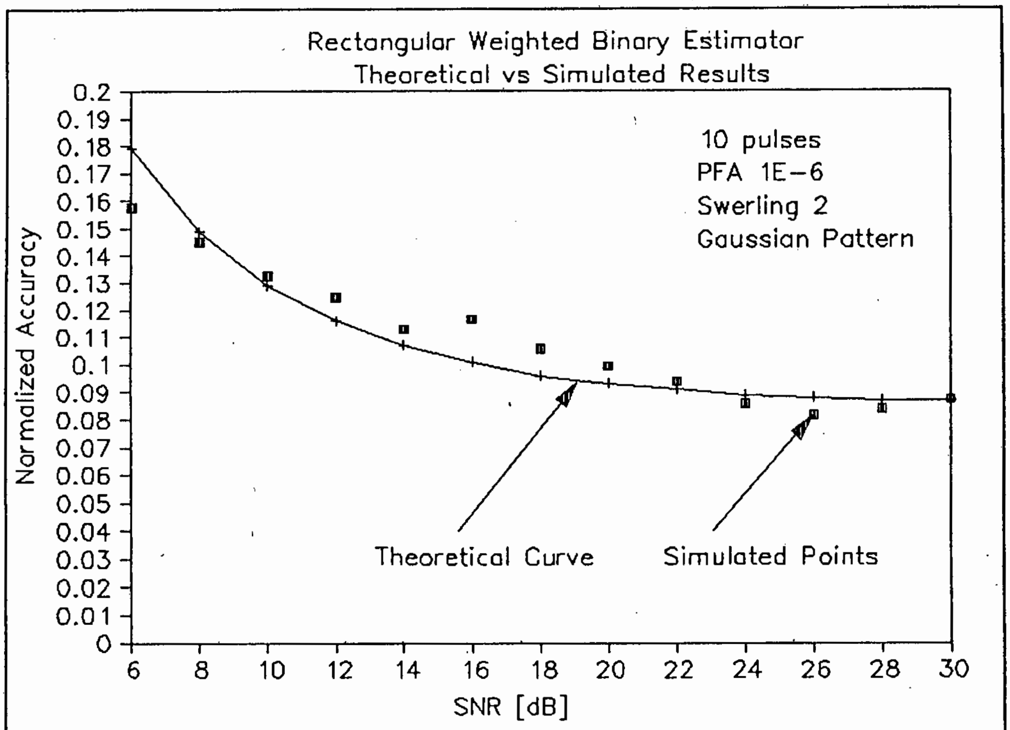

Figure 5.2.9-2: Rectangular weighted unbiased estimator vs simulated

Swerling [45] presented graphs of the minimum theoretical angular accuracy (Cramer-Rao lower bound) as a function of single pulse signal-to-noise ratio for both the non-fluctuating and fast-fluctuating target models assuming a gaussian antenna pattern. The graphs presented by Swerling are normalized by a factor $\sqrt{N}/\beta$ (N is the number of pulses within the 1/e power points of the antenna pattern and 2β is the 1/e power beamwidth). In order to achieve the corresponding graphs normalized to the half-power beamwidth, a scaling factor of 1.833 must be applied. The scaling factor follows from rewriting the expression in terms of the half-power parameters:

$$\frac{\sigma\sqrt{N}}{\beta} = \frac{\sigma\sqrt{[n/0.825]}}{\theta_3/1.665} \qquad (5.2.9\text{-}1)$$

The results presented by Swerling scaled for 10 pulses within the half-power beamwidth are shown in figure 5.2.9-3. In the graph the predicted theoretical results for the maximum likelihood and rectangular weighted unbiased estimator are also indicated for comparison.

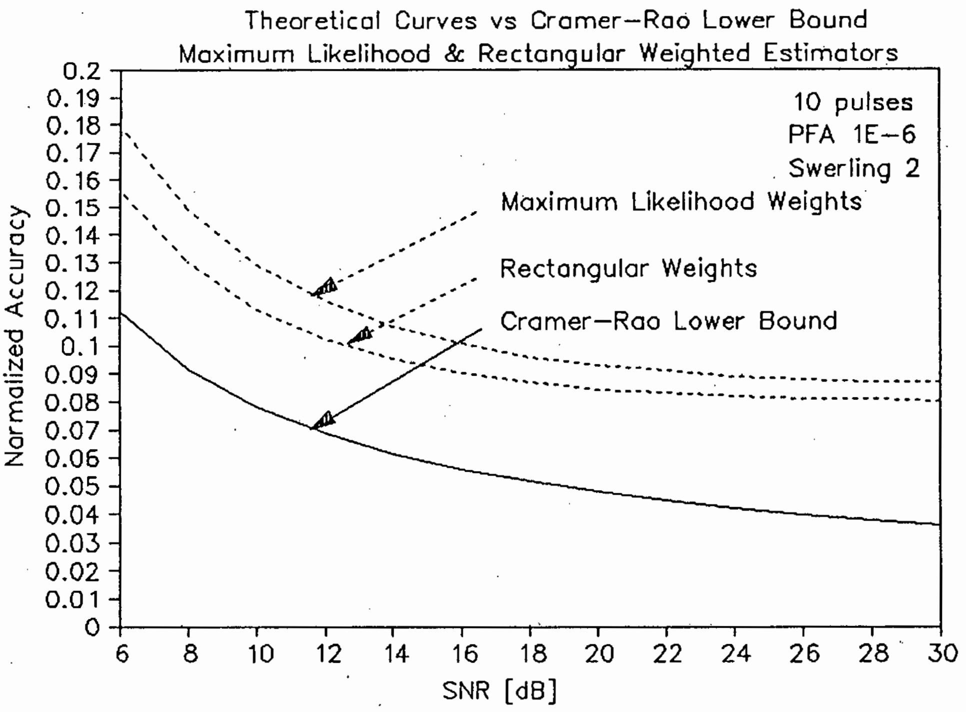

Figure 5.2.9-3: Cramer-Rao lower bound versus theoretical curves

6.0 CONCLUSIONS

6.1 SUMMARY

A method has been developed to enable the performance of different estimators to be evaluated. Two categories of estimators have been considered:

- unbiased estimators
- biased estimators.

Table 6.1-3 summarizes the target models evaluated for the different estimators assuming 10 pulses returned within the half-power beamwidth and a probability of false alarm out of the integrator of 1E-6. For each of the simulations 500 scans were applied per signal-to-noise value in order to achieve repeatability of results to the second digit after the decimal point in the normalized accuracy. For each of the runs, a least-squares curve fit was performed with a power curve of the form ax^b. The residual error was typically less than 10^{-2}. The table indicates the different estimators in the eights rows, while each of the columns represent a parameter evaluated. The numbers indicated within the matrix define the particular target models evaluated. The table shows that for the gaussian antenna pattern, all the swerling models have been considered. The results achieved with these evaluations showed that the success-run and sequential observer estimators yielded practically the same results as the binary moving window. These estimators were therefore not considered in the further evaluations. A similar argument applied to the 2-pole filter which yielded very similar results to that of the analog moving window estimates if a beam-splitting approach was used. Use of a peak-detected value yielded such poor results with fluctuating targets that this did not warrant further investigation.

In the evaluation of antenna pattern, adaptive thresholding, clutter and number of pulses (40) returned the object model was limited to the non-fluctuating case in order to remove any additional limitations imposed by radar cross-section fluctuation. It is expected that in most cases considered, the trends set by the non-fluctuating case will also be exhibited by the fluctuating cases. However, further investigations would be required to substantiate this.

The effects of clutter have only been considered for the binary moving window estimator largely due to long computation times required by the simulations. Due to the insensitivity of the binary estimator to interference, it may be expected that the full amplitude processing estimators will be more severely affected. However, a detailed study of the effects of clutter in various scenarios is required to enable a general statement to be made.

Table 6.1-1: Estimator key table

Code	Estimator	Class
0	Analogue moving window	Biased
1	Maximum likelihood	Unbiased
2	2-Pole	Biased
3	Binary moving window	Biased
4	Success-run	Biased
5	Sequential observer	Biased
6	Rectangular weighted binary window	Unbiased
7	Maximum likelihood weighted binary window	Unbiased
8	Batch Processor	Biased

Table 6.1-2: Target model key table

Code	Target model
0	Non-fluctuating
1	Swerling 1: scan-to-scan fluctuation
2	Swerling 2: pulse-to-pulse fluctuation
3	Swerling 3: scan-to-scan fluctuation
4	Swerling 4: pulse-to-pulse fluctuation
5	Log-normal: scan-to-scan fluctuation
6	Partially correlated from pulse-to-pulse

Table 6.1-3: Summary of evaluations

Estimator	Quantization	Thresholding	Gaussian Beam	Sinx/x Beam	Clutter	40 pulses
0	0	0	0,1,2,3,4,5,6	0	0	0
1		0	0,1,2,3,4,5,6	0		0
2		0	0,1,2,3,4			
3	0	0	0,1,2,3,4,5,6	0		0
4			0,1,2,3,4	0		
5			0,1,2,3,4			
6		0	0,1,2,3,4,5,6			0
7		0	0,1,2,3,4,5,6	0		0
8		0	0,1,2,3,4,5,6	0		0

6.2 FUTURE INVESTIGATIONS

The current simulations have provided the capability to evaluate different aspects of estimation. However, only a part of these capabilities have been utilized in this dissertation. Future work could concentrate amongst other areas on the following:

1. The effects of clutter on the different estimators (Chapter 5 paragraph 5.2.7). This would require different CFAR processing techniques to be evaluated as well in order to reduce the effects of clutter.

2. The improvements achievable by the application of specific plot extraction rules. Typical examples of such rules would be to reject detections which fall within the resolution of the initial detection, or a selection of the detection with the largest extent if multiple detections occur within a resolution cell. For extended targets some form of cluster recognition [1] could be applied.

6.3 CONCLUSIONS

The results achieved show an optimum performance for the non-fluctuating case with the maximum likelihood estimator as expected. The performance of the binary estimators indicates the reason for their popularity in practical systems, particularly due to their ease of implementation and relative insensitivity to scintillation. An improvement to the binary system is given by the batch processing technique which yields better detection and estimation performance than the pure binary system. A limitation to this method is the requirement to process full amplitude video within each batch, but compared to the full analogue processing, there is a distinct advantage.

The results achieved with clutter indicate that the received clutter power appears to the estimators as an additional noise source with corresponding deterioration in azimuth accuracy. Further studies are required to enable a general statement on the effects of clutter to be made.

The results achieved with different antenna patterns illustrate that a general rule relating performance to antenna pattern is not applicable amongst all estimators (assuming identical half-power beamwidths). The effects achieved with different target models are reasonably predictable for the different estimators.

APPENDIX A

ANGULAR MULTIPATH GEOMETRY

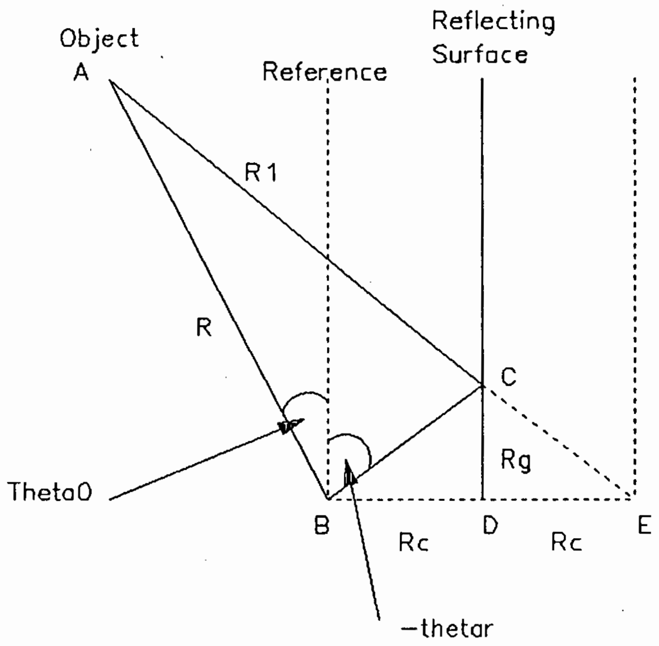

Figure A.1-1: Angular multipath geometry

Derivation:

$$\angle BCD = \|\theta_r\| \tag{D.1-1}$$

$$\angle BCA = 180 - 2\|\theta_r\| \tag{D.1-2}$$

$$\angle BAC = 2\|\theta_r\| - \|\theta_o - \theta_r\| \tag{D.1-3}$$

$$\frac{R}{\sin[180 - 2\|\theta_r\|]} = \frac{R_2}{\sin[2\|\theta_r\| - \|\theta_o - \theta_r\|]} \tag{D.1-4}$$

$$R_2 = \frac{\sin[2\|\theta_r\| - \|\theta_o - \theta_r\|]}{\sin[180 - 2\|\theta_r\|]} * R \tag{D.1-5}$$

$$R_c = R_2 \sin[\|\theta_r\|] \tag{D.1-6}$$

$$R_g = R_2 \cos[\|\theta_r\|] \tag{D.1-7}$$

$$\delta R = (R_1 + R_2) - R \tag{D.1-8}$$

PROBABILITY OF DETECTION VERIFICATION

Hand plotted points have been obtained via simulations of detection probability using 10^5 samples assuming a square law detector and linear non-coherent integration of 10 pulses.

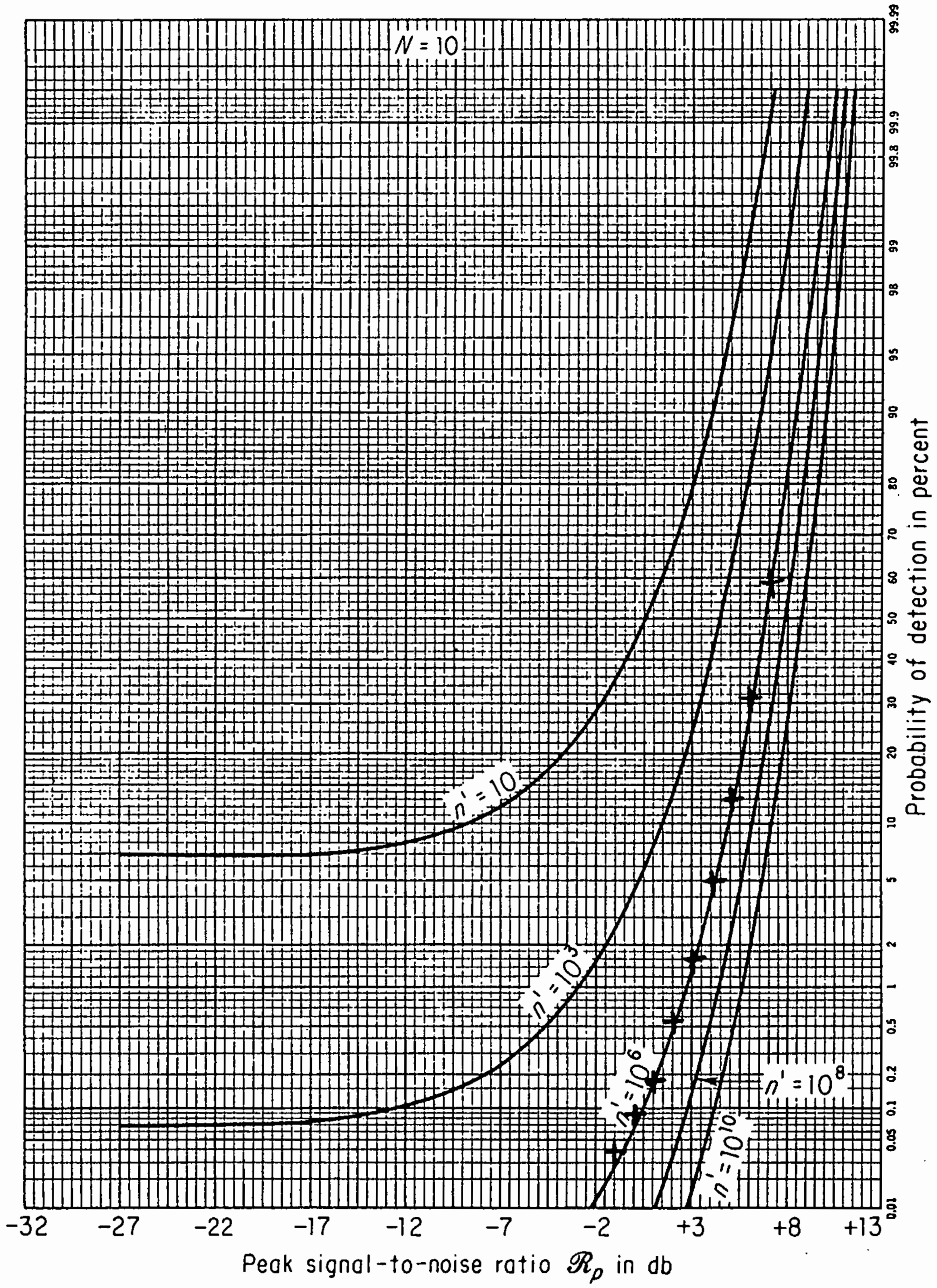

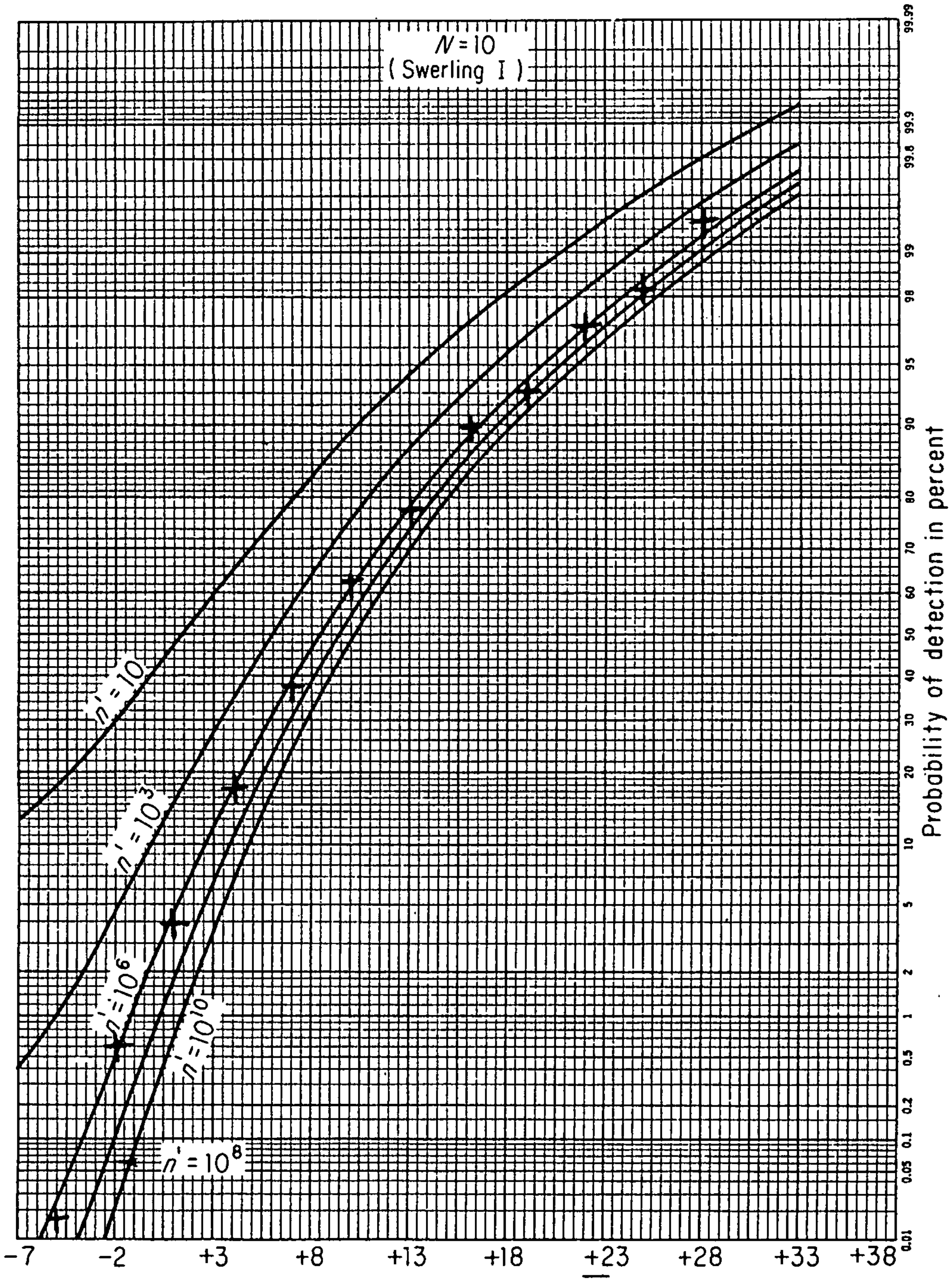N = 10
(Swerling I)
n' = 10
n' = 10^3
n' = 10^6
n' = 10^10
n' = 10^8
-7
-2
+3
+8
+13
+18
+23
+28
+33
+38
Peak signal-to-noise ratio $\overline{\mathscr{R}}_p$ in db
0.01
0.05
0.1
0.2
0.5
1
2
5
10
20
30
40
50
60
70
80
90
95
98
99
99.8
99.9
99.99
Probability of detection in percent

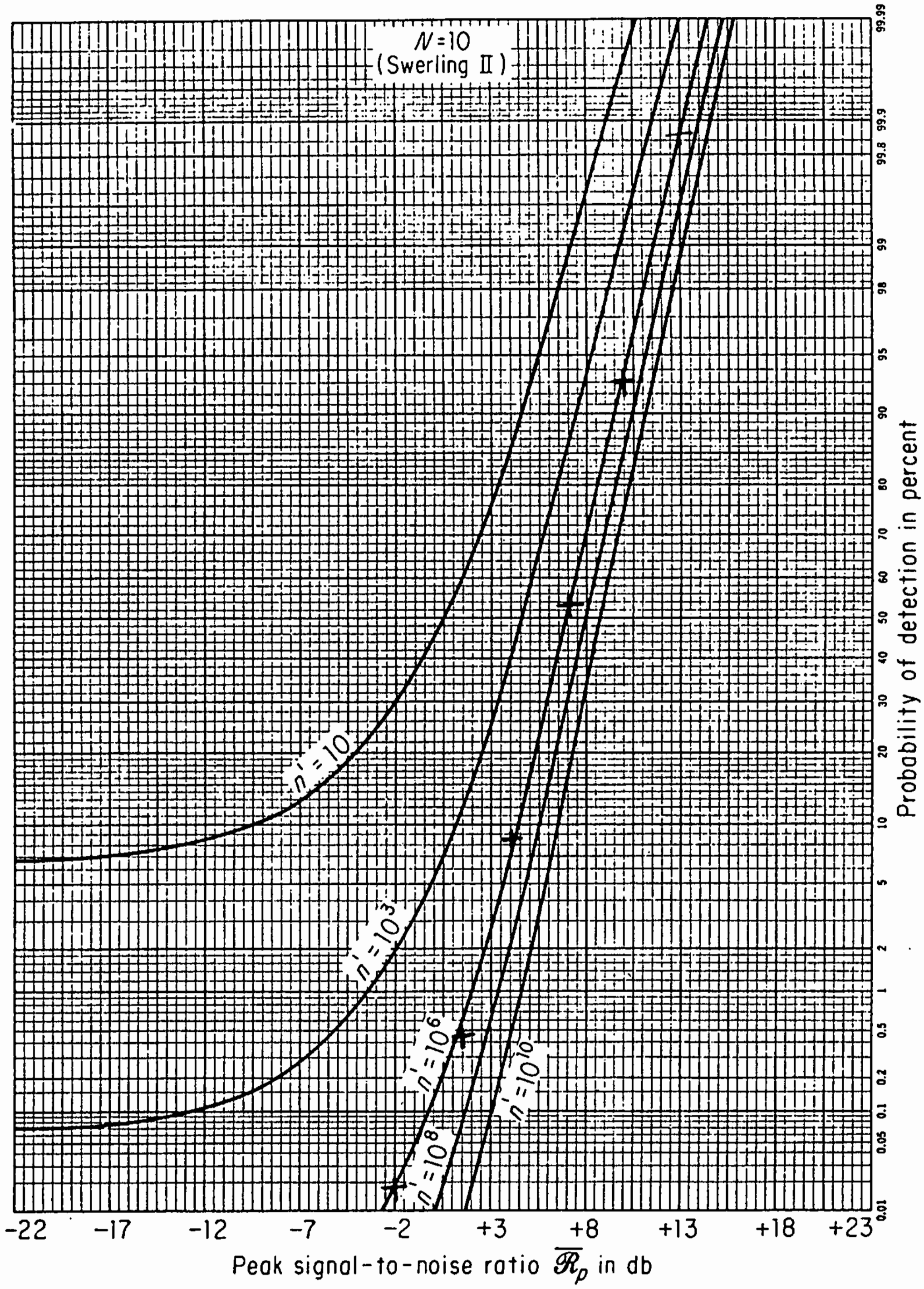

N=10
(Swerling II)
n'=10
n'=10^3
n'=10^6
n'=10^8
n'=10^{10}
-22
-17
-12
-7
-2
+3
+8
+13
+18
+23
Peak signal-to-noise ratio $\overline{\mathcal{R}_p}$ in db
0.01
0.05
0.1
0.2
0.5
1
2
5
10
20
30
40
50
60
70
80
90
95
98
99
99.8
99.9
99.99
Probability of detection in percent

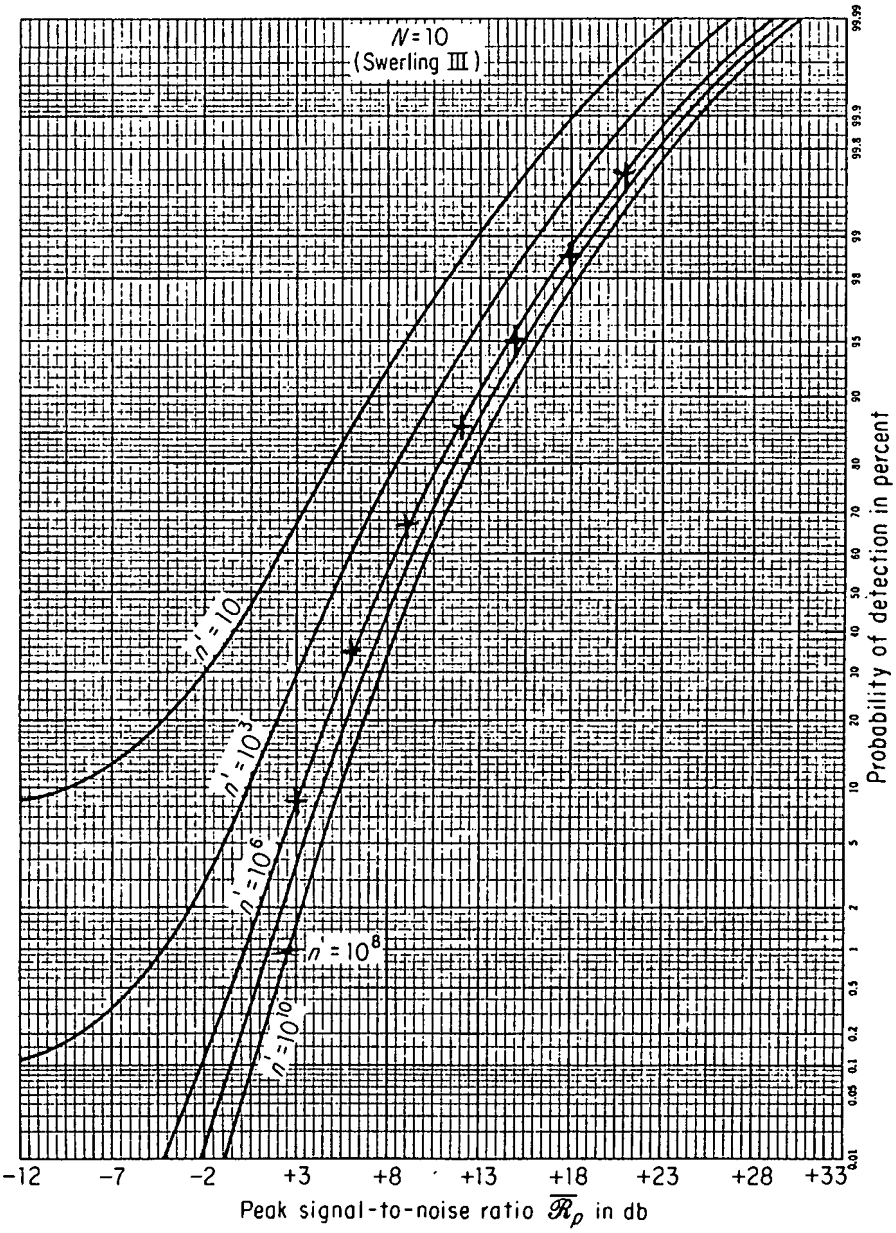
N=10
(Swerling III)
n' = 10
n' = 10^3
n' = 10^6
n' = 10^8
n' = 10^10
-12
-7
-2
+3
+8
+13
+18
+23
+28
+33
Peak signal-to-noise ratio $\overline{\mathcal{R}}_p$ in db
99.99
99.9
99.8
99
98
95
90
80
70
60
50
40
30
20
10
5
2
1
0.5
0.2
0.1
0.05
0.01
Probability of detection in percent

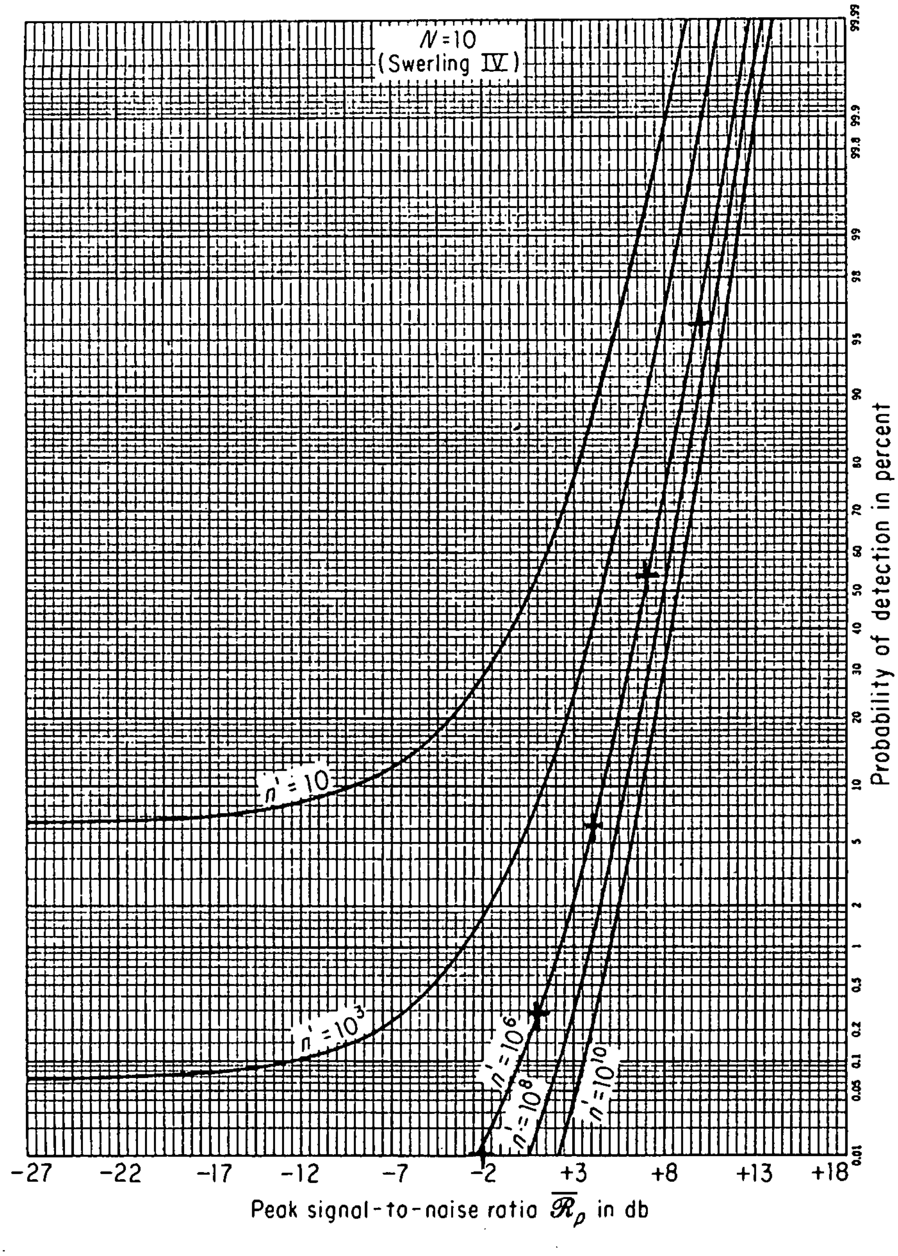

$N=10$
(Swerling IV)
$n'=10$
$n'=10^3$
$n'=10^6$
$n'=10^8$
$n'=10^{10}$
-27
-22
-17
-12
-7
-2
+3
+8
+13
+18
Peak signal-to-noise ratio $\overline{\mathcal{R}}_p$ in db
0.01
0.05
0.1
0.2
0.5
1
2
5
10
20
30
40
50
60
70
80
90
95
98
99
99.8
99.9
99.99
Probability of detection in percent

APPENDIX C

SIMULATION PROGRAM PARAMETERS

Table B-1: Target Parameters

Parameter	Options
range cell spread	
azimuth cell spread	
average radar cross-section	
target model	0,1,2,3,4,log-normal
doppler component	
number of independent pulses n_e-1	
range position	
azimuth position	

Table B-2: Clutter Parameters

Parameter	Options
range cell spread	
azimuth cell spread	
mean backscatter coefficient	
mean-to-median ratio	
number of spectral components	
frequency separation between spectral components	
spectral component amplitude distribution	
range start of clutter	
azimuth start of clutter	

Table B-3: Radar Parameters

Parameter	Options
first threshold false alarm probability	
signal-to-noise ratio	
signal-to-clutter ratio	
pulse length	
antenna transmit and receive gain	
transmit frequency	
pulse repetition frequency	
system losses	
noise figure	
noise temperature	
antenna rotation rate	
CFAR mean cell size	
CFAR guard cell size	
CFAR margin	
number of analogue-to-digital bits	
clip level	

Table B-4: Simulation Parameters

Parameter	Options
simulation start range	
simulation end range	
number of scans per trial	
number of trials	
clutter simulation	true/false
CFAR processing	true/false
greater-of CFAR	true/false
digital conversion	true/false

video type	linear/logarithmic
antenna pattern	gaussian,sinx/x,user
processing	binary/full amplitude
estimator weights	rectangular
	centre of gravity
	maximum likelihood
estimator type	binary moving window
	Success-run
	Sequential observer
	weighted binary
	analogue moving window
	two-pole
	weighted analogue
	batch processor
data processing rules	none
	resolution criteria
	maximum extent selection
	ambiguity midpoint

APPENDIX D

GENERATION OF A PARTIALLY CORRELATED RAYLEIGH TARGET

It is known from statistical theory that an exponential variate may be derived from two independent gaussian variates according to:

$$s = x^2 + y^2 \tag{A.1-1}$$

where:

s = exponential variate with characteristics

$$p_s(s) = (1/<s>)\ \exp(-s/<s>) \tag{A.1-2}$$

$$E(s) = <s> \tag{A.1-3}$$

$$\sigma_s^2 = <s>^2 \tag{A.1-4}$$

x, y = independent gaussian variates with characteristics

$$p_x(x) = (1/[\sigma_x\surd(2\pi)]\ \exp -[x^2/(2\sigma^2) \tag{A.1-5}$$

$$E(x) = 0 \tag{A.1-6}$$

$$Var(x) = \sigma_x^2 \tag{A.1-7}$$

Independent zero-mean gaussian variates (r_1 , r_2) with a standard deviation of one can be generated according to a method described by Box and Muller:

$$r_1 = \surd[-2\ln(u_1)] * \cos(2\pi u_2) \tag{A.1-8}$$

$$r_2 = \surd[-2\ln(u_1)] * \sin(2\pi u_2) \tag{A.1-9}$$

where:

u_1 and u_2 are uniform variates.

Transformation to gaussian variates with mean μ_x and standard deviation σ_x is achieved by:

$$x = \mu_x + \sigma_1\sigma_x \tag{A.1-10}$$

$$y = \mu_y + \sigma_2\sigma_y \tag{A.1-11}$$

In order to generate correlated exponential variates with a normalized autocorrelation function given by:

$$\rho(\tau) = \exp[-2\|\tau\|/\tau_c] \tag{A.1-12}$$

where:

$$\tau_c = \lambda/[2w_aL_x] \tag{A.1-13}$$

$$= 1/[\pi f_3] \tag{A.1-14}$$

with a corresponding power spectral density

$$S_s(w) \quad w_o/[1 + (f/f_3)] \tag{A.1-15}$$

the underlying gaussian variates are required to be first-order gauss-markov variates with an exponential autocorrelation function

$$\rho(\tau) = \exp(\beta_x\|\tau\|) \tag{A.1-16}$$

Blackman [10] provides a recursive relationship with which variates of a first-order gauss-markov process can be generated:

$$x(k+1) = x(k)\rho_x(k) + \surd[1-\rho_x^2(k)] * \sigma_x r(k) \tag{A.1-17}$$

where:

$\rho_x(k) = \exp(-\beta_x \| k \|)$ (A.1-18)

k = sampling interval

β_x = 1 / process correlation time constant

σ_x = process standard deviation

$r(k)$ = zero mean, unit standard deviation gaussian variate

$x(1)$ = gaussian sample with zero mean and standard deviation σ_x

The relationships between correlated gauss-markov processes a and b and the exponential variate s if transformation (A.1-17) is used, may be summarized by:

$E(s) = 2\sigma_x^2$ (A.1-18)

$\sigma_s^2 = 4\sigma_x^4$ i.e. $\sigma_s = 2\sigma_x^2$ (A.1-19)

$\rho_s(\tau) = \exp[-2\beta_x \| \tau \|]$ i.e. $\tau_x = 2\tau_s$ (A.1-20)

In order to generate a radar cross-section representing a Rayleigh scatterer, correlated exponential variates with unit mean and standard deviation may be applied:

$$\sigma = <\sigma> * s/<s> \qquad \text{(A.1-21)}$$

APPENDIX E

CLUTTER SIMULATION

The signal return from a clutter cell is assumed to be represented by an exponentially distributed power envelope, which results from gaussian distributed in-phase and quadrature components. In order to model the spatial dcorrelation of clutter, the underlying gaussian statistics should exhibit correlation. Mitchell [32] has shown that, assuming a gaussian shaped spectrum given by:

$$S(f) = \exp[-(\alpha f/f_3)^2 \qquad (C.1\text{-}1)$$

the corresponding autocorrelation function $R(\tau)$ is given by:

$$R(\tau) = \exp[-(\pi f_3 \tau_c/\alpha) \qquad (C.1\text{-}2)$$

The gaussian spectrum is represented by five spectral components spaced $0.6f_3$ apart [32]. The total returned clutter power is allocated to the five spectral components according to:

n	1	2	3	4	5
power	0.0104	0.2078	0.5637	0.2078	0.0104

The spectral frequencies are given by:

$$f_n = (n-3)\delta f \qquad \text{where: } \delta f = 0.6f_3 \qquad (C.1\text{-}3)$$

The land clutter parameters assumed are given by [43]:

$$\sigma^{o} = 0.00032/\phi \qquad \text{(C.1-4)}$$

$$\sigma_{v} = 0.32\text{m/s} \qquad \text{(C.1-5)}$$

$$\sigma_{c} = 2\sigma_{v}/\phi \qquad \text{(C.1-6)}$$

$$\sigma_{scan} = 0.265\ f_{prf}/n \qquad \text{(C.1-7)}$$

$$f_{3} = 2.35\sigma_{c} \qquad \text{(C.1-8)}$$

APPENDIX F

MAXIMUM ANGULAR ACCURACY OF A PULSED RADAR: RECURSIVE CALCULATION APPROACH.

Research Review, Department of Electrical and Electronic Engineering, University of Cape Town, vol. 14, Autumn 1989, p. 81-96.

MAXIMUM ANGULAR ACCURACY OF A PULSED RADAR: RECURSIVE CALCULATION APPROACH

J.J BRAS (ESD SOUTH), MEMBER, IEEE DR R M BRAUN, MEMBER, IEEE

ESD SOUTH, TECHNOPARK, STELLENBOSCH

ABSTRACT

A recursive method of calculating the maximum angular accuracy of a pulsed search radar is presented. The analysis and calculation techniques follow the approaches taken by P. Swerling [5], D. H. Cooper [2] and R. L. Mitchell and J. F. Walker [4].

INTRODUCTION

Radar systems are largely utilised to detect and estimate the position of particular objects in terms of range, azimuth and elevation.

The accuracy with which these parameters are estimated is of primary importance in the application of the radar system. Comparison between actual accuracy achieved by practical measurements and theoretically derived accuracies provide an important measure of the system performance.

The following paper presents recursive methods of calculating the maximum angular accuracy of a pulsed search radar employing binary quantisation of the received radar signal amplitude. P. Swerling [5] has examined the maximum angular accuracy of a pulsed search radar without quantisation.

In his paper, Swerling considers two fluctuation cases, namely the non-fluctuating case and the fast fluctuating case. In a subsequent paper, D. H. Cooper [2] has examined the effect of binary quantisation of the received radar signal amplitude for the non-fluctuating case. His analysis follows that of Swerling and he concludes that the additional limitation on angular accuracy imposed by the quantisation may in many cases be neglected.

This paper follows the theoretical analysis of maximum angular accuracy as derived by Swerling and Cooper. Calculation of the eventual accuracy expressions is done by employing recursive methods according to a paper by R. L. Mitchell and J. F. Walker [4], thereby providing a general approach for the calculation of angular accuracies for the Chi-square class of targets.

MAXIMUM ANGULAR ACCURACY

In his paper, Swerling [5] applies a theorem of statistical estimation to derive an expression for the maximum angular accuracy of an analytic, unbiased estimator. In applying the theorem, it is assumed that for each pulse the probability density function of observing a voltage v_i for a given signal-to-noise ratio x_i for the i-th pulse is existent and identical for all pulses within a scan. (A scan being interpreted as a single sweep of the beam across a target.) For pulse-to-pulse independence the joint probability density function of observing the voltages $v_1, v_2, \ldots, v_k$ as the antenna scans through a target sector is expressed as a product of the probability density functions for each pulse, i.e.

$$L\{v_1, v_2, \ldots, v_k | \Theta_T\} = \pi_{i=1}^{M} p(V_i/X_i) \tag{1}$$

where:

v_i = pulse amplitude for the i-th pulse. In the event of binary quantisation v_i equals 0 or 1;

Θ_π = target angular location;

x_i = power signal-to-noise ration for the i-th pulse;

M = number of pulses within the antenna beamwidth.

To account for the fact that the radar pulse generation may not be synchronised with the antenna rotation, the likelihood function (1) is averaged over the maximum antenna rotation $\Delta\Theta$ in one pulse repetition interval.

$$L = \frac{1}{\Delta\Theta} \int_{\Delta\Theta} \pi_{i=1}^{M} p(V_i/X_i)d\Theta \tag{2}$$

However, it is assumed that the variation of x_i over the interval $\Delta\Theta$ is sufficiently small to neglect this averaging process [5].

Expression (1) may also be written as:

$$\lambda = \operatorname{Ln}(L) = \sum_{i=1}^{M} \ln[p(V_i/X_i)] \tag{3}$$

for which the smallest possible error σ_{min} in estimating the target location Θ_T is given by [5].

$$\left(\frac{1}{\sigma_{min}}\right)^2 = E\left\{\left(\frac{\partial\lambda}{\partial\Theta_T}\right)^2\right\}(1-\rho^2) \tag{4}$$

where

ρ = The extent to which errors in estimating the signal-to-noise ratio X_o (when the nose of the beam is pointing at the target) affect errors in the angular estimation.

E(.) denotes the ensemble average.

It is shown [2] that ρ = o yielding

$$\left(\frac{1}{\sigma_{min}}\right)^2 = E\left\{\left(\frac{\partial\lambda}{\partial\Theta_T}\right)^2\right\} \tag{5}$$

Expression (5) may be analysed further [2] resulting in the final expression for r_{min}.

$$\left(\frac{1}{\sigma_{min}}\right)^2 = X_o^2 \sum_{i=1}^{M} \left(\frac{\partial q(X_i)}{\partial X_i}\right)^2 \left(\frac{\partial f(u)}{\partial u}\right)^2 \frac{1}{\beta^2} \cdot \frac{1}{(q(X_i) - q(X_i^2))} \tag{6}$$

where:

X_o = power signal-to-noise ratio when the nose of the beam is pointing at the target;

$q(X_i)$ = probability that the quantised signal for the ith pulse given a pulse signal-to-noise ratio of xi will be 1;

$f(u_i)$ = a symmetrical function representing the beam pattern factor;

$d[q(X_i)]/dX_i$ = derivative of q(xi) to xi.

For the non-fluctuating case, the limitation in angular accuracy is caused by receiver noise. Due to the noise being assumed independent from pulse to pulse, the likelihood function is expressed by (1) and σ_{min} by (5).

For the fast fluctuating case, a further limitation in accuracy is introduced by the target cross-section fluctuation. Once again pulse-to-pulse independence is assumed allowing σ_{min} to be expressed by (5). However, in this case the single pulse signal-to-noise ratio is considered to be the average ratio over all target fluctuations [5].

RECURSIVE CALCULATIONS

Equation (5) forms the basis for the calculation of σ_{min}. In this equation, the functions q(xi), ∂[q(xi)]/∂(xi) and ∂[f(ui)]/∂(ui) need to be evaluated.

Assuming square-law detection followed by integration of N equally weighted pulses, Mitchell and Walker [4] derived recursive expressions for q(xi) applicable to non-fluctuating as well as the Chi-square class of fluctuating targets given by:

$$w(x,X) = \frac{1}{\Gamma(k)} \left(\frac{K}{X}\right)^K X^{K-1} \varepsilon\left(\frac{-K x}{X}\right) \tag{7}$$

The parameter K distinguishes various target cases:

K = 1 : Swerling Case 1 {Rayleigh target, slow fading]
K = 2 : Swerling Case 3
K = N : Swerling Case 2 {Rayleigh target, rapid fading}
K = 2N: Swerling Case 4
K = infinity: non-fading case
0<K<1 = Weinstock target for scan-to-scan fading
K<N = Weinstock target for pulse-to-pulse fading
1<K<N = Block-correlated Rayleigh target

NON-FLUCTUATING TARGETS

Swerling [5] has shown that for square-law detection in the presence of Gaussian noise, the probability density function of V (the integrated signal-plus-noise variable) conditional on X (the sum of single-pulse signal-to-noise ratio's) is given by:

$$p(V|X) = \left(\frac{V}{X}\right)^{\frac{N-1}{2}} e^{-V-X} \quad \Gamma_{N-1}\,(2\sqrt{VX}), \tag{8}$$

The probability of detection is then given by [5].

$$P_D\,(X,N) = \int_{V=t}^{\infty} p(V/X)dV \tag{9}$$

which may be rewritten as [4]:

$$P_D(X,N) = \sum_{j=o}^{\infty} a(j,X)\; g(N+j,t) \tag{10}$$

$$g(N+j,t) = \frac{1}{\Gamma(N+j)} \int_t V^{N+j-1}\, e^{-V}\, dV \tag{11}$$

$$a(j,X) = \frac{Xj}{\Gamma(j+1)}\, e^{-x} \tag{12}$$

The single pulse detection probability q(x) is given by (10) with N = 1.

Expressions (11) and (12) can be written recursively:

$$a(j+1,\, X) = \frac{X}{j+1}\; a(j,X) \tag{13}$$

$$a(o,X) = e^{-X}$$

$$g(N+j+1,t) = g(N+j,t) + b(j,t) \tag{14}$$

$$g(1,t) = e^{-t} \qquad \{N = 1\}$$

$$b(j+1,t) = \frac{t}{j+1}\; b(j,t) \tag{15}$$

$$b(o,t) = e^{-t}$$

The series may be truncated once [4]:

$$1 - \sum_{j=0}^{J} a(j,X) < \text{error}$$

An expression for $\partial[q(x))]/\partial(x)$ is obtained by taking the derivative of the series expansion for q(x).

$$\frac{\partial q(x)}{\partial x} = \frac{\partial P_D(x,N)}{\partial x} = \tag{16}$$

$$\sum_{j=o}^{\infty} g(N+j,t)\;.\;[a_1(j,X) - a_2(j,X)] \tag{17}$$

$$a_1(j,X) = \frac{X^{j-1}}{(j-1)!}\; e^{-X}$$

$$a_2(j,X) = \frac{X^j}{j!}\; e^{-X} \tag{18}$$

It can be shown that the series for $\partial[q(x)]/\partial(x)$ is convergent. Expression (17) and (18) may be written recursively:

$$a_1(j+1,X) = {}^{X}/_{j}\; a_1(j,X) \;, \quad j \geq 1 \tag{19}$$

$$a_1(o,x) = 0$$

$$a_1(1,x) = e^{-X}$$

$$a_2(j+1,x) = \frac{X}{j+1}\; a_2(j,X) \tag{20}$$

$$a_2(o,x) = e^{-X}$$

FLUCTUATING TARGETS

It can be shown [4] that for the Chi-square class of targets, q(X,N) is given by:

(21)

$$P_D(X,N) = \sum_{j=0}^{\infty} a(j,X) \quad g(N+j,\ t)$$

(22)

$$a(j,X) = \frac{1}{\Gamma(j+1)} \cdot \frac{\Gamma(k+j)}{\Gamma(k)} \left(\frac{K}{k+X}\right)^k .$$

$$\left(\frac{X}{K + X}\right)^j$$

A recursive expression for (22) may be derived [4].

(23)

$$a(j+1,X) = \frac{X \cdot (1+{}^j/_k)}{(1+{}^X/_h)(j+1)} \quad a(j,X);$$

$$a(o,X) = \left(\frac{K}{K + X}\right)^K$$

As with the non-fluctuating case, the series may be truncated once:

$$1 - \sum_{j=0}^{J} a(j,X) < \text{error}$$

In the event of single-pulse detection, N = 1.

The derivative ∂[q(x)]/∂(x) is obtained by taking the derivative of the series expansion (21):

(24)

$$\frac{\partial}{\partial X} \{P_D(X,N\} = \sum_{j=0}^{\infty} c(j,k)[a_1(j,X)-a_2(j,X)]$$

(25)

$$c(j,k) = \frac{\Gamma(k+j)}{\Gamma(k)} \left(\frac{K}{K+X}\right)^{K+1} \frac{1}{(K+X)}$$

$$c(j+1,k) = (k+j)\ c(j,k)$$

$$c(o,k) = \frac{K^{K+1}}{(K+X)^{K+2}}$$

(26)

$$a_1(j,X) = \frac{1}{(j-1)!} \left(\frac{X}{K+X}\right)^{j-1}$$

$$a_1(j+1,X) = \frac{1}{j} \left(\frac{X}{K+X}\right) a_1(j,X) \quad j \geq I$$

$$a_1(o,X) = o;\ a_1(1,X) = 1$$

(27)

$$a_2(j,X) = \frac{1}{j!} \left(\frac{X}{K+X}\right)^j$$

$$a_2(j+1,X) = \frac{1}{(j+1)} \quad \frac{X}{(K+X)} \quad a_2(j,X)$$

$$a_2(o,X) = 1$$

BEAM PATTERN FACTOR

In addition to evaluation of expressions for q(x) and ∂[q(x)]/∂(x), the beam pattern factor needs to be accounted for as well in calculating σ_{min}. This pattern factor f(u) incorporates the weighting of the returned pulse signal-to-noise ratio's by the antenna beam. A general expression for the i'th returned pulse is given by:

(28)

$$xi = x0 \quad f\left(\frac{\Theta_i - \Theta_r}{\beta}\right)$$

where:

x0 = average axial signal-to-noise ratio;
xi = average returned signal-to-noise ratio for the ith pulse;
Θi = angle pointed to by the nose of the beam for the ith pulse;
Θr = target angular location;
β = factor relating to beamwidth [5].

Following the approach by Swerling [5], a Gaussian pattern factor may be defined by:

$$f(u) = e^{-u^2} \qquad (29)$$

In this case β is related to 1/e power points of the beam, and the beamwidth is defined as 2β. For the half-power points, 2β evaluates to 1,66 Θ_3. The derivative of f(u) is given by:

$$\frac{Z f(u)}{Z u} = -2ue^{-u^2} \qquad (30)$$

Further, Θ_i is defined by:

$$\Theta_i = \Theta_1 + (i - 1)\Delta\Theta \qquad (31)$$

where

$$\Delta\Theta = \frac{2\beta}{N} \quad ; \quad N = \text{number of pulses} \qquad (32)$$

$\Delta\Theta$ must be small enough to allow the averaging process of (2) to be neglected.

RESULTS

Calculations were performed using the recursive approach for the non-fluctuating target (figure 1) and these results were compared with those given by Cooper (figure 2). Although it is not possible to determine the deviation in results achieved with the recursive calculation from those calculated by Cooper due to the fact that Cooper's results are given in graph, comparison with values read from the graph supplied by Cooper show very close similarity.

CONCLUSION

The recursive approach to calculating the maximum angular accuracy provides a computationally efficient and easily implemented solution. The number of iterations required for acceptable accuracy is not inhibitive [4]. However, due to exponential values being calculated, it is necessary to monitor underflow situations for small exponent values.

REFERENCES

[1] Brennan, L.E. and Reed, I.S. : 'A Recursive Method of Computing the Q Function', IEEE Transactions on Information Theory, April 1965, pp. 312 - 313

[2] Cooper, D.H. : 'Binary Quantization of Signal Amplitudes : Effect for Radar Angular Accuracy', IEEE Transactions on Aerospace and Navigational Electronics, March 1964, pp. 65 - 72

[3] Hovanessian, S.A. and Ahn, H.H. : 'Calculation of Probability of Detection with Target Scintillation', IEEE Transactions on Aerospace and Electronic Systems, Vol. AES-9, No. 2, March 1973, pp. 300 - 305

[4] Mitchell, R.L. and Walker, J.F. : 'Recursive Methods for Computing Detection Probabilities', IEEE Transactions on Aerospace and Electronic Systems, Vol. AES-7, No. 4, July 1971, pp. 671 - 676

[5] Swerling, P. : 'Maximum Angular Accuracy of a Pulsed Search Radar', Proceedings of the IRE, September 1956, pp. 1146 - 1155

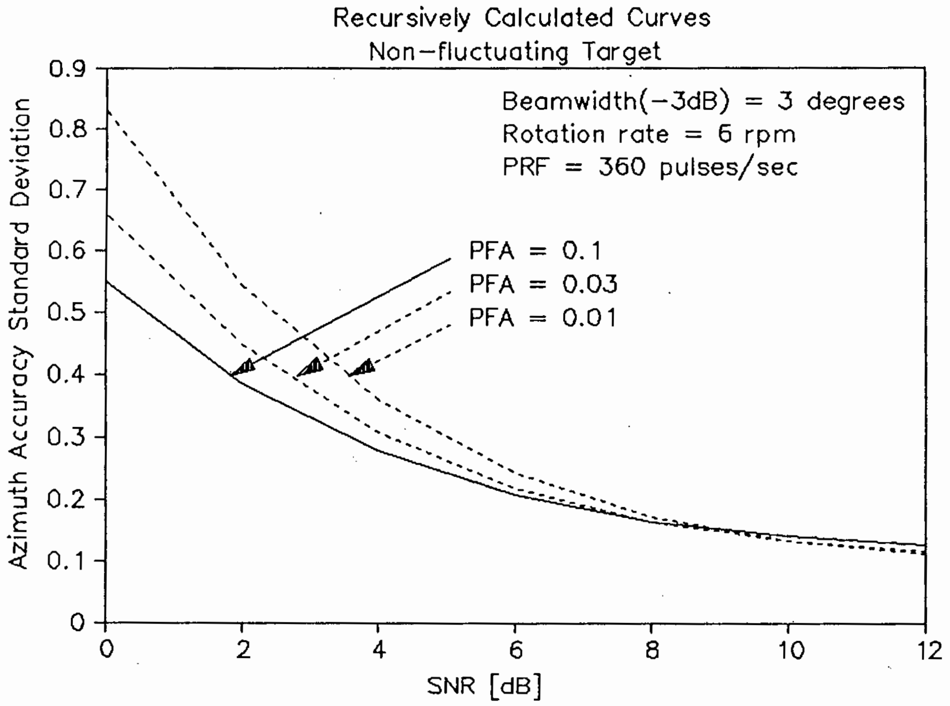

Figure 1: Recursively calculated results

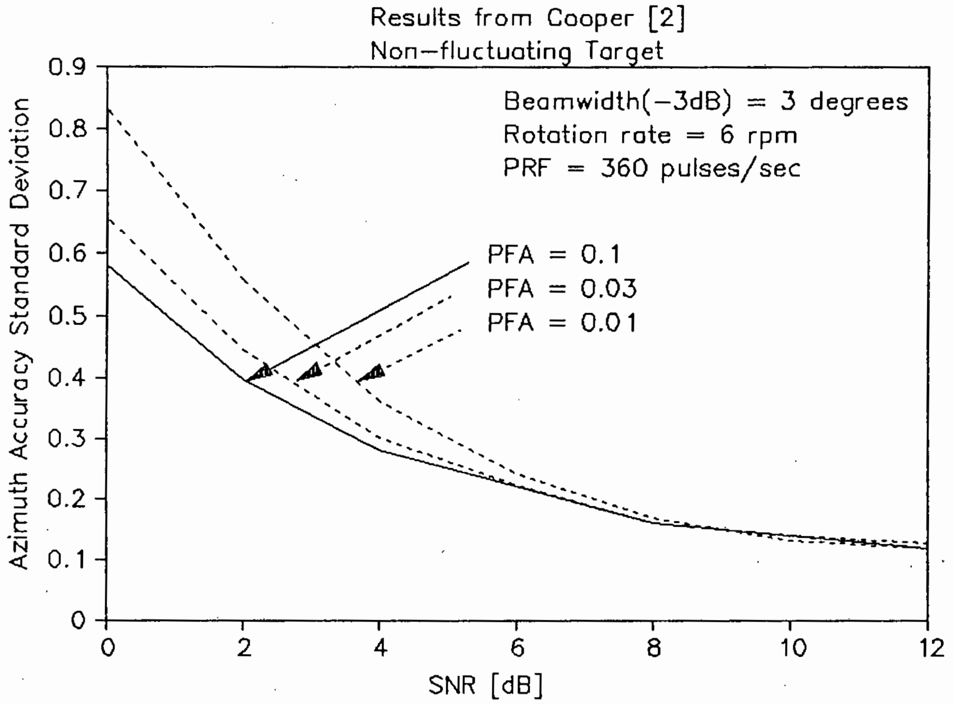

Figure 2: Results from Cooper [2]

APPENDIX G

A SIMULATION OF AZIMUTH ACCURACY IN PULSED SURVEILLANCE RADAR

IEEE South African Symposium on Communications and Signal Processing Proceedings, 30 August 1991, Pretoria, p. 36-41.

$$P_r(t) = \frac{P_t(t-\tau)\, G_t G_r\, \lambda^2 \sigma}{(4\pi)^3 R^4}$$

To express this equation in terms of a voltage relationship, the transmitted power is defined as a function of a complex voltage signal:

$$\psi_t(t) = \mu(t) .\ \exp\,(j2\pi fct)$$

The transmitted signal is reflected by a scatterer which is defined in terms of a complex reflection coefficient γ. This reflection coefficient represents that portion of the transmitted signal voltage which is reflected, and the phase shift introduced to the reflected signal.

The reflected signal may thus be expressed as :

$$\psi_r(t) = \psi_t(t - \tau) \left[\frac{G_t G_r\, \lambda^2}{(4\pi)^3 R^4} \right]^{\frac{1}{2}} .\ \gamma$$

This equation is valid if it is assumed that the signal scatterer may be considered as a stationary point scatterer, and the antenna is assumed stationary. For a moving scatterer and scanning antenna, the antenna gain, complex reflection coefficient, round trip delay time and scatterer range may no longer be considered as constants, but become functions of time. Mitchell [5] has shown that, for a processing interval T, the received signal from a point scatterer may be expressed as

$$\psi_r(t) = u_t(t-\tau)\, \frac{\lambda}{(4\pi)^{1.5}} \cdot \frac{1}{R^2} \left[G_t G_r \right]^{\frac{1}{2}} \gamma$$

$$\exp\left(\frac{-j4\pi R}{\lambda}\right) \exp[j2\pi(fc+fd)t]$$

if it is assumed that

1. The total range displacement of the scatterer during the processing interval is small compared to the range resolution of the system.
2. The change in doppler frequency for an accelerating scatterer is small compared to the doppler resolution of the system.
3. The angle rotated by the scanning antenna during the processing interval T is small compared to the angular resolution of the system.

The simulation of the received signal from distributed scatterers is achieved by superimposing all the individual returns to form a composite signal. However, for large numbers of scatterers, this technique becomes to computationally intensive. By grouping the scatterers which are unresolvable in terms of range, azimuth and doppler into resolution cells and representing the return from such a cell by a single phasor the computational load can be reduced.

Mitchell [5] states that for a system transmitting a coherent train of pulses at uniform intervals, the received pulse train can be simulated with a simplified expression:

$$\psi_r(\theta,t,eT_r) = \sum_m \sum_n \frac{\lambda}{(4\pi)^{1.5}\, R_m{}^2}\, U(\theta,\tau_m,fn)\, \mu_{pt}(t-\tau_m)$$

$$\exp(j2\pi f_n eTr)$$

The phasor $U(\Theta,\tau,fn)$ represents the return from a resolution cell at pointing angle Θ, range delay τ, and with a doppler frequency fn. For independent scatterers, the ensemble average of the complex reflection coefficients within the resolution cell may be considered as the average radar cross section of the cell, and the power of the phasor representing this cell is given by :

$$\overline{\left| U(\Theta,\tau) \right|^2} = \sum_e \sigma(\Theta_e,\tau)\, G_t(\Theta_e - \Theta)\, G_r(\Theta_e - \Theta)$$

AZIMUTH ESTIMATORS

Azimuth estimators aim to establish the angular location of an object within the radar resolution cell. Theoretically, if the antenna beam pattern were known exactly, and no noise entered the system from any source, the azimuth accuracy would be limited by the quantisation of the antenna position encoder. In practice, however, the existence of receiver noise, scatterer radar cross-section fluctuation and other noise sources limit the achievable azimuth accuracy. The ideal estimator attempts to minimise the influence of noise as effectively as possible by sensing the derivative of the system response function [6]. For the pulsed radar system, this is effectively the sequence of received pulse returns from the scatterer weighted by the antenna gain pattern.

FIGURE 2: SWERLING 0; PFA 1E-6

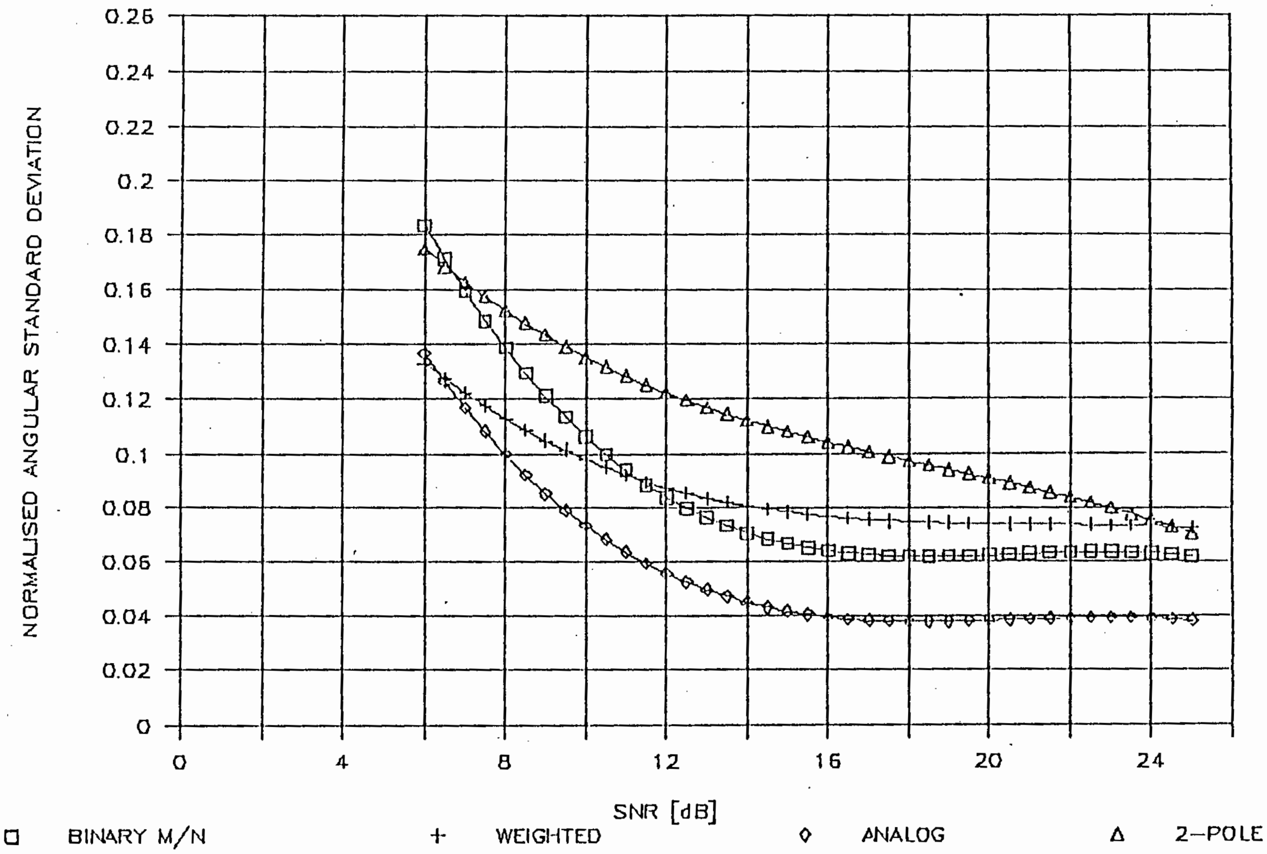

FIGURE 3: SWERLING 1; PFA 1E-6

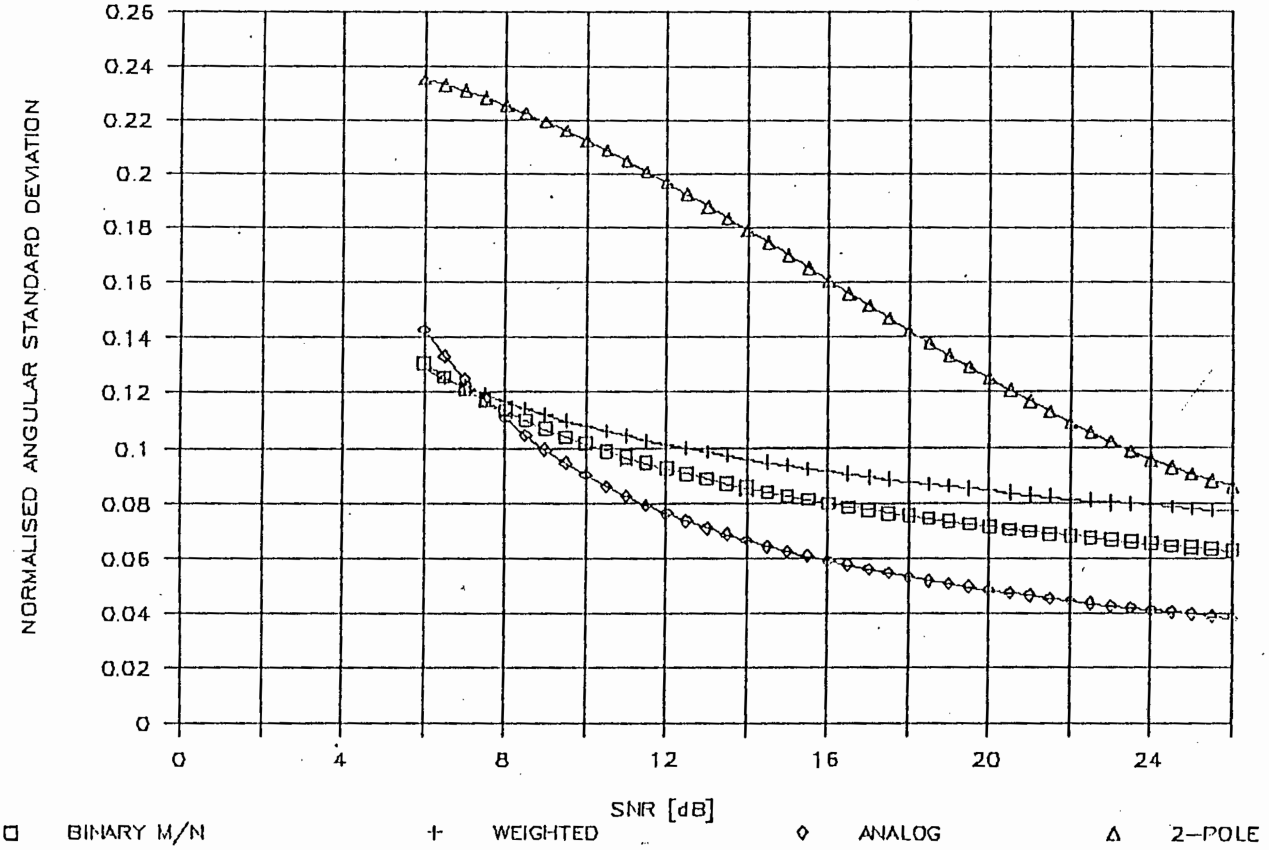

FIGURE 4: SWERLING2, PFA 1E-6

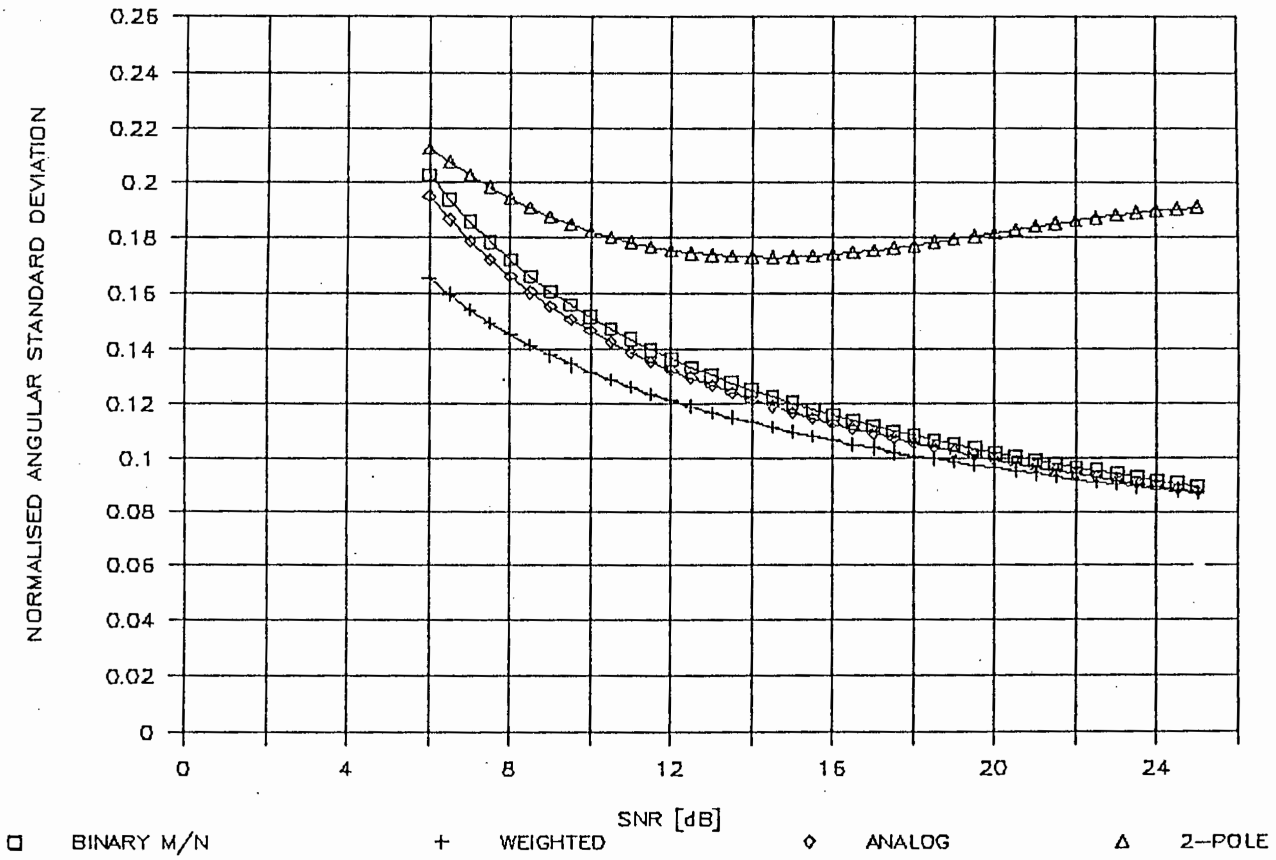

FIGURE 5: PARTIALLY CORRELATED TARGET

FOURIER CURVE FIT; SNR=10dB

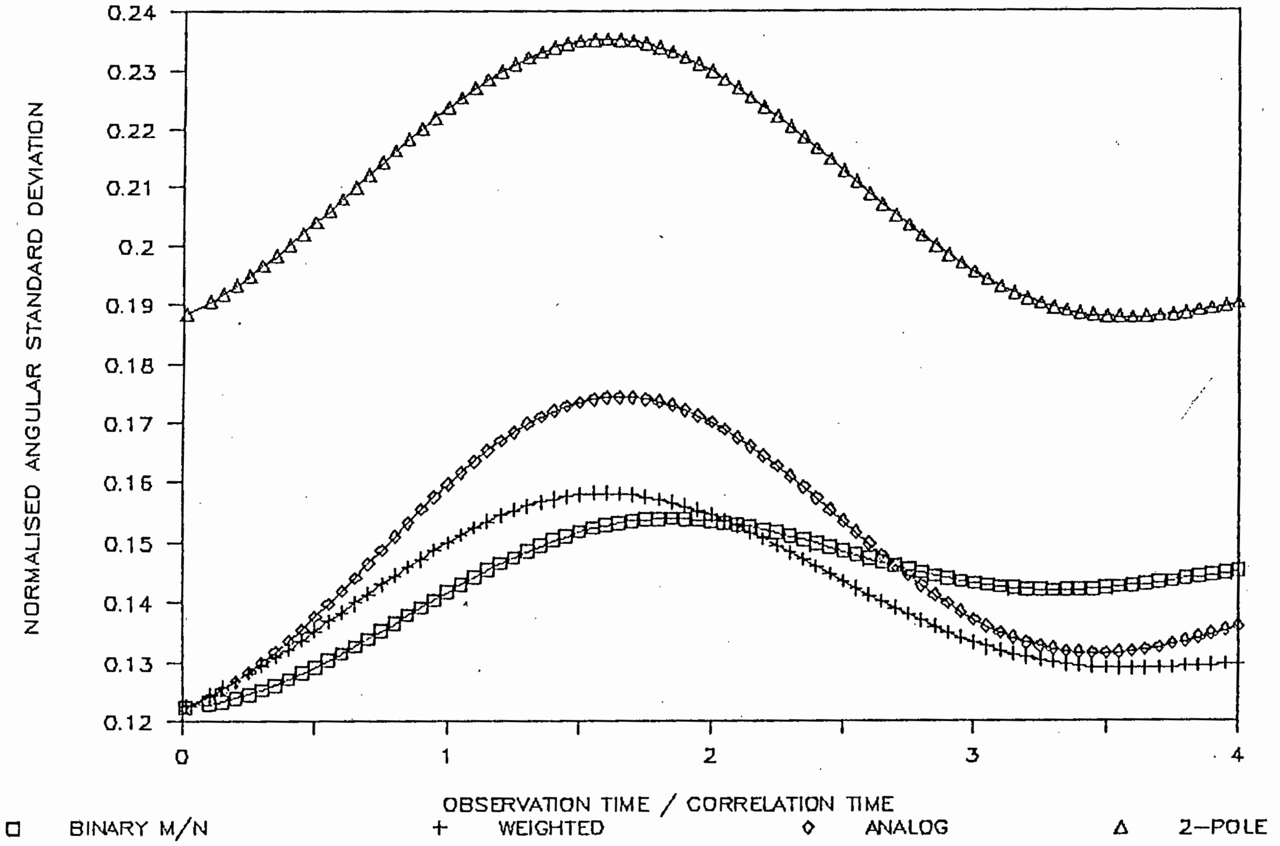

REFERENCES

1. Accarino, N. and Giaccari, E., "A new approach to radar plot extraction for ATC applications", IEEE International Radar Conference, Arlington, VA, 28-30 April 1980, p. 391-396.

2. Barton, D.K. and Ward, H.R., "Handbook of radar measurement", Artech House Inc., Dedham, MA, 1984^2.

3. Barton, D.K., "Land clutter models for radar design and analysis", Proceedings of the IEEE, vol. 73, no. 2, February 1985, p. 198-204.

4. Barton, D.K., "Low-angle radar tracking", IEEE Proceedings, vol. 62, no. 6, June 1974, p. 687-704.

5. Barton, D.K., "Modern radar system analysis", Artech House, Inc., Norwood, MA, 1988.

6. Barton, D.K et.al., "Radar Evaluation Handbook", Artech House, Inc., Norwood, MA, 1991.

7. Barton, D.K., "Radar measurement accuracy in log-normal clutter", EASCON '71 Record, p. 246-251.

8. Barton, D.K., "Radar System Analysis", Artech House, Inc., Dedham, MA, 1979^2.

9. Bernstein, R., "An analysis of angular accuracy in search radar", IRE National Convention Record, vol. 3, pt. 5, 1955, p. 61-78.

10. Blackman, S.S., "Multiple target tracking with radar applications", Artech House, Inc., Dedham, MA, 1896, p. 213-247.

11. Blake, L.V., "Radar range performance analysis", Lexington Books, Lexington MA,1980.

12. Blythe, J.H. et.al., "Binary plot extraction using digital integrating counters", Proceedings of the IRE, vol. 121, no. 1, November 1974, p. 1345-1350.

13. Cantrell, B.H. and Trunk, G.V., "Angular accuracy of a scanning radar employing a two-pole filter", IEEE Transactions on Aerospace and Electronic Systems, vol. AES-9, no. 5, September 1973, p. 649-880.

14. Cooper, D.H., "Binary quantization of signal amplitudes: effect for radar angular accuracy", IEEE Transactions on Aerospace and Navigational Electronics, March 1964, p. 65-72.

15. Cramer, H., "Mathematical methods of statistics", Princeton University Press, Princeton, 1946.

16. DiFranco, J.V. and Rubin, W.L., "Radar Detection", Artech House, Inc., Dedham, MA, 1980.

17. Dinneen, G.P. and Reed, I.S., "An analysis of signal detection and location by digital methods", Transactions of the IRE, vol. IT-2, no. 1, March 1956, p. 29-38.

18. Edrington, T.S., "The amplitude statistics of aircraft radar echoes", Transactions of the IRE, vol. MIL-9, no. 1, January 1965, p. 10-16.

19. Fehlner, L.F.:, "Marcum's and Swerling's data on target detection by a pulsed radar", Applied Physics Laboratory, John Hopkins University, Silver Spring, Md., Report TG-451, 2 July 1962.

20. Galati, G. and Studer, F.A., "Angular accuracy of the binary moving window detector", IEEE Transactions on Aerospace and Electronic Systems, vol. AES-18, no. 4, July 1982, p. 416-422.

21. Hanle, E., "Cross-section variations with different target classes and their influences to detection and tracking", IEEE International Conference on Radar, 24-28 April 1989, Paris, p. 135-140.

22. Hansen, V.G., "Performance of the analog moving window detector", IEEE Transactions on Aerospace and Electronic Systems, vol. AES-6, no. 1, March 1970, p. 173-179.

23. Hansen, V.G., "Simple expressions for determining radar detection thresholds", IEEE Transactions on Aerospace and Electronic Systems, vol. AES-18, no. 4, July 1982, p. 510-584.

24. Hansen, V.G., "Topics in radar signal processing: part 1", Microwave Journal, vol. 27, no. 3, March 1984, p. 24-46.

25. Henn, J.W. et.al., "Land clutter study: low grazing angles (backscattering)", Radar 82, IEE Conference Publication 216, October 1982, p. 250-253.

26. Jackson, L.B., "Digital filters and signal processing", Kluwer Academic Publishers, Dordrecht, 1986^3, p. 96-97.

27. Kanter, I., "Exact detection probability for partially correlated Rayleigh targets", IEEE Transactions on Aerospace and Electronic Systems, vol. AES-22, no. 2, March 1986, p. 184-195.

28. Kreyszig, E., "Advanced engineering mathematics", John Wiley & Sins, Inc., New York, 1983^5.

29. Likharev, V.A., "Digital-computer simulation of signal detection and parameter estimation problems", Radio Engineering, vol. 24, no. 10, 1969, p. 96-100.

30. Marcum, J.I., "A statistical theory of target detection by pulsed radar", IRE Transactions on Information Theory, vol. IT-6, no. 2, April 1960, p. 59.

31. Minkler, G. and Minkler, J., "CFAR", Magellan Book Company, Baltimore, MD, 1990, p. 19-40.

32. Mitchell, R.L., "Radar signal simulation", Artech House, Inc., Dedham, MA, 1976.

33. Nathanson, F.E., "Radar design principles", McGraw-Hill Book Company, Inc., New York, 1969.

34. Pachares, J. "A table of bias levels useful in radar detection problems", IRE Transactions on Information Theory, vol. IT-6, April 1960, p. 269-308.

35. Peebles, P.Z., "The generation of correlated log-normal clutter for radar simulations", IEEE Transactions on Aerospace and Electronic Systems, November 1971, p. 1215-1217.

36. Pham, K.K., "Improvement of visibility in ground clutter", IEEE International Conference on Radar, 24-28 April 1989, Paris, p. 79-84.

37. Rohling, H., "Radar CFAR thresholding in clutter and multiple target situations", IEEE Transactions on Aerospace and Electronic Systems, vol. AES-19, no. 4, July 1983, p. 608-621.

38. Schleher, D.C.:, "MTI and Pulsed Doppler Radar", Artech House, Inc., Norwood, MA, 1991.

39. Schleher, D.C.:, "MTI Radar", Artech House, Inc., Dedham, MA., 1980^2, p. 19-61.

40. Schleher, D.C.:, "Automatic detection and radar data processing", Artech House, Inc., Dedham MA, 1987^2, p. 1-86.

41. Scholefield, P.H.R., "Statistical aspects of ideal radar targets", IEEE Proceedings, vol. 55, no. 4, April 1967, p. 587-589.

42. Skolnik, M.I., "Introduction to radar systems", McGraw-Hill Book Company, New York, 1980^2, p. 399-410.

43. Skolnik, M.I., "Radar Handbook", McGraw-Hill Book Company, New York, 1990^2, p. 8.1-23, p. 15-12, p. 18.34-45.

44. Swerling, P., "Detection of fluctuating pulsed signals in the presence of noise", IRE Transactions on Information Theory, vol. IT-3, no. 3, September 1957, p. 175-178.

45. Swerling, P., "Maximum angular accuracy of a pulsed search radar", Proceedings of the IRE, vol. 4, no. 9, September 1956, p. 1146-1155.

46. Swerling, P., "Recent developments in target models for radar detection analysis", AGARD Avionics Tech. Symp. Proceedings, Istanbul, Turkey, 25-29 May 1975, CP-60-70, p. 7.1-16.

47. Trunk, G.V., "Comparison of two scanning radar detectors: the moving window and the feedback integrator", IEEE Transactions on Aerospace and Electronic Systems, vol. AES-7, no. 2, March 1971, p. 395-398.

48. Trunk, G.V., "Survey of radar ADT", NRL Report 8698, Naval Research Laboratory, Washington D.C.:, 30 June 1983.

49. Urkowitz, H., "Signal theory and random processes", Artech House, Inc., Norwood, MA, 1983, p. 308.

50. Walter, C.M., "A quantitive analysis of automatic target detection-position estimation schemes observing scintillating targets in noise", IRE National Convention Record, vol. 6, pt. 5, 1958, p. 107-119.

51. Walter, C.M. et.al., "Comparative evaluation of several azimuth estimating procedures using digital processing and search radar simulation", IRE Transactions on Aeronautical and Navigational Electronics, vol. ANE-5, June 1958, p. 114-121.

52. Weiner, M.A., "Detection probability for partially correlated Chi-square targets", IEEE Transactions on Aerospace and Electronic Systems, vol. AES-24, no. 4, July 1988, p. 411-416.

53. Woodward, M.A., "Probability and information theory, with applications to radar", Permagon Press, New York, 1964.